NOTE TO USERS

This reproduction is the best copy available.

UMI

University of Alberta

Fabrication and Characterization of Silicon Nanowires and Metal Nanostructures

By

Vicki Wai-Shum Lui ©

A thesis submitted to the Faculty of Graduate Studies and Research in partial fulfillment of the requirements for the degree of Master of Science

Department of Chemistry

Edmonton, Alberta

Fall 2005

Library and Archives Canada

Published Heritage Branch

395 Wellington Street
Ottawa ON K1A 0N4
Canada

Bibliothèque et Archives Canada

Direction du Patrimoine de l'édition

395, rue Wellington
Ottawa ON K1A 0N4
Canada

0-494-09230-0

Your file *Votre référence*
ISBN:
Our file *Notre référence*
ISBN:

NOTICE:
The author has granted a non-exclusive license allowing Library and Archives Canada to reproduce, publish, archive, preserve, conserve, communicate to the public by telecommunication or on the Internet, loan, distribute and sell theses worldwide, for commercial or non-commercial purposes, in microform, paper, electronic and/or any other formats.

The author retains copyright ownership and moral rights in this thesis. Neither the thesis nor substantial extracts from it may be printed or otherwise reproduced without the author's permission.

AVIS:
L'auteur a accordé une licence non exclusive permettant à la Bibliothèque et Archives Canada de reproduire, publier, archiver, sauvegarder, conserver, transmettre au public par télécommunication ou par l'Internet, prêter, distribuer et vendre des thèses partout dans le monde, à des fins commerciales ou autres, sur support microforme, papier, électronique et/ou autres formats.

L'auteur conserve la propriété du droit d'auteur et des droits moraux qui protège cette thèse. Ni la thèse ni des extraits substantiels de celle-ci ne doivent être imprimés ou autrement reproduits sans son autorisation.

In compliance with the Canadian Privacy Act some supporting forms may have been removed from this thesis.

While these forms may be included in the document page count, their removal does not represent any loss of content from the thesis.

Conformément à la loi canadienne sur la protection de la vie privée, quelques formulaires secondaires ont été enlevés de cette thèse.

Bien que ces formulaires aient inclus dans la pagination, il n'y aura aucun contenu manquant.

Canada

Abstract

Silicon nanowires were made via oxide-assisted growth (OAG) and electrochemical etching. Growth mechanisms for the various products of the OAG synthesis were proposed based on scanning electron microscopy (SEM). The etching synthesis produced silicon nanowires along with silver dendrites, both of which were characterized by SEM. The nanowires (both syntheses) were etched with HF to yield hydride-terminated wires, though the electrochemically produced wires showed less success. Some nanowires (OAG) exhibited weak photoluminescence.

Metal nanostructures on semiconductors were synthesized by galvanic displacement. Silver plates were formed on GaAs with silver salts. With $AgNO_3$, both phases of silver were present and large, stacked structures formed. When Ag_2SO_4 was used, only the cubic phase was evident and the plates lie flat on the substrate. The twinning growth mechanism is discussed. Also, regular and semi-regular polyhedral shapes of gold were formed on InP, also via twinning. Other systems studied include Ag/Ge, Pt/InP, and Ag/InP.

Acknowledgements

There are a number of people I would like to thank for helping me with my project. Without them, this project would not have been possible. I would like to thank my supervisors, Jillian Buriak and Jonathan Veinot, for their direction, guidance, and expertise. I thank Jeffrey Stryker for his guidance and support. Besides my advisory committee members, there are many others for whom I would like to express appreciation and gratitude: Mohammad (Navid) Hormozi Nezhad for synthesis of samples of metal nanostructures on semiconductor substrates (described in Chapter 3); Daniel Salamon for his instruction, support, and expertise on the scanning electron microscopes; Janet Macdonald for characterization of my samples on the transmission electron microscope; Steve Launspach for training me and helping me obtain X-ray diffraction patterns; Matthieu Versavel and Shane Crerar for obtaining other X-ray diffraction patterns for me; Robert Konzuk for instruction on the use of the tube furnace; and Thomas Etsell, Ken Westra, Hani Henein, Barry Wiskel, and Tim Hatchard for their helpful discussions. Even though I cannot name all the various technical and support staff of the Departments of Chemistry and of Chemical and Materials Engineering, I am very grateful to them as they were very supportive and helpful and I would not be able to do research without them. I would also like to express thanks to my family, friends, and the Buriak and Veinot groups for their friendship and support.

Table of contents

1 Introduction 1

1.1 'There's plenty of room at the bottom' 1

1.2 The nanoscale 2

1.3 Nano in nature 4

1.3.1 Cellular structures 4

1.3.2 Insect wings 4

1.3.3 Mollusk shells 5

1.4 'Old' synthetic nanostructures 5

1.4.1 Gold ruby glass 5

1.4.2 Guinier-Preston zones 6

1.4.3 Langmuir-Blodgett films 8

1.5 Modern nano 8

1.5.1 Scanning probe microscopy 10

1.5.2 Thiols on gold 12

1.5.3 Microcontact printing 13

1.5.4 Dip pen nanolithography 14

1.5.5 Buckminsterfullerene and related structures 14

1.5.6 Quantum Dots 16

1.5.7 Luminescent silicon 17

1.5.8 Photonic bandgap materials 18

1.5.9 Nanobiology 19

1.5.10 Biomimetics 20

1.6 The future of nano 21

1.7 Project motivation and goals 21

1.8 References 23

2 Oxide-assisted growth of silicon nanowires 28
2.1 Introduction 28
2.2 Experimental procedure 33
2.2.1 Materials 33
2.2.2 Synthesis of silicon nanowires 34
2.2.3 Etching of silicon nanowires 35
2.2.4 Characterization 36
2.2.4.1 Scanning electron microscopy (SEM) *36*
2.2.4.2 Transmission electron microscopy (TEM) *37*
2.2.4.3 Energy dispersive X-ray spectrometry (EDX/EDS) *37*
2.2.4.4 X-ray diffraction (XRD) *38*
2.2.4.5 Fourier-transform infrared spectrometry (FTIR) *38*
2.2.4.6 Fluorometry/Photoluminescence (PL) *38*
2.3 Results 39
2.3.1 As-grown products 39
2.3.1.1 Zone I *41*
2.3.1.2 Zone II *43*
2.3.1.3 Zone III *46*
2.3.1.4 Zone IV *46*
2.3.1.5 Zone V *49*
2.3.2 Etching of silicon nanowires 50
2.3.3 Photoluminescence 53
2.4 Discussion 54
2.4.1 Growth mechanism 54
2.4.1.1 Zones I, II *56*
2.4.1.2 Zone IV *65*
2.4.1.3 Zone V *66*
2.4.2 Etching of silicon nanowires 69
2.4.3 Photoluminescence 70

2.5 Conclusion 71
2.6 References 72

3 Metal nanostructures on semiconductor substrates.. 77
3.1 Introduction 77
3.2 Experimental 81
3.2.1 Materials 81
3.2.1.1 Reagents for substrate preparation and cleaning 81
3.2.1.2 Bath reagents and additives 82
3.2.1.3 Semiconductors 82
3.2.2 Synthesis procedure 83
3.2.2.1 Metal deposition 83
3.2.2.1.1 Au on InP 83
3.2.2.1.2 Pt on InP 84
3.2.2.1.3 Ag on InP 84
3.2.2.1.4 Ag on GaAs 84
3.2.2.1.5 Ag on Ge 84
3.2.2.2 Si nanowires and Ag dendrites (Ag on Si) 85
3.2.2.2.1 Etching synthesis 85
3.2.2.2.2 Etching refinement 85
3.2.3 Characterization 86
3.2.3.1 Scanning electron microscopy (SEM) 86
3.2.3.2 Energy dispersive X-ray spectrometry (EDX/EDS) 86
3.2.3.3 X-ray diffractometry (XRD) 86
3.2.3.4 Open-circuit potential (OCP) measurements 86
3.3 Results and Discussion 87
3.3.1 Au on InP 87
3.3.1.1 Results 87
3.3.1.2 Discussion 90
3.3.2 Pt on InP 94

3.3.2.1 Results *94*
3.3.2.2 Discussion *95*
3.3.3 Ag on InP **96**
3.3.3.1 Results *96*
3.3.3.2 Discussion *97*
3.3.4 Ag on GaAs **98**
3.3.4.1 Results *98*
3.3.4.2 Discussion *106*
3.3.5 Ag on Ge **124**
3.3.5.1 Results *124*
3.3.5.2 Discussion *125*
3.3.6 Si nanowires and Ag dendrites (Ag on Si) **126**
3.3.6.1 Results *126*
3.3.6.2 Discussion *131*
3.4 Conclusion **135**
3.5 References **137**

4 Conclusion **142**
4.1 Silicon nanowires **142**
4.2 Metal nanostructures on semiconductor substrates **142**

List of tables

2 Oxide-assisted growth of silicon nanowires

Table 2.1 Parameters used in electron microscopy.....37

3 Metal nanostructures on semiconductor substrates

Table 3.1 Reduction potentials.....79

List of figures

1 Introduction

Figure 1.1 Objects at different length scales 3
Figure 1.2 Blue *Morpho* butterfly 5
Figure 1.3 Abalone shell 6
Figure 1.4 Lycurgus Cup 7
Figure 1.5 Guinier-Preston zones 7
Figure 1.6 Langmuir-Blodgett film technique 8
Figure 1.7 Scanning probe microscopy 11
Figure 1.8 STM image 11
Figure 1.9 Thiols on gold 12
Figure 1.10 Microcontact printing 13
Figure 1.11 Dip pen nanolithography 14
Figure 1.12 Fullerene structures 15
Figure 1.13 Quantum dots 16
Figure 1.14 Luminescent silicon 17
Figure 1.15 Photonic bandgap material 19
Figure 1.16 Orthogonal self-assembly 20
Figure 1.17 Layerered zeolite crystals 20

2 Oxide-assisted growth of silicon nanowires

Figure 2.1 Process of attachment of Si nanowires to bulk Si surface 29
Figure 2.2 Silicon nanowire nucleation and growth process 32
Figure 2.3 Schematic of experiment apparatus 34
Figure 2.4 Macroscopic products 40
Figure 2.5 Zone I products 42
Figure 2.6 Copper-containing structure 44
Figure 2.7 Zone II products 45
Figure 2.8 Zone III products 47

Figure 2.9 Zone IV products 48
Figure 2.10 Zone V products 51
Figure 2.11 FTIR spectra of etched products 52
Figure 2.12 Growth sequence of octopus-like structure 58
Figure 2.13 Tapered ends of nanowires 59
Figure 2.14 Nucleation on a nanowire 59
Figure 2.15 Facetted tips 60
Figure 2.16 Zone I clumps 61
Figure 2.17 Leftover SiO reagent 62
Figure 2.18 Substrate surfaces showing spectrum of colours 63
Figure 2.19 Protrusions on Zone I tips 64
Figure 2.20 Spheroidization mechanism 65
Figure 2.21 Impingement of SiO particles 68
Figure 2.22 Schematic of observation of roughened products 69

3 Metal nanostructures on semiconductor substrates

Figure 3.1 Electroless deposition processes 78
Figure 3.2 Etching mechanism of silicon nanowires 80
Figure 3.3 Au on InP with H_2SO_4 87
Figure 3.4 Au on InP with 0.1% HBr for 24 h 88
Figure 3.5 Au on InP with 2% HBr for 30 min 89
Figure 3.6 Au on InP with 2% HBr for 24 h 90
Figure 3.7 Re-entrant grooves in twinning 92
Figure 3.8 Pt on InP with H_2SO_4 for 1 h 95
Figure 3.9 Ag on InP. 97
Figure 3.10 Ag on GaAs with very dilute $AgNO_3$ 98
Figure 3.11 Ag on GaAs with 10^{-3} mol/L $AgNO_3$ for 10 min 99
Figure 3.12 Thickness of Ag plates 100
Figure 3.13 Ag on GaAs with 10^{-3} mol/L $AgNO_3$ for 30 min 101
Figure 3.14 Ag on GaAs with 10^{-3} mol/L $AgNO_3$ for 1h: centre of substrate 102
Figure 3.15 Ag on GaAs with 10^{-3} mol/L $AgNO_3$ for 1h: substrate edge 103

Figure 3.16 Ag on GaAs with 10^{-3} mol/L $AgNO_3$ for 21 h 104
Figure 3.17 Coalescence of Ag plates.....105
Figure 3.18 Ag on GaAs with 10^{-3} mol/L $AgNO_3$ for 21 h: background 106
Figure 3.19 Ag on GaAs with pre-purged 10^{-3} mol/L $AgNO_3$ for 30 min.....107
Figure 3.20 Ag on GaAs with 10^{-3} mol/L Ag_2SO_4 108
Figure 3.21 XRD spectra of Ag plates on GaAs substrate 109
Figure 3.22 Graphs from OCP experiments performed of $AgNO_3$ on GaAs .110
Figure 3.23 Ag plates with 120° and 60° corners.....112
Figure 3.24 Schematic demonstrating successive nucleations 113
Figure 3.25 Measurements of angle of nucleation of Ag plates 114
Figure 3.26 Nucleations of Ag plates parallel to edge of original plate 115
Figure 3.27 Parallel Ag plates.....115
Figure 3.28 Complex structure showing caved-in Ag plates.....116
Figure 3.29 Close packing schemes of spheres 118
Figure 3.30 Twinning of new plates 120
Figure 3.31 Ag on Ge in the presence of BMT.....124
Figure 3.32 Ag on Ge with SDS for 3 h 126
Figure 3.33 Ag on Ge with 10^{-3} mol/L SDS for 24 h 126
Figure 3.34 Optical photograph of Si substrate etched with HF/$AgNO_3$ 127
Figure 3.35 Etching synthesis of Si nanowires: overview of products.....128
Figure 3.36 Silicon nanowires 129
Figure 3.37 Silver dendrites.....130
Figure 3.38 Silver dendrites farther from substrate surface.....131
Figure 3.39 Etching in different directions.....132
Figure 3.40 Less etched Si substrate.....133
Figure 3.41 Cross-sections of silicon wires/pillars.....134

1 Introduction

1.1 'There's plenty of room at the bottom'

Nanometre-scale science and technology, or nanoscience and nanotechnology (collectively referred to as 'nano'), has flourished in the last few years. Why has this field suddenly become so popular? A major starting point that instigated modern nano research was a historic talk, entitled 'There's Plenty of Room at the Bottom,' given by 1965 Nobel Physics laureate Richard Feynman at the California Institute of Technology in December 1959.[1] The aptly titled speech not only talked about how much information could fit in a tiny space (bottom size regime), but it also talked about the potential of the nano field of study. Feynman predicted the future prominence and impact of nanoscience and nanotechnology:

> What I want to talk about is the problem of manipulating and controlling things on a small scale. As soon as I mention this, people tell me about miniaturization, and how far it has progressed today. They tell me about electric motors that are the size of the nail on your small finger. And there is a device on the market, they tell me, by which you can write the Lord's Prayer on the head of a pin. But that's nothing; that's the most primitive, halting step in the direction I intend to discuss. It is a staggeringly small world that is below. In the year 2000, when they look back at this age, they will wonder why it was not until the year 1960 that anybody began seriously to move in this direction.

In 1974, Norio Taniguchi of Tokyo Science University first coined the term 'nanotechnology' as follows:[2]

> 'Nanotechnology' is the production technology to get the extra high accuracy and ultrafine dimensions, i.e., the preciseness and fineness on the order of 1 nm, 10^{-9} m in length. The name of 'nanotechnology' originates from this nanometre. In the processing of materials, the smallest bit size of stock removal, accretion or flow of materials is probably of one atom or one molecule, namely 0.1-0.2 nm in length. Therefore, the expected limit size of fineness would be of the order of 1 nm. Accordingly, 'nanotechnology' mainly consists of the processing of separation, consolidation and deformation of materials by one atom or one molecule. Needless to say, the measurement and control techniques to measure the preciseness and fineness of 1 nm play a very important role in this technology.

(Note that the coinage of the term is often mistakenly attributed to K. Eric Drexler in his book *Engines of Creation* in 1986.[3]) Today, there are hundreds of terms with the root *nano-*, which is taken from the Greek *nanos*, meaning *dwarf*,[4] and more terms are continually being added.

1.2 The nanoscale

Before we delve into nano any further, some definition of size scale is appropriate. The size regime of nanometre-scale science and technology is also called the mesoscale. If we base definitions of length scale on how the IUPAC (International Union of Pure and Applied Chemistry) defines a micropore, mesopore, and macropore,[5] then the microscale (microscopic length scale) would refer to a length scale of 2 nm or less, the macroscale (macroscopic length scale) a length scale of 50 nm or more, and the mesoscale (mesoscopic length scale) the intermediate regime between these two extremes. Figure 1.1 gives examples of objects at different length scales. In reality, the definitions outlined above are

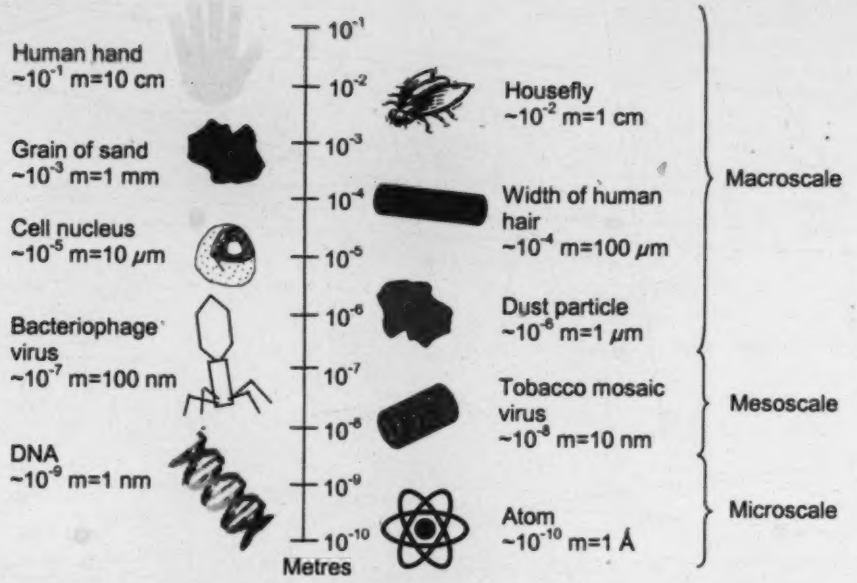

Figure 1.1. Objects at different length scales. The measurements listed for the objects are orders of magnitude and not exact measurements.

more fluid and even a few hundred nanometres may qualify as mesoscale. The microscale concerns the behaviour and characteristics of individual atoms and molecules with discrete states. In the macroscopic regime, continuum models are applied in which atoms and molecules behave together as an aggregate whole, and the lower limit of this regime will depend on the system. Simplistically, the mesoscopic scale seeks to describe systems in which the atoms and molecules behave as small clusters; when compared to the microscopic and macroscopic regimes, it may be thought of as a broken continuum.[6]

One note of caution: sometimes the microscale is thought of as the micrometre scale, which is actually part of the macroscale. In this context, the mesoscale becomes the nanoscale, while lengths below a nanometre may simply be thought of as the atomic and molecular scale. The microscale in this context no longer refers to dimensions 2 nm or smaller. Although the present document deals primarily with objects and phenomena on the nano- or mesoscale, we will avoid using the terms *microscale* and *microscopic* to avoid confusion. When the word *macroscopic* is used, it will generally be used to describe what can be observed with the naked eye.

Though various aspects of nano have been around for decades, only the past few years have seen the burgeoning of the field. Many new discoveries and advances fuel the excitement and drive for even more growth in this field. Nano has become important because of its potential to change the world in which we live: from materials with superior strength and flexibility to sensors to detect minute concentrations of poisonous gas, from revolutionary drugs and medical research to computing devices that operate at the speed of light. The key to nature at this scale is control and manipulation through various parameters and processes. Tailoring the size, shape, composition, and arrangement of nanostructures is crucial to designing objects and materials with specific properties and functions.

1.3 Nano in nature

1.3.1 Cellular structures

Though nano is only recently being intensely studied and exploited by humankind, it has always been present in nature. Life at the cellular level operates on the nanometre scale; for example, the ribosome, the organelle that translates ribonucleic acid (RNA) into protein, is about 20 nm in diameter.[7] Cell membranes are about 10 nm thick, consisting of a phospholipid bilayer that is covered ('functionalized') with carbohydrate side chains and embedded with proteins.[7] Biological processes occur at the nanoscale in order to facilitate transport through increased surface-area-to-volume ratio and smaller distances that organelles, ions, etc. must travel.[7,8]

1.3.2 Insect wings

Insect wings often appear iridescent. The colour arises not from pigments but from the physical structure of the wings.[9,10] For example, the blue *Morpho* butterfly has hierarchical grating-like structures in its wings (see Figure 1.2). The feature size of these gratings is on the nanometre scale, causing the wings to diffract visible light.

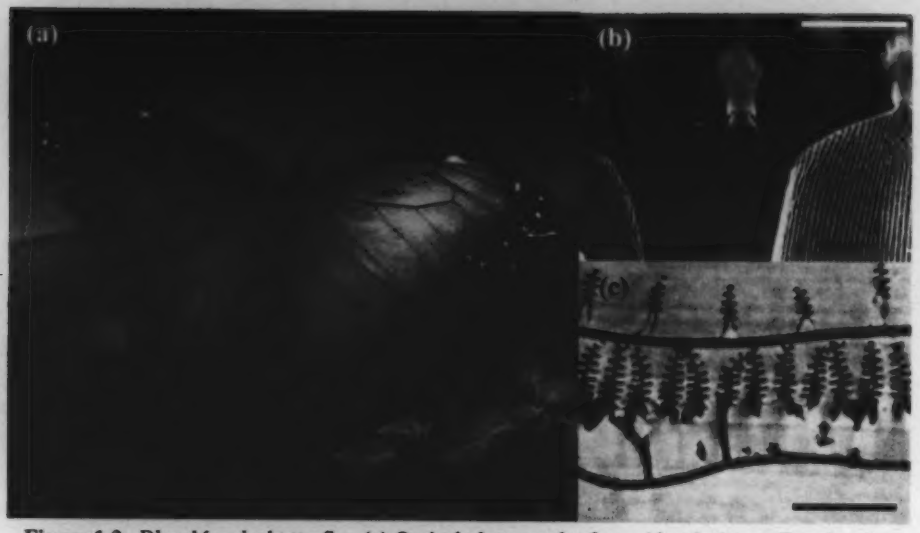

Figure 1.2. Blue *Morpho* butterfly. (a) Optical photograph of top side of wings. (Reprinted from reference 11.) (b) Scanning electron micrograph of scales in wings. Scale bar=30 μm. (c) Transmission electron micrograph of cross-section of a scale. Scale bar=2 μm. ((b) and (c) reprinted from reference 10.)

1.3.3 Mollusk shells

Another example is seen in the shells of mollusks. The nacre of abalone shells consists of 200-500-nm- and 20-30-nm-thick alternating sheets of inorganic calcium carbonate ($CaCO_3$) and organic protein, respectively (Figure 1.3).[12-15] Like the butterfly wings, these layers contribute to iridescence. In addition, even though nacre is 95% calcium carbonate and 5% protein, both of which are weak materials, this layered structure results in a composite that has 500-3000 times the fracture toughness of pure calcium carbonate alone—the brittle material in chalk.

1.4 'Old' synthetic nanostructures

1.4.1 Gold ruby glass

It has been mentioned that only in the past few years has nano research really flourished. However, in the 17th century, it was discovered that gold could be used to impart a red colour to glass, producing what is known as gold ruby glass. The discovery is normally credited to Johann Kunckel, Andreas Cassius, or Johann Glauber.[16] The colloidal gold in gold ruby glass is about 5-70 nm.[17,18]

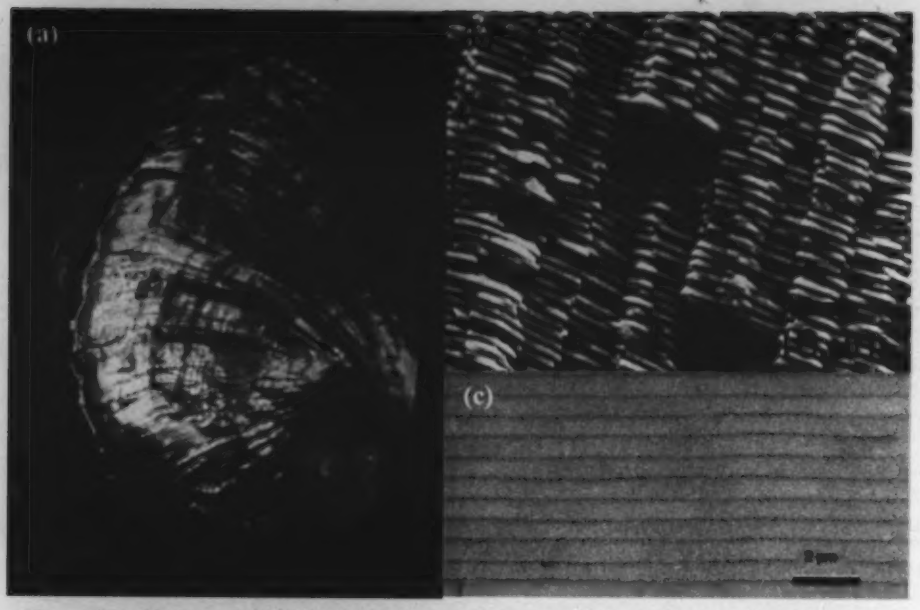

Figure 1.3. Abalone shell. (a) Optical photograph showing iridescence. (b) The calcite crystals are layered and arranged in columns. ((a) and (b) reprinted from reference 14.) (c) The layers of calcium carbonate and protein (darker lines) are clearly shown in this cross-section. (Reprinted from reference 13.)

Though these early glassmakers could not have known how large the colloids were, they were knowingly exploiting the effect of gold powder. The ancient Romans also made gold ruby glass, albeit probably accidentally. One example made by this early civilization is the Lycurgus Cup from the 4th century, shown in Figure 1.4. In reflected light, the cup appears green, but when a light is shone from inside the cup and is transmitted, the cup appears red.[17,18]

1.4.2 Guinier-Preston zones

Property enhancement through manipulation of materials at nanoscale dimensions may be seen in the age-hardening of alloys. Alfred Wilm discovered this phenomenon in 1906.[19] Merica, Waltenberg, and Scott explained it in 1919.[19] In 1938, Guinier and Preston inferred from their X-ray studies that certain tiny structural features were responsible.[20-24] Using modern technology such as transmission electron microscopy and X-ray diffraction, it has been determined that these structural features within alloys of aluminum with 4% copper are disc-like copper precipitates, called Guinier-Preston (GP) zones, that are only a few

atomic planes thick and up to a few tens of nanometres in diameter.[25] They are oriented parallel to the {100} planes of the matrix (see Figure 1.5). As precipitate particles, they block dislocation motion, limiting the plasticity of the metal matrix, thereby hardening the material.

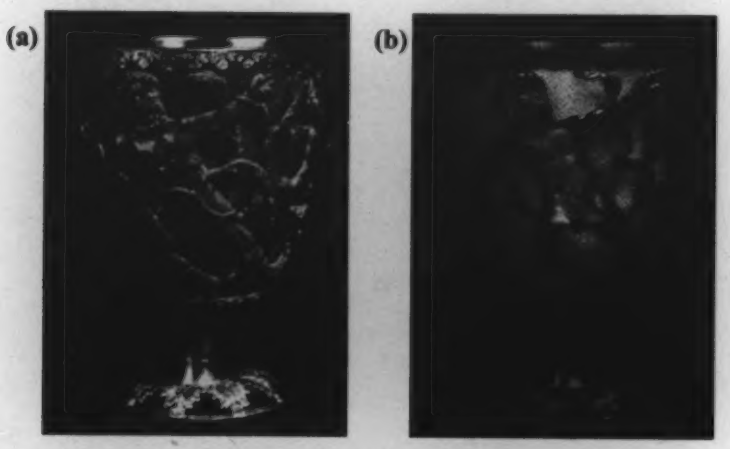

Figure 1.4. Lycurgus Cup. (a) In reflected light, the Cup appears green. (b) The Cup appears red when light is shone from inside. (Reprinted from reference 18.)

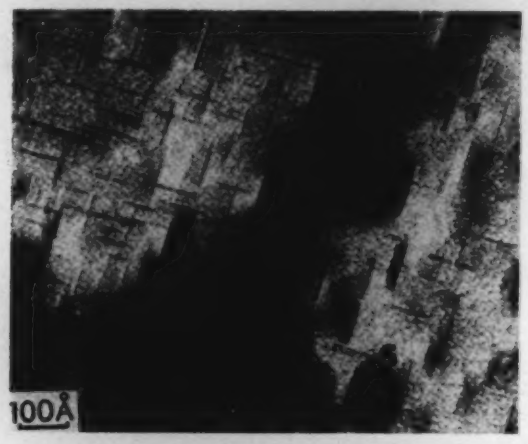

Figure 1.5. Guinier-Preston zones. The matrix is single crystal aluminum with copper impurities. Most of the copper GP zones in the image are perpendicular to the plane of the image and appear as lines of darker contrast. Zones R and S are in the plane of the image and appear as discs. (Reprinted from reference 25.)

1.4.3 Langmuir-Blodgett films

Katharine Blodgett and Irving Langmuir collaborated in the 1930s to develop a technique for depositing successive layers of surfactant-like compounds onto a substrate.[26-28] (A surfactant is a molecule with a polar head and a non-polar organic/carbon-based chain.) A film of the molecule forms on top of a water surface in a trough with a movable barrier (Figure 1.6a). The barrier moves to compress this surface layer (Figure 1.6b). As the substrate is lowered or raised through the water surface at a right angle, a monolayer of the molecule is deposited (Figure 1.6c-e). This process can be repeated thousands of times.[28] Though the technique was developed in the 1930s, it was not until a few decades later that researchers saw its practical applications including optical coatings, electronics coatings, and biological research.[29]

1.5 Modern nano

In the preceding discussion, a few key examples from the vast number of long-known nanostructures were presented. These unique materials and their fascinating properties may have led Feynman to his prophetic vision of

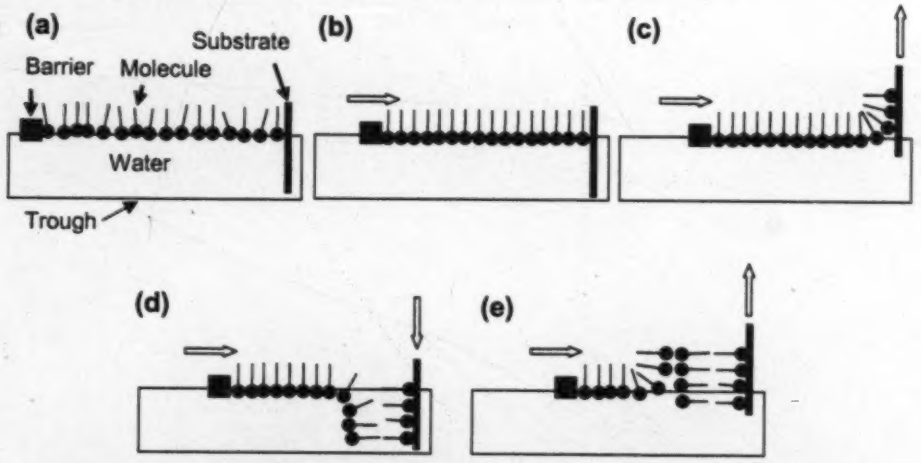

Figure 1.6. Langmuir-Blodgett film technique. (a) The film is spread over the surface of the water. (b) The barrier moves to compress the film. (c) The substrate is moved upwards while the barrier is moved to deposit the first monolayer. (d) The substrate is lowered to deposit a second monolayer in tail-to-tail configuration. (e) The substrate is raised to deposit the third monolayer in head-to-head configuration.

nanoscience and nanotechnology. However, there is another figure who figures prominently in the field of miniaturization; Gordon Moore, co-founder of Intel, made a prediction in 1965 that the number of transistors (per unit square area) on a computer chip would double every year.[30] In that year, there were 64 transistors on a chip. In 1975, he updated his predicted doubling rate to every 2 years.[31] This observation is now known as Moore's Law and it has held true ever since. Later this year, 40 years after his first prediction, Intel will launch a chip that boasts more than 1.7 billion transistors.[31] It is projected that in 2012 that that number will rise to 10 billion.[32] However, we are quickly approaching the fundamental limit of Moore's Law using current microfabrication techniques.

Modern microfabrication facilities utilize a top-down or subtractive approach, that is, silicon (or some other semiconductor) is etched down from bulk sizes.[33] One of the primary limitations in fabrication is the wavelength of radiation used to transfer a mask image onto a silicon wafer. To make smaller features, a smaller wavelength is required. The critical dimension of the features needs to be much larger than the wavelength to avoid diffraction effects. As this wavelength becomes increasingly small, it becomes more and more difficult to reproduce reliable devices as requirements in the optics and alignment systems become more stringent and a different photoresist is needed. In addition, there are device issues facing electronic components of this size. With smaller channel lengths in transistors (the distances electrons travel), subthreshold leakage current becomes significant—essentially, too much current is flowing when the device is in the 'off' state. The oxide necessary to control the switching function of a transistor scales with device size and becomes thinner as well, so gate leakage current presents a major dilemma as the oxide ceases to behave as an electrical insulator. In addition to reliability issues, these leakage currents contribute to power consumption and heat evolution. Furthermore, there is a Moore's Law analogue for cost, commonly known as Moore's Second Law: fabrication costs double every three years, making progress very costly and difficult. With these challenges facing the microelectronics and microfabrication industry, new

approaches to device fabrication must be developed if the industry is to continue advancing in accordance with Moore's Law.

The bottom-up (or additive) approach exploits the chemist's expertise. This approach entails assembling atoms together to make an aggregate: atoms form small building blocks (e.g., molecules), which in turn self-assemble into ordered patterns. Much of modern nanoscience and nanotechnology research is focussed on developing these bottom-up approaches in an effort to overcome the limitations of Moore's Law, besides advancing fundamental understanding out of pure scientific curiosity. In addition to trying to make smaller, faster, more powerful, yet cheaper electronic devices, nano research is also geared towards applications in other fields, such as materials science and engineering and medicine. A few more examples of advances in nano will help to elucidate what the field encompasses and to highlight some of the developments since Feynman's historic talk.

1.5.1 Scanning probe microscopy

Scanning probe microscopy (SPM) is a generic term used for an analytical technique in which a probe tip scans across a surface in raster fashion to produce a two-dimensional image of the surface with respect to some characteristic, for example, topology or magnetic field. The earliest example is the scanning tunnelling microscope (STM), invented in 1981 by Heinrich Rohrer and Gerd Binnig for which they won the 1986 Nobel Prize in Physics.[34-36] A piezoelectric element moves an atomically sharp metal tip (e.g., platinum) across a sample surface while the tip is electrically biased with respect to the surface (Figure 1.7a). A tunnelling current is produced in which electrons travel from the tip to the surface, or vice versa, depending on the bias. The tunnelling current drops off exponentially with tip-sample distance (i. e., the tip and sample are not in physical contact). In essence, the electronic density function is probed with an STM and often correlates to the topology. In addition to its imaging capability down to the atomic level, the STM is used to pick up specific individual atoms and molecules

and drop them off at will by control of the voltage bias (Figure 1.8).[37-39] This is precisely what Feynman had predicted:[1]

> ... I am not afraid to consider the final question as to whether, ultimately—in the great future—we can arrange the atoms the way we want; the very atoms, all the way down!

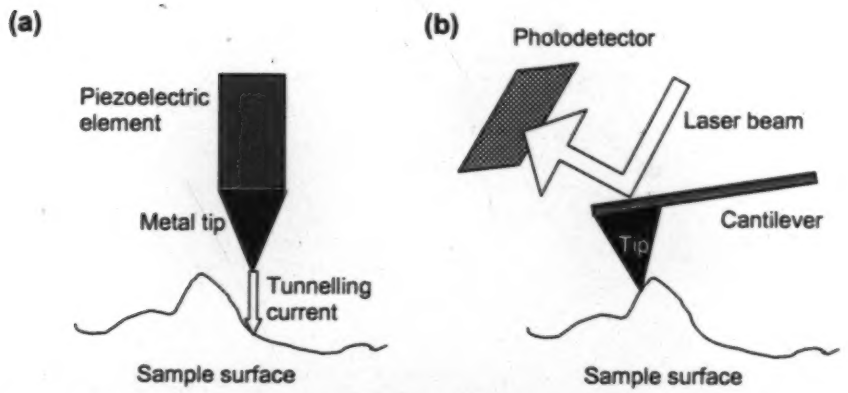

Figure 1.7. Scanning probe microscopy. (a) Scanning tunnelling microscopy. A tunnelling current travels between the tip and surface. (b) Atomic force microscopy (contact mode). The tip follows the surface while a laser beam is reflected off the cantilever onto a photodetector.

Figure 1.8. STM image. Copper atoms were picked up and deposited individually onto an iron (111) surface by an STM and subsequently scanned with the STM. The image reads "atom" in Chinese. (Reprinted from reference 39.)

Another popular scanning probe microscope is the atomic force microscope (AFM), invented in 1986 by Binnig, Quate, and Gerber.[40] A tip on a cantilever is rastered across a surface in order to determine the topology of the surface. In contact mode, wherein the tip is in contact with the sample, the position of a laser beam on a photodetector is determined by the deflection of the cantilever as it follows the surface rising and falling (Figure 1.7b). In non-contact mode, the deflection of the cantilever depends on the van der Waals force between the tip and sample. In tapping (intermittent) mode, the tip is vibrated so that it touches the surface then retracts. The phase difference between the driving force and actual position/direction gives topological information. Other variations include magnetic force microscopy[41] and lateral force (friction) microscopy.[42]

1.5.2 Thiols on gold

Thiols are molecules with a sulphur-hydride (–SH) functionality. They are known to bind to gold (and silver) easily through the sulphur atom with the possible formation of hydrogen (H_2) gas, though the issue of the fate of the hydrogen atoms is still unresolved.[43-47] Organic chains with thiol groups tend to align themselves in a particular fashion, or self-assemble, on gold surfaces, forming what is known as a self-assembled monolayer or SAM (Figure 1.9). (Langmuir-Blodgett films are related to SAMs.) Applications include using the SAM as a form of resist on a substrate and imparting functionality (e.g., hydrophobicity) to a surface.[43,48] We will describe a couple methods in which

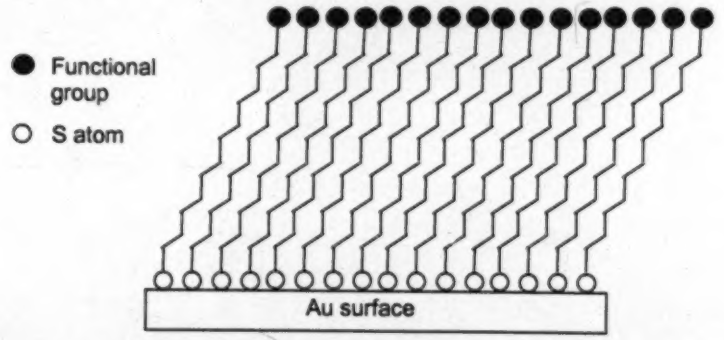

Figure 1.9. Thiols on gold. The organic chains attach by way of the sulphur atom and may have an additional functional group.

thiols are often deposited onto gold. These methods are more widely applicable to a range of surfaces and molecules of compatible chemistry.

1.5.3 Microcontact printing

Rubber-stamping is a very familiar childhood activity. However, stamping features on the nanoscale is not familiar to most people. In microcontact printing (μCP), the polymer of choice for these rubber nanostamps is poly(dimethylsiloxane) (PDMS).[48] Through conventional photolithography, a silicon master is made with the desired relief pattern. The PDMS prepolymer is poured over the master and cured through ultraviolet (UV) light to produce the stamp, which can then be lifted off from the master. Up to about 50 stamps may be replicated on one master. When the stamp is dipped into a molecular 'ink' and subsequently pressed onto a surface, it produces a pattern on the surface. For example, thiols on gold are often patterned in this way. This process is illustrated in Figure 1.10. In contrast to hard lithography, such as photolithography and electron beam lithography, which utilizes hard materials and harmful radiation, this technique is a form of soft lithography, employing 'soft' materials, such as organic molecules and polymers.

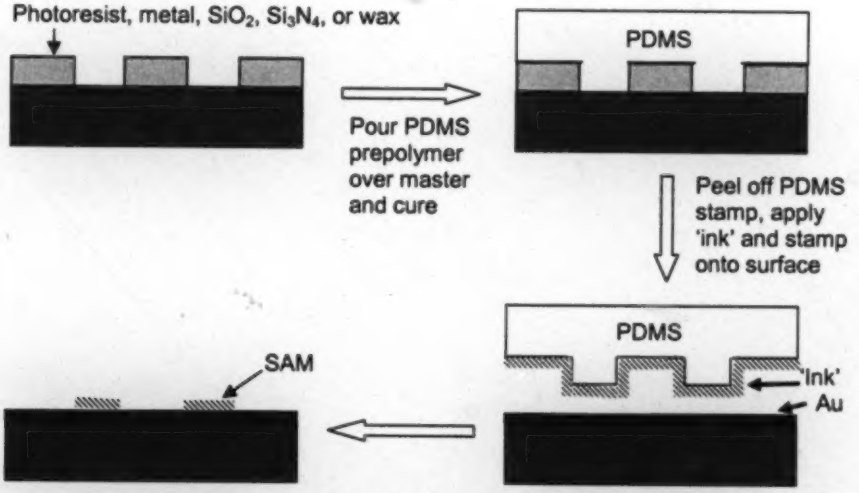

Figure 1.10. Microcontact printing. Schematic illustration of process from making master to patterning surface in desired fashion with molecular 'ink.' (Adapted from reference 48.)

1.5.4 Dip pen nanolithography

With the advent of scanning probe microscopy with nanometre resolution comes the possibility of writing with nanometre resolution—dip pen nanolithography (DPN).[49] Using an AFM, a probe tip ('pen') is dipped into an 'ink' of a molecule and scanned across a surface in order to deposit the molecule through a water meniscus derived from ambient humidity (Figure 1.11). For example, the ink can be a thiol and the surface can be gold. The result is a fine line of thiols that are lined up against each other. In contrast to μCP, which involves a multi-step fabrication process but parallel patterning procedure (many stamps, many features on a stamp), DPN is a very simple but serial writing process. (Serial here means that the pattern is built point by point sequentially as the pen moves.) Because it is sequential, the writing process can be slow; however, this technique allows for greater control and finer features.

1.5.5 Buckminsterfullerene and related structures

The 1996 Nobel laureates in Chemistry, Sir Harold W. Kroto, Richard E. Smalley, and Robert F. Curl, Jr., discovered the C_{60} molecule while performing experiments related to interstellar matter.[50,51] This molecule is named buckminsterfullerene after the architect Richard Buckminster Fuller who designed buildings with related structures. The 7-angstrom 'buckyball' structure is a truncated icosahedron, like a soccerball (Figure 1.12a), consisting of 12 pentagonal and 20 hexagonal faces with 60 equivalent carbon atoms at the

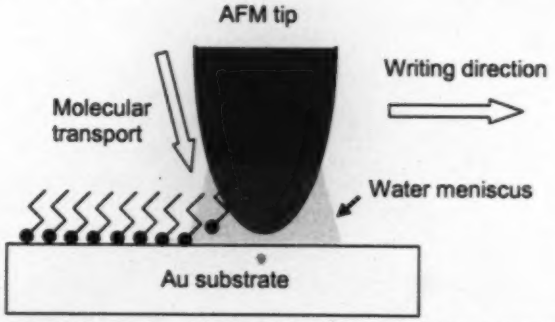

Figure 1.11. Dip pen nanolithography. The AFM tip delivers fine lines of a self-assembled monolayer. (Adapted from reference 49.)

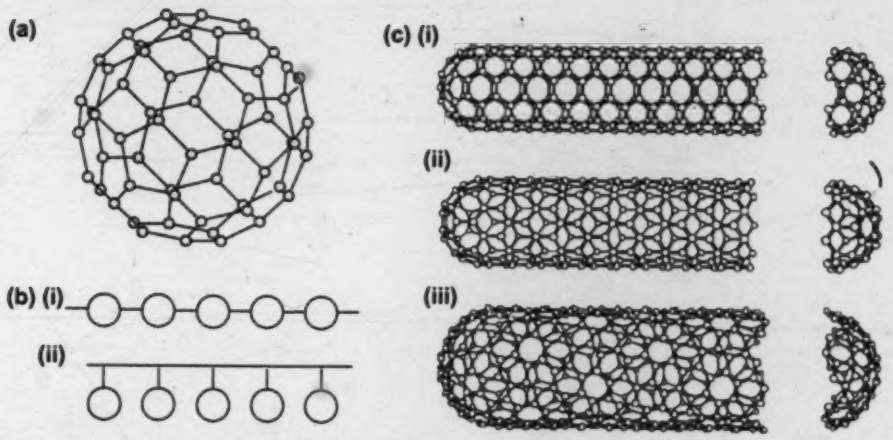

Figure 1.12. Fullerene structures. (a) C_{60}, buckminsterfullerene. (b) Polymers incorporating C_{60} molecules in a pearl necklace-type fashion (i) and pendant necklace-type fashion (ii). (c) Carbon nanotube rolled up in different ways: (i) 'zigzag,' (ii) 'armchair,' (iii) general chirality. ((a) and (c) reprinted from reference 51.)

vertices that are bonded to each other along the 90 edges. Because it has alternating single and double bonds, it is considered a conjugated molecule and has potential applications in molecular electronics. In its face-centred cubic structure, it has a direct bandgap of at least 1.5 eV and may therefore possibly be used in optoelectronic applications. It may be doped with other atoms; for example, when doped with potassium, it forms K_3C_{60} and is superconducting at 19 K. Because of its ability to reversibly accept and donate electrons, it may be used in catalytic applications. It has also been used to cage other atoms. Buckyballs may form the chain in polymeric materials ('pearl necklace', Figure 1.12b(i)) or they may be the functional groups ('pendant necklace', Figure 1.12b(ii)). Other 'fullerene' molecules, such as C_{70}, have been synthesized too.

Another related structure is the carbon nanotube (CNT), or 'buckytube,' discovered by Sumio Iijima in 1991.[51,52] The body of a CNT is a rolled-up graphene sheet and it may be terminated at each end with half of a fullerene (Figure 1.12c). The aspect ratio (length to diameter) can exceed 1000. Because of the high atomic order (few defects) and covalent bonding between the carbon atoms, the CNT exhibits a very high elastic modulus (1 TPa) and a very high ultimate tensile strength (at least 30 GPa),[53,54] higher than those of steel (200 GPa and 1.9 GPa, respectively, for high tensile steel). Because of these mechanical

properties, it is already used in strengthening materials, for example, polyethylene.[54] Depending on its diameter and the way the graphene sheet is rolled up, a CNT can be either metallic or semiconductive.[51] Simple circuits have been assembled, demonstrating possible use in molecular electronics.[55,56] However, much effort is still needed in order to be able to selectively synthesize one type of CNT or the other.[57] The CNT has also been shown to have field-emission properties, useful for display applications.[58]

1.5.6 Quantum Dots

In the section on gold ruby glass, we have mentioned the use of gold, which has its characteristic golden colour in bulk size, a red colour in colloids ~5 nm or larger, and a black colour in colloids ~2 nm. Much like the size dependence of the colour of gold, the photoemissive properties of semiconductor nanoparticles ('quantum dots') also depend on their size. For example, in the macroscale, cadmium selenide (CdSe) emits red light at 716 nm. However, in the mesoscale, cadmium selenide crystallites can emit any colour in the visible spectrum when excited by UV light.[59,60] The emission wavelength is dependent on the crystallite size; as the crystal gets smaller, the wavelength of emission becomes smaller (Figure 1.13). Equivalently, the frequency increases, similar to

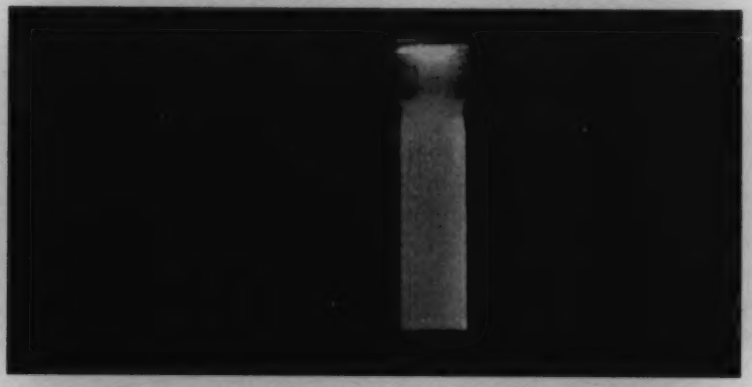

Figure 1.13. Quantum dots. These are colloids of zinc-sulphide-capped cadmium selenide nanocrystals (short form notation: (CdSe)ZnS) dispersed in hexane and illuminated with 365-nm UV light. From left to right, the photoluminescence peaks are located at 470, 480, 520, 560, 594, and 620 nm. The sizes of the CdSe cores increase from about 2 nm to 5.5 nm from left to right. (Reprinted from reference 60.)

how the resonant frequency of a column of air (e. g., in a musical instrument) increases as the length of the column is decreased. The name 'quantum dot' is derived from this quantum size dependence within a 'zero-dimensional' space (dot). Not only can the colour be tuned, but the emission is also very intense and well resolved. Hence, applications of semiconductor quantum dots range from optoelectronics for display and lighting applications to bioassaying to replace fluorescent markers with inferior properties (shorter lifetime, less resolved peaks, less bright).[61,62]

1.5.7 Luminescent silicon

Silicon is a semiconductor with an indirect bandgap, the consequence of which is it normally does not emit light. However, it has been shown that nanocrystalline silicon emits visible light. There are two main forms of luminescent silicon: silicon nanoparticles[63,64] (quantum dots) (Figure 1.14a) and porous silicon, which is a spongy network of nanowires and nanocrystallites produced by etching of a silicon wafer (Figure 1.14b).[65,66] Nanostructured silicon luminesces when UV light is shone on it (photoluminescence),[63-66] when it is electrically stimulated (electroluminescence),[67,68] or when it is reacted with

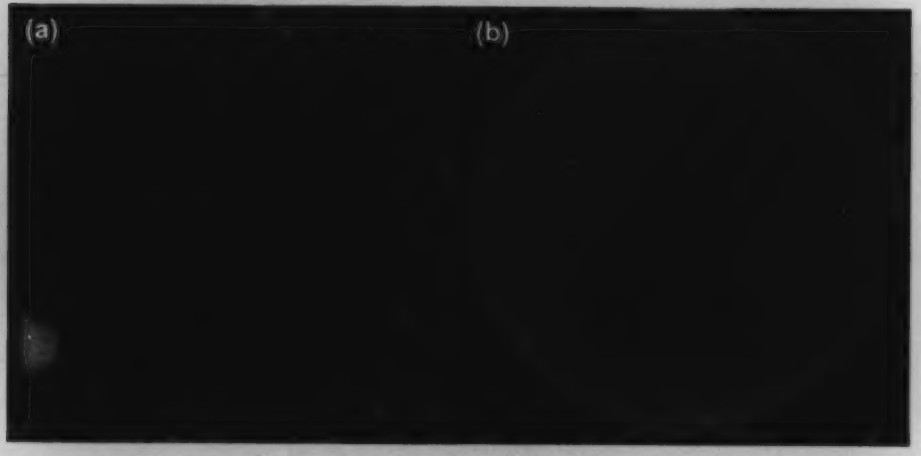

Figure 1.14. Luminescent silicon. (a) Silicon nanoparticles. The hydride-terminated particles are of size 2.1±0.3 nm. The emission peak (735 nm) corresponds to red-near IR. The blue field is due to the UV lamp. (Reprinted from reference 64.) (b) Porous silicon. UV light is shone, enabling red emission. The material was hydride-terminated, with the patterned area further reacted to yield a dodecenyl surface. (Reprinted from reference 66.)

certain chemicals (chemiluminescence).[69,70] The proposed mechanism involves a decrease in the non-radiative electron-hole recombination rate.[71] The exciton (electron-hole pair) is confined to a space with dimensions smaller than the exciton Bohr radius, which is essentially the natural physical separation of an excited electron and its hole in a bulk material. Because of this confinement, it is less likely for the electron-hole pair to be quenched by defects within the crystal. As described in the above section on quantum dots, silicon nanostructures also exhibit size-tuneable luminescence. (The bulk bandgap corresponds to infrared light.) Most preparations result in red-light-emitting silicon; however, other colours, such as blue, have been reported.[72] Nanomaterials that emit light, especially with tuneable luminescence, may be used for lighting and display applications. Porous silicon also has potential to become a sensitive gas sensor for military and safety applications, due to the sensitivity of its optical properties to the chemical environment (see Figure 1.14b).[66,73]

1.5.8 Photonic bandgap materials

In the same way that a semiconductor has an electronic bandgap, an interval of energies that electrons cannot possess, photonic bandgap (PBG) materials, as the name suggests, have a photonic bandgap, an interval of energies that photons cannot possess. PBG materials are made of dielectric materials (e. g., silicon) and have a regular structure, such as periodic pores[74] or an inverted structure of cubic close-packed spheres (the voids between the spheres are filled and the spheres themselves have been etched away, see Figure 1.15).[75,76] When a defect is introduced, such as a missing or enlarged pore (periodic pore structure) or an interstitial defect (inverted packed sphere structure), light within the forbidden energy interval may travel through. PBG materials are being studied for optical computing and telecommunication applications to enable computation and data transfer at the speed of light.

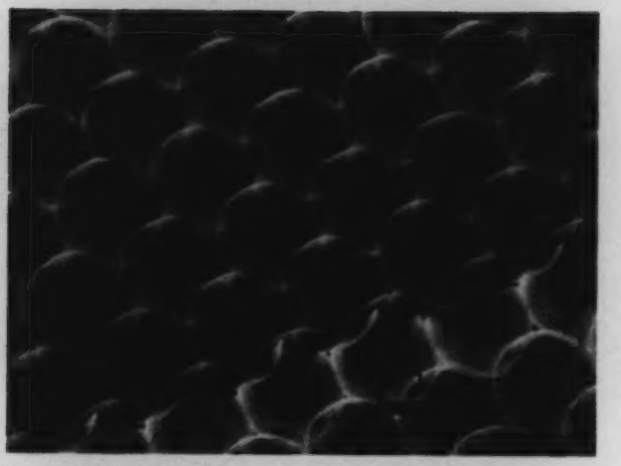

Figure 1.15. Photonic bandgap material. Colloidal silica spheres were self-assembled into a crystal structure. The voids between the spheres were filled with silicon. The spheres were subsequently etched away. The resulting structure shown is called an inverted opal. (Reprinted from reference 75.)

1.5.9 Nanobiology

Above, it was mentioned that nature has been operating on the nanoscale level long before the birth of modern nano research. Some researchers have decided to harness nature's power and combine it with existing synthetic techniques or with other aspects of nano. For example, the complementary base-pairing of deoxyribonucleic acid (DNA) has been used in a technique called orthogonal self-assembly[77] in order to selectively bind nanoparticles to surfaces (Figure 1.16).[78] The surface has a single strand of DNA on it. A nanoparticle tethered with DNA of a complementary base sequence is introduced in the vicinity. Then the DNA attached to the nanoparticle hybridizes to the surface-bound DNA. By detection of the tethered nanoparticle through AFM or scanning electron microscopy, high resolution DNA detection is attained. Orthogonal self-assembly is also amenable to use with quantum dots, which have already been tethered to biological molecules, enabling detection of desired molecules or cells with high, well-resolved photoluminescence signals.[62] This assembling technique offers promise when used in supramolecular assembly of many nanostructures as well.[78]

1.5.10 Biomimetics

Research is also active in biomimetics, the field of building materials, structures, and devices that mimic those found in nature. For example, researchers study the abalone shell and try to design and synthesize an engineering material with similar or better fracture toughness.[79] In addition, by attempting to imitate structures found in nature, new self-assembly routes may be found that will lead to a better understanding of growth mechanisms of the building blocks (e. g., crystals). The structure shown in Figure 1.17 consists of layers of zeolite crystals with polyelectrolyte linker molecules between the

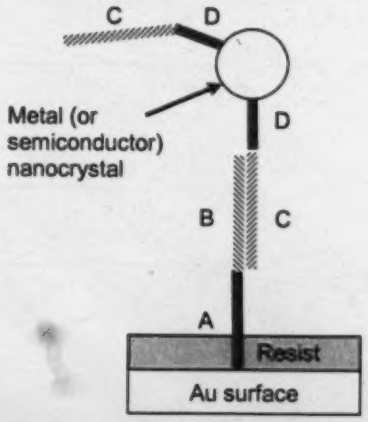

Figure 1.16. Orthogonal self-assembly. The gold surface is patterned with a DNA strand consisting of sequences A and B. A resist layer is used to prevent nanoparticles from adsorbing to the gold through non-specific binding. The nanoparticle is functionalized with DNA strands consisting of sequences C and D. Sequences B and C are complementary and will hybridize, causing nanoparticles to be bound to the surface only where the surface is patterned with A-B DNA strands. (Adapted from reference 78.)

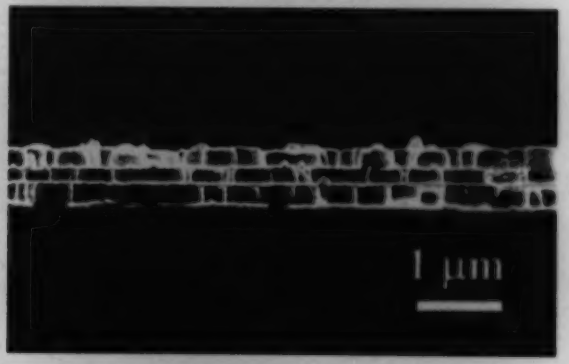

Figure 1.17. Layerered zeolite crystals. The crystals self-assemble onto a glass substrate with polyelectrolyte linkers between the layers. (Reprinted from reference 80.)

layers.[80] The dimensions of this structure are comparable to those found in the abalone shell.

1.6 The future of nano

Top-down approaches are well established within the microelectronics and microfabrication industry. Bottom-up approaches are of very intense interest and are just beginning to be used commercially. For the microelectronics and microfabrication industry, the future of nano likely involves combining the two approaches. Though it may well be that devices on the nanoscale are superior to devices fabricated via top-down approaches, we humans are of the macroscale and live on the macroscale and therefore need the bottom-up devices to be integrated with top-down devices. Because nano is really simply science, it involves workers in all fields of science and engineering, from chemistry to physics to biology to materials science to electrical engineering. In the future, we should expect to see more collaborative efforts and also workers who will be knowledgeable in many 'traditional' disciplines.

1.7 Project motivation and goals

Many of the abovementioned examples of nanoscience and nanotechnology are directly related in some way to the field of electronics and, more specifically, computing or telecommunications. Indeed, a vast amount of the research done in the nano field is geared towards electronics. As stated earlier, it becomes increasingly difficult to fabricate devices of a diminishing size, as everything must be scaled down in the process of miniaturization: channel lengths, gate oxides, and metal interconnects.

Semiconductors have long played a central role in microelectronics due to their intrinsic characteristic of tuneable conductivity. Unlike metals, which have overlapping valence and conduction bands, semiconductors have a bandgap between these two bands. They can be made more conductive by the addition of

dopants that alter their band structure or by application of an electric field, i.e., they can be switched on or off.

Silicon is the primary semiconductor used due to both its passivating oxide and its abundance in the Earth's crust.[33] It is used in a wafer format (relatively large) in integrated circuits. However, as shown in the above discussion on quantum dots and luminescent silicon, semiconductors on the nanoscale exhibit unusual properties. In this project, silicon nanowires are produced in order to access their unique properties. For example, it has been shown that silicon nanowires have a higher carrier mobility than that of planar silicon devices.[81] Furthermore, silicon nanowires can act not only as electronic devices but also as the interconnects between devices. Through simple, versatile chemical reactions (hydrosilylation described in Chapter 2), silicon surfaces may be modified by molecules or polymers with various properties, for example, insulating, conductive, biologically active, and sensing. Through these molecules, silicon nanowires may be covalently attached to a bulk silicon surface to enable integration. This has the advantage that the same chemistry, which has been shown to be effective on bulk silicon surfaces, can be used on both the bulk silicon substrate and the silicon nanowires. After demonstrating that silicon nanowires can be functionalized, it may be possible to develop complex architectures. For example, differently functionalized silicon nanowires may be attached to different regions of the same substrate. It may also be possible to attach nanowires to each other in a controlled fashion using these same molecules. Thus, miniaturization in electronics may be realized through using a technology that is significantly different from the existing top-down approach that is the staple of the microelectronics industry.

Another approach to miniaturization is simply improving the individual components of the transistor or replacing them with something better. For instance, the metal interconnects used in integrated circuits has been replaced from physically vapour-deposited aluminum to electrochemically deposited copper.[82] Though this is a huge improvement, as copper is more electrically conductive than aluminum, there is still room for progress. Narrower metal lines

are more resistive, as the effect of grain boundaries becomes more prominent. More closely spaced lines are also more capacitive. Thus, it would be useful to study how metals deposit onto semiconductors.

Besides silicon, there are other technologically important semiconductors. Both gallium arsenide (GaAs) and indium phosphide (InP) are direct bandgap semiconductors with higher electron mobilities than that of silicon, enabling their use in optoelectronics and wireless communications. The second major focus of this project examines metal deposition on various semiconductors via galvanic displacement, with emphasis on silver (Ag) on gallium arsenide and gold (Au) on indium phosphide. The Ag/GaAs system is particularly studied as it is virtually uncovered by the existing literature. A further advantage of this system is that silver is noble and is the most electrically (and thermally) conductive element. Galvanic displacement is employed because of its simplicity, efficiency, relatively small waste generation, and amenability to different metals and substrates. As shape and size control is important in the synthesis of nanostructures, the deposition studied includes nanostructures of various shapes and sizes. The Ag/GaAs and Au/InP systems may prove to be particularly beneficial if the metal forms adherent bonds to the substrate, as this is a very likely possibility.

1.8 References

(1) Feynman, R. P. *Engineering and Science* **1960**, *23*, 22.

(2) Taniguchi, N. On the Basic Concept of 'Nano-Technology', *Proceedings of the International Conference of Production Engineering*; Japan Society of Precision Engineering: Tokyo, 1974; p. 18.

(3) Drexler, K. E. *Engines of Creation: The Coming Era of Nanotechnology*; Anchor Books: New York, 1986.

(4) "nano-." Merriam-Webster Online Dictionary. http://www.m-w.com (accessed August 2005).

(5) IUPAC. *IUPAC Compendium of Chemical Terminology*, 2nd ed.; McNaught, A. D., Wilkinson, A., Eds.; Royal Society of Chemistry: Cambridge, UK, 1997.

(6) Alivisatos, A. P. *Science* **1996**, *271*, 933.

(7) Campbell, N. A. *Biology*, 3rd ed.; The Benjamin/Cummings Publishing Company, Inc.: Redwood City, CA, 1993.

(8) Banavar, J. R.; Maritan, A.; Rinaldo, A. *Nature* **1999**, *399*, 130.

(9) Wong, T. H.; Gupta, M. C.; Robins, B.; Levendusky, T. L. *Opt. Lett.* **2003**, *28*, 2342.

(10) Vukusic, P.; Sambles, J. R.; Lawrence, C. R.; Wootton, R. J. *Proc. R. Soc. Lond. B* **1999**, *266*, 1403.

(11) Blue Morpho Butterfly, Saint Louis Zoo. http://www.stlzoo.org/animals/abouttheanimals/invertebrates/insects/butterfliesandmoths/bluemorpho.htm (accessed August 2005).

(12) Menig, R.; Meyers, M. H.; Meyers, M. A.; Vecchio, K. S. *Acta Mater.* **2000**, *48*, 2383.

(13) Lin, A.; Meyers, A. *Mat. Sci. Eng. A* **2005**, *390*, 27.

(14) Tan, T. L.; Wong, D.; Lee, P. *Opt. Express* **2004**, *12*, 4847.

(15) Currey, J. D. *Proc. R. Soc. Lond. B* **1977**, *196*, 443.

(16) Bowey, A. M. Gold Ruby Glass Made in Gibraltar. http://www.glass.co.nz/gibruby.htm (accessed August 2005).

(17) Wagner, F. E.; Haslbeck, S.; Stievano, L.; Calogero, S.; Pankhurst, Q. A.; Martinek, K.-P. *Nature* **2000**, *407*, 691.

(18) Department of Scientific Research, The British Museum. The Lycurgus Cup. http://www.thebritishmuseum.ac.uk/science/lycurguscup/sr-lycurgus-p1.html (accessed August 2005).

(19) *Nanostructured Materials: Processing, Properties and Potential Applications*; Koch, C. C., Ed.; Noyes Publications: Norwich, NY, 2002.

(20) Guinier, A. *Nature* **1938**, *142*, 569.

(21) Calvert, J.; Jacquet, P.; Guinier, A. *C. r. hebd. séances Acad. sci.* **1938**, *206*, 1972.

(22) Guinier, A. *C. r. hebd. séances Acad. sci.* **1938**, *206*, 1641.

(23) Preston, G. D. *Nature* **1938**, *142*, 570.

(24) Preston, G. D. *Proc. R. Soc. Lond. A* **1938**, *167*, 526.

(25) Phillips, V. A. *Acta Metall.* **1973**, *21*, 219.

(26) Blodgett, K. B. *J. Am. Chem. Soc.* **1934**, *56*, 495.

(27) Blodgett, K. B. *J. Am. Chem. Soc.* **1935**, *57*, 1007.

(28) Blodgett, K. B.; Langmuir, I. *Phys. Rev.* **1937**, *51*, 964.

(29) Roberts, G. G.; Vincett, R. S.; Barlow, W. A. *Phys. Technol.* **1981**, *12*, 69.

(30) Moore, G. E. *Electronics* **1965**, *38*, 114.

(31) Maney, K. Moore's Law began as guess that grew in power over time. http://www.usatoday.com/tech/columnist/kevinmaney/2005-04-12-maney_x.htm (accessed August 2005).

(32) Service, R. Intel's Breakthrough. http://www.technologyreview.com/articles/05/07/issue/feature_intel.0.asp (accessed August 2005).

(33) Madou, M. J. *Fundamentals of Microfabrication: The Science of Miniaturization*, 2nd ed.; CRC Press: New York, 2002.

(34) Binnig, G.; Rohrer, H.; Gerber, C.; Weibel, E. *Appl. Phys. Lett.* **1982**, *40*, 179.

(35) Binnig, G.; Rohrer, H.; Gerber, C.; Weibel, E. *Phys. Rev. Lett.* **1982**, *49*, 57.

(36) Binnig, G.; Rohrer, H. *IBM J. Res. Dev.* **1986**, *30*, 355.

(37) Eigler, D. M.; Schweizer, E. K. *Nature* **1990**, *344*, 524.

(38) Stroscio, J. A.; Eigler, D. M. *Science* **1991**, *254*, 1319.

(39) IBM. STM Image Gallery. http://www.almaden.ibm.com/vis/stm/atomo.html (accessed August 2005).

(40) Binnig, G.; Quate, C. F.; Gerber, C. *Phys. Rev. Lett.* **1986**, *56*, 930.

(41) Saenz, J. J.; Garcia, N.; Grutter, P.; Meyer, E.; Heinzelmann, H.; Wiesendanger, R.; Rosenthaler, L.; Hidber, H. R. *J. Appl. Phys.* **1987**, *62*, 4293.

(42) Meyer, G.; Amer, N. M. *Appl. Phys. Lett.* **1990**, *57*, 2089.

(43) Bain, C. D.; Whitesides, G. M. *Angew. Chem. Int. Ed. Eng.* **1989**, *28*, 506.

(44) Fenter, P.; Eberhardt, A.; Eisenberger, P. *Science* **1994**, *266*, 1216.

(45) Delamarche, E.; Michel, B.; Kang, H.; Gerber, C. *Langmuir* **1994**, *10*, 4103.

(46) Nuzzo, R. G.; Zegarski, B. R.; Dubois, L. H. *J. Am. Chem. Soc.* **1987**, *109*, 733.

(47) Lee, J.-G.; Lee, J.; Yates, J. T., Jr. *J. Am. Chem. Soc.* **2004**, *126*, 440.

(48) Xia, Y.; Whitesides, G. M. *Angew. Chem. Int. Ed.* **1998**, *37*, 550.

(49) Piner, R. D.; Zhu, J.; Xu, F.; Hong, S.; Mirkin, C. A. *Science* **1999**, *283*, 661.

(50) Kroto, H. W.; Heath, J. R.; O'Brien, S. C.; Curl, R. F.; Smalley, R. E. *Nature* **1985**, *318*, 162.

(51) Dresselhaus, M. S.; Dresselhaus, G.; Eklund, P. C. *Science of Fullerenes and Carbon Nanotubes*; Academic Press: Toronto, 1996.

(52) Iijima, S. *Nature* **1991**, *354*, 56.

(53) Yu, M.-F.; Files, B. S.; Arepalli, S.; Ruoff, R. S. *Phys. Rev. Lett.* **2000**, *84*, 5552.

(54) Srivastava, D.; Wei, C.; Cho, K. *Appl. Mech. Rev.* **2003**, *56*, 215.

(55) Tans, S. J.; Verschueren, A. R. M.; Dekker, C. *Nature* **1998**, *393*, 49.

(56) Bachtold, A.; Hadley, P.; Nakanishi, T.; Dekker, C. *Science* **2001**, *294*, 1317.

(57) Collins, P. G.; Arnold, M. S.; Avouris, P. *Science* **2001**, *292*, 706.

(58) de Heer, W. A.; Chatelain, A.; Ugarte, D. *Science* **1995**, *270*, 1179.

(59) Murray, C. B.; Norris, D. J.; Bawendi, M. G. *J. Am. Chem. Soc.* **1993**, *115*, 8706.

(60) Dabbousi, B. O.; Rodriguez-Viejo, J.; Mikulec, F. V.; Heine, J. R.; Mattoussi, H.; Ober, R.; Jensen, K. F.; Bawendi, M. G. *J. Phys. Chem. B* **1997**, *101*, 9463.

(61) Peng, X.; Manna, L.; Yang, W.; Wickham, J.; Scher, E.; Kadavanich, A.; Alivisatos, A. P. *Nature* **2000**, *404*, 59.

(62) Chan, W. C. W.; Nie, S. *Science* **1998**, *281*, 2016.

(63) Wilson, W. L.; Szajowski, P. F.; Brus, L. E. *Science* **1993**, *262*, 1242.

(64) Hessel, C.; Veinot, J. G. C. *Chem. Mater.*, to be submitted for publication, 2005.

(65) Canham, L. T. *Appl. Phys. Lett.* **1990**, *57*, 1046.

(66) Stewart, M. P.; Buriak, J. M. *Angew. Chem. Int. Ed.* **1998**, *37*, 3257.

(67) Chen, L.-Y.; Chen, W.-H.; Hong, F. C.-N. *Appl. Phys. Lett.* **2005**, *86*, 193506.

(68) Halimaoui, A.; Oules, C.; Bomchil, G.; Bsiesy, A.; Gaspard, F.; Herino, R.; Ligeon, M.; Muller, F. *Appl. Phys. Lett.* **1991**, *59*, 304.

(69) Ding, Z.; Quinn, B. M.; Haram, S. K.; Pell, L. E.; Korgel, B. A.; Bard, A. J. *Science* **2002**, *296*, 1293.

(70) McCord, P.; Yau, S.-L.; Bard, A. J. *Science* **1992**, *257*, 68.

(71) Alivisatos, A. P. *Science* **1996**, *271*, 933.

(72) Belomoin, G.; Therrien, J.; Smith, A.; Rao, S.; Twesten, R. *Appl. Phys. Lett.* **2002**, *80*, 841.

(73) Létant, S. E.; Sailor, M. J. *Adv. Mater.* **2000**, *12*, 355.

(74) Noda, S.; Chutinan, A.; Imada, M. *Nature* **2000**, *407*, 608.

(75) Blanco, A.; Chomski, E.; Grabtchak, S.; Ibisate, M.; John, S.; Leonard, S. W.; Lopez, C.; Meseguer, F.; Miguez, H.; Mondia, J. P.; Ozin, G. A.; Toader, O.; van Driel, H. M. *Nature* **2000**, *405*, 437.

(76) Vlasov, Y. A.; Bo, X.-Z.; Sturm, J. C.; Norris, D. J. *Nature* **2001**, *414*, 289.

(77) Martin, B. R.; Dermody, D. J.; Reiss, B. D.; Fang, M.; Lyon, L. A.; Natan, M. J.; Mallouk, T. E. *Adv. Mater.* **1999**, *11*, 1021.

(78) Schwartz, P. V. *Langmuir* **2001**, *17*, 5971.

(79) Clegg, W. J.; Kendall, K.; Alford, N. M.; Button, T. W.; Birchall, J. D. *Nature* **1990**, *347*, 455.

(80) Lee, G. S.; Lee, Y.-J.; Yoon, K. B. *J. Am. Chem. Soc.* **2001**, *123*, 9769.

(81) Cui, Y.; Zhong, Z.; Wang, D.; Wang, W. U.; Lieber, C. M. *Nano Lett.* **2003**, *3*, 149.

(82) Vereecken, P. M.; Binstead, R. A.; Deligianni, H. Andricacos, P. C. *IBM J. Res. Dev.* **2005**, *49*, 3.

2 Oxide-assisted growth of silicon nanowires

2.1 Introduction

Moore's Law, which states that the number of transistors per unit chip area doubles approximately every 12-24 months, has driven the cost of electronics down exponentially, all the while computing power has exponentially increased.[1] According to the Semiconductor Industry Association (SIA), in 2004, "more transistors were produced—and at a lower cost—than grains of rice."[1] However, this law is based on current silicon microfabrication technology in which large pieces of silicon are etched down, also known as the 'top-down' approach. There is a fundamental limit beyond which the feature size cannot be reduced further without much difficulty and performance deterioration.[2] Analysts predict that this limit may be reached by 2015 or 2020, and therefore reduction of computing cost will no longer offset inflation in other areas, negatively impacting the economy.[1] Thus is the driving force for developing 'bottom-up' approaches in which atoms and molecules are assembled to form small building blocks, which in turn compose larger functional units. The goals of bottom-up approaches are to reduce cost, increase computing power and speed, and increase reliability.

One of the building blocks that researchers are turning to is the silicon nanowire. Silicon is a natural choice since it is a well-established and well-researched material within the semiconductor industry. It is the second most abundant element in the Earth's crust (after oxygen) and has a stable, passivating native oxide layer, unlike the water-soluble oxide of germanium and the 'leaky' oxides of gallium arsenide.[2] As a nanowire, it has the potential to make devices much smaller, all the while it should enable interfacing with bulk silicon surfaces (*vide infra*).

In the current project, the objective of using silicon nanowires was to interface them with bulk silicon surfaces through organic molecules. Silicon nanowires were to be produced via a literature approach. After synthesis, they were to be hydride-terminated through etching with hydrofluoric acid (HF)

(Figure 2.1a).[3] The hydride terminations may be reacted with alkenyl or alkynyl functional groups through hydrosilylation (Figure 2.1b).[3] Through a bisalkene or bisalkyne, the nanowire may be covalently attached to a similarly hydride-terminated then hydrosilylated silicon surface (Figure 2.1c). The silicon-carbon

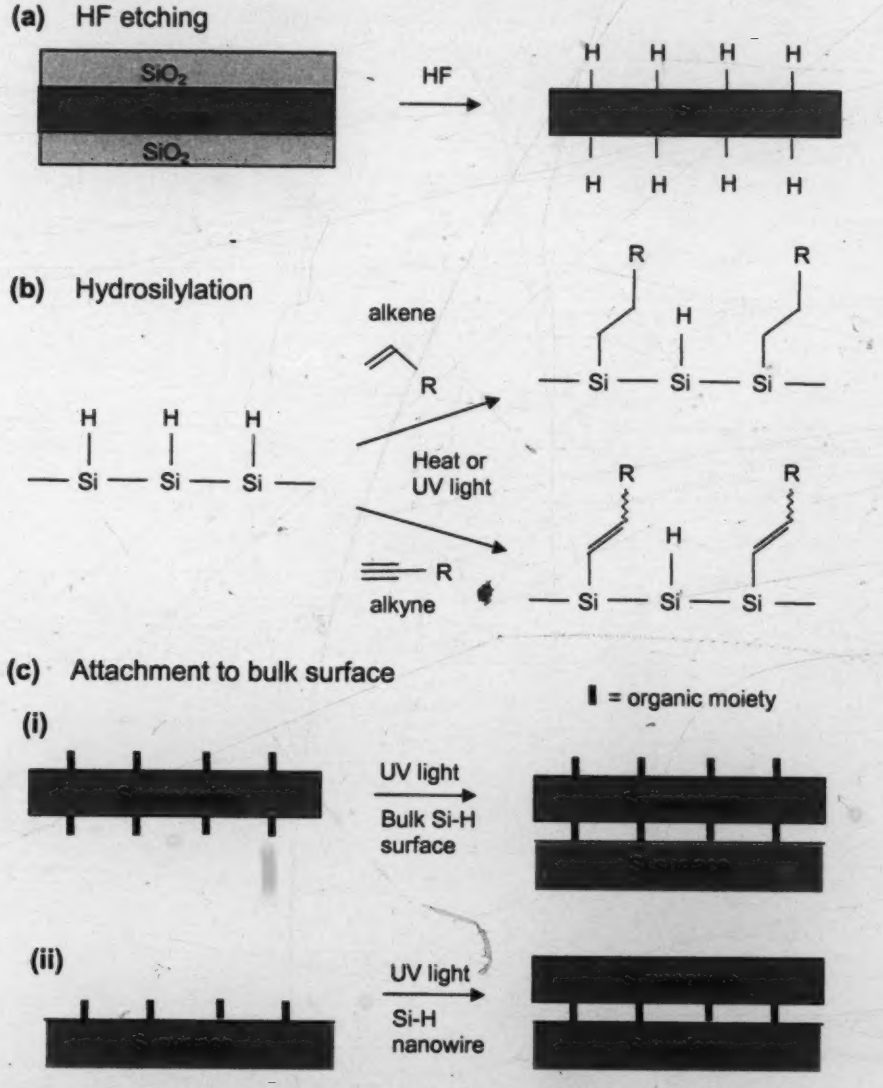

Figure 2.1. Process of attachment of Si nanowires to bulk Si surface. (a) HF-etching of Si nanowire to remove SiO_2, which may be a thin native oxide or a thick sheath, and to hydride-terminate surface. (b) Hydrosilylation with alkene and alkyne to yield alkyl and alkenyl terminations, respectively. (c) (i) Attachment of hydrosilylated Si nanowire to hydride-terminated bulk Si surface. (ii) Attachment of hydride-terminated Si nanowire to hydrosilylated bulk Si surface.

(Si-C) bond has been shown to be very stable,[3] unlike some other bonds proposed to drive molecular electronics.[4] Furthermore, when the reacting functional group is an alkyne, the resulting organic moiety has a double bond (conjugation), potentially enabling electron delocalization and therefore direct electronic communication. Because hydrosilylation is well known for bulk silicon surfaces and the resulting bond is demonstrably strong, we should expect the same for the Si-C bond formed via hydrosilylation on silicon nanowires.

There exists a number of routes to synthesize silicon nanowires, including the vapour-liquid-solid (VLS) method (original and variants),[5-12] lithography and dry etching,[13,14] electrochemical etching,[15,16] scanning tunnelling microscopy (STM),[17] among others.[18-20] In this project, one of the methods employed was the oxide-assisted growth (OAG) method. The OAG method was discovered by Lee and co-workers while trying to prepare silicon nanowires via the VLS growth method.[21-23] In the VLS method, a silicon target mixed with a metal catalyst is heated up such that the metal and silicon form a metal silicide liquid drop.[6] As more silicon is added to the drop, the drop becomes saturated, and, to prevent supersaturation, the silicon precipitates out of the drop. As more and more silicon reagent is added, it continues to precipitate from the drop, causing a nanowire to form.[a] Lee et al. used an iron catalyst and laser ablation to vaporize the silicon-iron target. However, when they looked at their products under the transmission electron microscope, they discovered that the expected drop of metal found at one end of the nanowire, a feature characteristic of the VLS mechanism, was not present.[23,24] Based on this observation, they concluded that a different growth mechanism was responsible for at least some of the nanowires. They had discovered what they dubbed the 'oxide-assisted growth' method and proposed a growth mechanism by which their growth method operated.

It is believed that the mechanism occurs as follows. The reagent consists of silicon monoxide (SiO) powder,[25-39] a mixture of Si and SiO_2

[a] This particular form of the technique is a variant of the original chemical vapour deposition (CVD) technique developed in the 1960's in which a vapour of a silicon-containing compound flowed over a single crystalline silicon substrate with liquid metal droplets.[5] This technique produces epitaxial whiskers. The silicon is originally in vapour form, then forms a metal silicide in liquid form, finally precipitating out as a solid, hence, 'vapour-liquid-solid.'

powder,[23,24,37,40-48] a mixture of SiO_2 and Ge powder,[45] a mixture of SiC and SiO_2,[49] a mixture of Si and Fe_2O_3,[44] or some other powder which when heated or laser-ablated would create a vapour of SiO (see equations below).[45] The vaporization of SiO occurs readily at a temperature of ~1200°C or greater. SiO is an easily oxidizable, quasi-stable substance and not a stoichiometric, saturated compound like SiO_2; it is a kinetic product while SiO_2 is a thermodynamic product. Depending on the actual composition, it may be more accurate to describe it as SiO_x, where the local value of x varies between 1 and 2. After the SiO vapour particles are formed, they are carried downstream to a cooled substrate (ideally ~930-950°C) where the SiO disproportionates into Si and SiO_2.[41,45] The equations that describe the process are as follows.

Formation of SiO vapour (dependent on reagent)

$$\left.\begin{array}{l} SiO(s) \rightarrow SiO(g) \\ Si(s) + SiO_2(s) \rightarrow 2SiO(g) \\ SiO_2(s) + Ge(s) \rightarrow SiO(g) + GeO(g) \\ SiC(s) + SiO_2(s) \rightarrow Si(s) + SiO(g) + CO(g) \\ \vdots \end{array}\right\} \quad (1)$$

Disproportionation

$$2SiO(g) \rightarrow Si(s) + SiO_2(s) \quad (2)$$

The proposed structure formed, based on density-functional theory calculations, is a Si nanocluster covered with a shell of SiO_x; this is the nucleus of a nanowire.[50] When the droplet lands on the substrate, some of the silicon atoms bond to the substrate surface, while the other atoms are open to the flow of reagent particles.[50,51] Due to its high curvature,[b] it is proposed that the shell of SiO_x is in a semi-liquid state, much like how the melting point of a nanocluster decreases

[b] curvature = 1/r, where r = radius of curvature

with nanocluster size.[27] Because of this state, it is more reactive and thus is a preferential site for another droplet to condense. When a new droplet condenses, the silicon of the droplet precipitates onto the original crystalline silicon nucleation site and SiO_2 is expelled to form a stable, protective sheath, preventing lateral growth.[45] Again, the new tip of SiO_x has a high curvature and is reactive. Another droplet condenses and the process repeats itself. As more reagent droplets are deposited, a nanowire grows, consisting of a silicon core and a silicon dioxide shell. This process is illustrated in Figure 2.2. It should also be noted that, at the nanoscale, the interfacial energy of the silicon core/silicon dioxide shell likely plays a role. The {111} and {100} crystal faces of silicon are the most stable planes and are at the surfaces of most of the cores, indicating that the wires grow in the <112> direction.[32,45] The stable silicon oxide shell also prevents lateral growth of the nanowires.[45] There are also numerous crystal defects in the wire and tip, increasing the reactivity of the wire and contributing to the fast growth rate of the nanowires.[45] In addition to nanowires, nanoparticle chains are also often formed. Their formation is dependent on temperature, annealing time, and ambient pressure.[27,28,37] Other products are found in other regions as well, dependent on the substrate temperature.

The basic procedure is to allow heated SiO vapour to flow down a tube onto a surface of cooler temperature. An inert gas (nitrogen, argon, helium) is

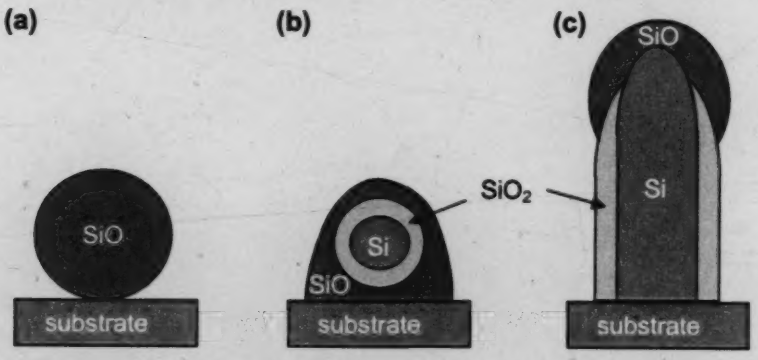

Figure 2.2. Silicon nanowire nucleation and growth process. (a) An amorphous silicon monoxide particle lands on the substrate. (b) Disproportionation occurs to form an amorphous silicon dioxide sheath on a crystalline silicon core. (c) The nanowire forms through continuous deposition of SiO. (Adapted from reference 43.)

used as the carrier gas to transport the reagent particles down to the cool substrate. As stated earlier, a variety of sources, such as SiO powder and Si/SiO_2, can be used, as long as SiO can be produced in vapour form. In cases where the target is a mixture and not pure SiO, laser ablation is used to vaporize the target, while a furnace is used to heat up the substrate. When pure SiO powder is used, laser ablation is not necessary, as a furnace is sufficient to both thermally evaporate the source material and to heat up the substrate.

The general standard procedure outlined above is amenable to modification to grow ultra-fine nanowires in zeolites,[52,53] other structures on the silicon nanowires,[54-62] and hybrid nanowires.[63] Furthermore, the OAG and VLS growth methods may be combined to take advantage of the respective benefits of each method.[64,65]

2.2 Experimental procedure

2.2.1 Materials

Silicon wafers ((100) orientation, n-type, phosphorus-doped, resistivity 0.5-1 Ω·cm) were obtained from Silicon Quest International. Piranha solutions were prepared by mixing sulphuric acid (H_2SO_4) (98%, CMOS grade, J. T. Baker) and hydrogen peroxide (H_2O_2) (30%, J. T. Baker) in a 3:1 volume ratio. Silicon monoxide (SiO) reagent (Goodfellow) was 99.9+% pure with maximum particle size of 45 μm and average particle size of 9.3 μm and was used as supplied. The main impurity was aluminum at 0.08%. Though the purity is stated as 99.9+%, this purity of SiO goes down as it is oxidized when exposed to air, becoming SiO_x.. Etching solutions were prepared from HF (49%, CMOS grade, J. T. Baker) and diluted with 18-MΩ·cm water (Barnstead NANOpure Diamond purifier) or ethanol. All water used for rinsing or diluting was deionized using the aforementioned purifier.

2.2.2 Synthesis of silicon nanowires

Silicon nanowires were synthesized according to a modified literature procedure[30] with the apparatus shown in Figure 2.3. Silicon wafers were cleaved into long rectangular pieces (about 19 mm × 76 mm) and cleaned by rinsing with organic solvent (acetone, pentane) or by standard piranha treatment (mixture as above) at about 80°C followed by rinsing with deionized water. The substrates were then placed inside an aluminum oxide (Al_2O_3, alumina) reaction tube (20-mm inner diameter, 91.4-cm (36") length, supplied by Vesuvius McDanel) with the upstream end of the pieces ~2.5 cm downstream from the centre of the tube. The tube was placed inside a tube furnace of ~41-cm (16") length. Different configurations of the substrates were used and these are illustrated in Figure 2.3. About 0.4 g of silicon monoxide reagent was placed directly in the centre of the tube by a spatula. Purging of the tube to eliminate oxygen proceeded by connecting one end of the alumina tube to an argon gas cylinder and the other end to an oil bubbler through plastic tubing.[c] The argon flow rate varied from ~8-15

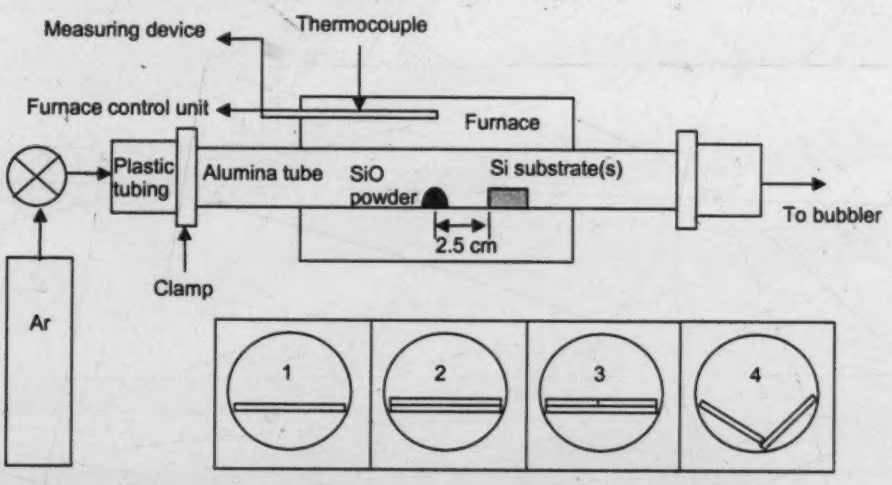

Figure 2.3. Schematic of experimental apparatus. The Type S (platinum-iridium) thermocouple was inserted between the tubular heating element and the alumina tube. Various substrate configurations as seen looking into the tube are shown in the inset. 1: Single substrate. 2: Two stacked substrates of equal size. 3: Similar to 2 but with two smaller substrates on top. 4: Two substrates in a 'V' configuration.

[c] In contrast to the literature procedure, no evacuation of the tube was performed.

standard cubic centimeters per minute (sccm), resulting in a flux of ~2.5-5 sccm/cm^2.[d] After 1-3 hours of purging, the tube furnace began heating up, first by ramping the temperature of the centre of the tube to 800-1050°C at 50C°/min, then by reaching the final temperature of 1300-1430°C at 20C°/min. The furnace could be heated to a maximum of ~1430°C, as at a higher temperature, the native oxide on the silicon carbide heating element would begin desorbing. The furnace was maintained at the final temperature for 3-5 hours with continuous flow of argon before cooling at a rate of 20C°/min until the furnace could not cool any faster than this rate. At room temperature, the products were removed from the tube, followed by characterization or etching.

2.2.3 Etching of silicon nanowires

The following is a summary of the basic procedures used in an attempt to etch the oxide from the products obtained from the vapour-phase synthesis.

(1) The entire substrate was immersed in dilute (1-6%) aqueous HF, followed by dip-rinsing into a series of solvents (water, ethanol, pentane).

(2) Some product was scraped off, placed in a beaker with dilute (1-6%) HF, removed with pipette and placed into various solvents, the last of which was centrifuged to concentrate the product.

(3) Some product was scraped off, crushed, and sonicated in solvent in a microcentrifuge tube, and centrifuged. The supernatant was removed and dilute HF was added and allowed to sit for a few minutes. The vial then went through a series of centrifugations, supernatant removal, and addition of water to remove the HF. The final solvent used to disperse the product was ethanol.

(4) Part of the substrate was placed over a container with 6% aqueous HF or a 1:1 volume mixture of 49% aqueous HF and ethanol in order to allow the HF vapour to etch the product. Due to the nature of the by-products, no rinsing was needed (although ethanol was used sometimes).

---

[d] The experiments performed by Lee et al. employed a tube of inner diameter 50 mm. The flux they used was ~2.5 sccm/cm^2.

2.2.4 Characterization

Nanoscience and nanotechnology require the use of many different types of instrumentation in addition to traditional synthetic apparatus. The following techniques were employed in the current work. The abbreviation used for a characterization method is often used for the instrument as well; for example, SEM may refer to scanning electron microscopy or scanning electron microscope. The particular meaning of the abbreviation in each instance will be obvious from the specific context. We describe briefly each type of analysis to assist the reader before giving details on the actual instrument used.

2.2.4.1 Scanning electron microscopy (SEM)

The scanning electron microscope is an instrument whereby an electron gun emits high energy electrons in a raster fashion to bombard a sample and the subsequently scattered particles/energy is outputted in order to image the sample.

The primary SEM used for the present studies was a Hitachi S-4800, with a resolution down to 1 nm. The as-grown products on their original substrates were characterized in secondary electron detection mode. This instrument is also capable of transmission mode to produce scanning transmission electron microscopy (STEM) images. This mode was used to characterize isolated products dispersed in ethanol or tetrahydrofuran and drop-coated onto carbon-coated copper TEM grids (supplied by SPI). The parameters for both modes are given in Table 2.1.

The other SEM used was a Hitachi S-3000N, a variable-pressure SEM (VP-SEM). Though its resolution is not as fine as that of the S-4800, it is capable of operating within a pressure range of 1-270 Pa., besides high-vacuum mode. The finest resolution on this instrument is 4.5 nm in variable-pressure mode. It was operated in variable-pressure mode to examine some particularly delicate products and the SiO reagent leftover after synthesis. The parameters are given in Table 2.1.

Table 2.1. Parameters used in electron microscopy.

Hitachi S-4800		Hitachi S-3000N		JEOL 2010	
Source	Tungsten cold field emission	Source	Tungsten hairpin filament	Source	Lanthanum hexaboride (LaB_6)
Voltage	5-15 kV	Voltage	5-15 kV	Voltage	200 kV
Working distance	2-15 mm	Working distance	3-8 mm	Camera length	100 cm

2.2.4.2 Transmission electron microscopy (TEM)

The transmission electron microscope is an instrument that, like the SEM, emits high energy electrons to bombard a sample. However, unlike the SEM in which detectors are placed above the sample, the TEM uses a detector below the sample to detect electrons transmitted through the thin sample. Because the sample is thin, there are fewer scattering interactions and a smaller interaction volume of the beam with the sample. Thus, the resolution on a TEM can be much higher than that on an SEM. The TEM can be used in imaging mode to obtain images in real space or in diffraction mode to obtain crystal structure information (selected area electron diffraction or SAED) in reciprocal space.

The TEM used was a JEOL 2010, which is capable of imaging down to a resolution of 2.3 Å and of providing SAED patterns. It was used to characterize products dispersed in ethanol or tetrahydrofuran and drop-coated onto carbon-coated copper TEM grids (SPI). The parameters are listed in Table 2.1.

2.2.4.3 Energy dispersive X-ray spectrometry (EDX/EDS)

The energy dispersive X-ray spectrometer is an instrument which emits high energy electrons at a sample and detects the consequent X-rays dispersed from it. As the electrons collide with the atoms of the sample, the atoms release the excess energy in a number of forms, one of which is X-ray energy. The X-ray energy spectrum of each element is unique. Thus EDX is used to analyze the elemental composition of a sample.

In the present experiments, the EDX system was integrated with the Hitachi S-4800. Because the SEM already has an electron source, there is no need for the EDX system to have one of its own and thus the additional instrumentation included an X-ray detector only. The detector was an Oxford Instruments Inca x-sight. The voltage and working distance were 15 kV and 15 mm, respectively. The resolution was 1 μm.

2.2.4.4 X-ray diffraction (XRD)

The X-ray diffractometer is an instrument which emits X-rays from a source (such as copper metal). The X-rays diffract off of the crystal planes of a material to allow investigation of the crystalline nature of a substance.

The powder X-ray diffractometers used were the Bruker AXS D8 Discover and an Inel XRG 3000. The radiation wavelengths were those of copper Kα (λ=1.54184 Å) and copper Kα_1 (λ=1.54056 Å), respectively.

2.2.4.5 Fourier-transform infrared spectrometry (FTIR)

The Fourier-transform infrared spectrometer is an instrument which emits infrared radiation at a sample, then detects behind the sample which frequencies were transmitted through the sample in order to gain chemical bonding information.

FTIR spectra of etched products were obtained using a Nicolet Nexus 670. The detector used was deuterated triglycine sulphate/KBr. In addition to the usual transmission mode, diffuse reflectance mode was also employed with the DRIFTS (Diffuse Reflectance Infrared Fourier Transform Spectroscopy) attachment.

2.2.4.6 Fluorometry/Photoluminescence (PL)

The fluorometer or spectrophotometer is an instrument that can emit radiation at a range of frequencies and measure the frequencies at which a sample photoluminesces.

Some products were isolated and dispersed in dry tetrahydrofuran (PureSolv) and examined for photoluminescence with a CARY Eclipse Fluorescence Spectrophotometer equipped with a xenon flash lamp and an emission monochromator with a wavelength range of 190-900 nm. Products on the original substrate were analyzed with the same instrument. In addition, an ultraviolet (UV) lamp was used to shine light at 365 and 254 nm on some as-grown samples for visual inspection.

2.3 Results

2.3.1 As-grown products

Fine nanowires form within a specific temperature range (*vide infra*), outside of which other products are formed. Product morphology is largely dependent upon deposition temperature. Photographs of typical products are shown in Figure 2.4a, b. Note that there is usually a lot more product on the top exposed surface than on the bottom. For comparison, products from reference 30 of Lee et al. are shown and described. Where the products are similar, it is probable that a similar growth mechanism is operative as well. They identify zones within the deposition profile that can be differentiated with the naked eye. There is a close correspondence of the products obtained here to those reported by them. For consistency and ease of comparison, labels used here will correspond to those used in the literature, with the letter L denoting the corresponding zones in the products of reference 30. For example, Zone II refers to a zone in the current work and Zone LII to the corresponding zone in reference 30. A schematic is shown in Figure 2.4c to illustrate the locations and lengths of corresponding literature zones if they were scaled down to a comparative length scale of the current products.

It should be noted that because of the differences in the experimental design (i. e., tube, tube furnace, evacuation, etc.), exact zone correspondence to reference 30 was not possible. Furthermore, products exhibited variations from run to run, as was noted by others as well.[27,30] It is likely that in order to obtain

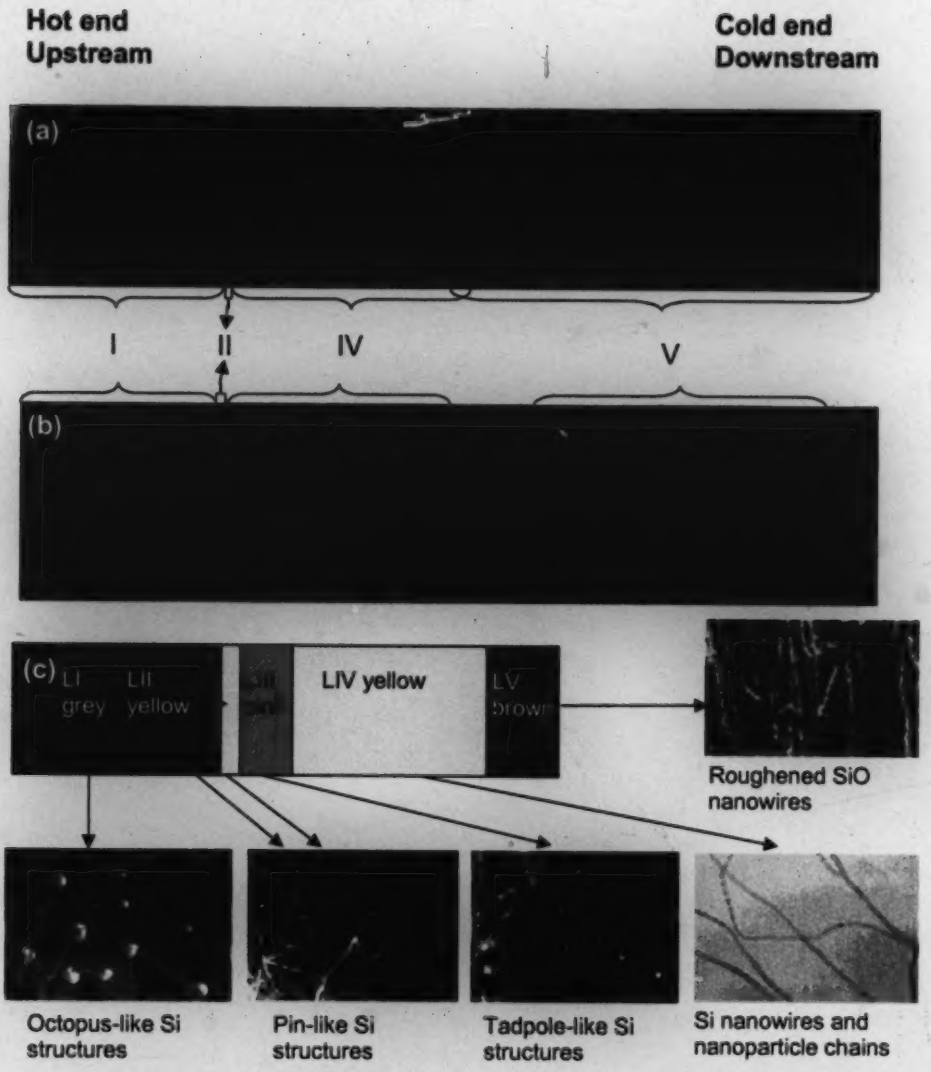

Figure 2.4. Macroscopic products. Optical photographs of (a) the top exposed surface and (b) the bottom exposed surface of different substrates. The bottom typically has less product deposition. The approximate locations of the different zones are shown. (c) Schematic showing the colours and relative lengths of the different zones in reference 30, scaled down so that the positions of the zones match those obtained with the current work. The electron micrographs, taken from reference 30, are representative of what can be found in each zone.

exactly the same products as those in reference 30, a shallower temperature gradient may be needed, as well as a slower heating rate.

As a result of the temperature gradient along the substrate during growth, except for Zone II, the boundaries of the different zones are not well defined.

Even under the SEM, though Zone II has a clear boundary, the dominant product found there may also be found in the surrounding zones; likewise, products found primarily in other zones may also be found in Zone II or other zones. Besides a spatial temperature gradient along the substrate, there is also a temporal thermal gradient experienced during heating and cooling. This effect may be responsible for the secondary products found in the different zones. The present discussion will point out both the dominant and minor products. Unless otherwise specified, images (including those from reference 30) are micrographs taken using the SEM.

2.3.1.1 Zone I

Zone I looks macroscopically similar to Zone LI. It is a grey-brown colour with some yellow, while Zone LI is described as dark grey.[30] This region extends 15-20 mm, from an area of estimated temperature 1350°C to one of 1250°C, measured with a thermocouple. This range agrees with the literature measurement of 1320°C to 1250°C for Zone LI. The texture of Zone I is bumpy due to clumps. At the downstream end of Zone I, the clumps become more yellow. Electron micrographs of structures found in Zones I and LI are shown in Figure 2.5. SEM reveals that these clumps consist of octopus-like structures (spheres with multiple tapered nanowires) at the upstream end of Zone I and pin-like structures (spheres with single tapered nanowires) in the downstream region. These products are the dominant structures. They have spheres (or tips) ranging from about 500 nm to 10 μm in diameter and attached wires that are 150 nm to 1 μm in diameter at the attachment point (base). The average and maximum diameters of these structures become smaller as the temperature decreases (farther downstream). These diameters roughly agree with those reported in the literature.[30] Exposed lengths of some wires are up to 50 μm and it is reasonable that some wires are much longer. At the upstream end of this zone, the octopus-like structures give rise to related irregularly shaped morphologies, such as the flower-like structure in Figure 2.5d. Some nanowires, 20-200 nm in diameter, are also found, growing out of the tips of the octopus- and pin-like structures. The

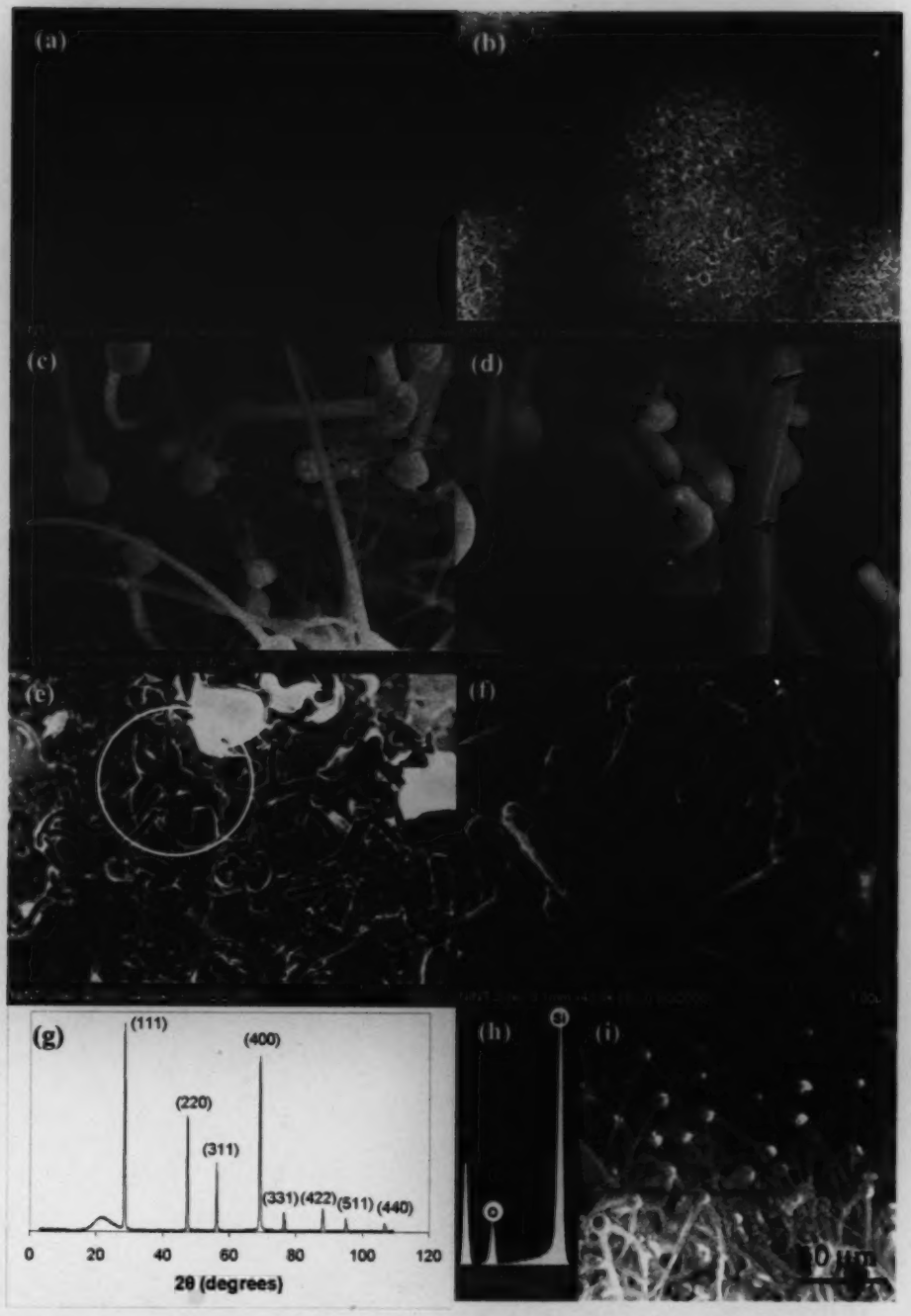

Figure 2.5. Zone I products. (a) and (b) Clumps at different magnifications. (c) Octopus- and pin-like structures and fine nanowires. (d) Disordered flower-like structure. The arrows point to bifurcation and coalescence. (e) Other disordered structures. The circled structure has wires seamlessly fused to it. (f) Short bars. (g) XRD spectrum. (h) EDX spectrum. (i) Octopus- and pin-like structures and nanowires (background) from reference 30.

existence of these nanowires was reported previously.[30] There seems to be some other structures which Lee et al. label 'short bars' but which they found in Zone LII. However, it is not unreasonable to find these structures in Zone I due to the temperature gradient, both spatially and temporally. The XRD spectrum consists of well-defined peaks, showing that Zone I is polycrystalline silicon with no grain texture (no preferential orientation of crystals). The polycrystallinity is due to the many silicon structures that are likely single crystalline, either in whole or at least in its individual constituents of tips and wires (TEM SAED was performed on similar structures in Zone II and showed that tips and probably wires are single crystalline.) Although the nanowires may grow in a preferential crystal direction, the orientation of individual structures with respect to each other is random. All of these structures are made of silicon and oxygen, as shown by EDX. The oxygen appears in the EDX spectrum probably due to the amorphous SiO_x sheath on the structures. EDX performed on the 'edge' and 'centre' of a wire in the TEM shows a higher amount of oxygen in the edge. XRD shows a peak that appears to arise from an amorphous phase. A TEM image of a similar structure in Zone II (*vide infra*) shows a thin sheath on a crystalline core.

In some samples, there are also a few structures in Zone I and Zone III/IV with metallic elements appearing in the EDX spectrum. These structures appear to be nanowires grown through the VLS mechanism, as metal is found in the tip. A handful of structures like the one shown in Figure 2.6 contain copper, apparently in a round tip raised above a rectangular base. Traces of iron, aluminum, and calcium are found in another sample. These structures are found in areas that had structures grown through the OAG mechanism as well.

2.3.1.2 Zone II

Zone II is the narrowest zone, yet it appears to be the densest zone with respect to amount of product. The product grew around a temperature of 1250°C, while Zone LII grew in a region from 1250°C to 1230°C.[30] Nanostructures form a yellow ridge-like structure in this area, with a height up to 5 mm and a width of

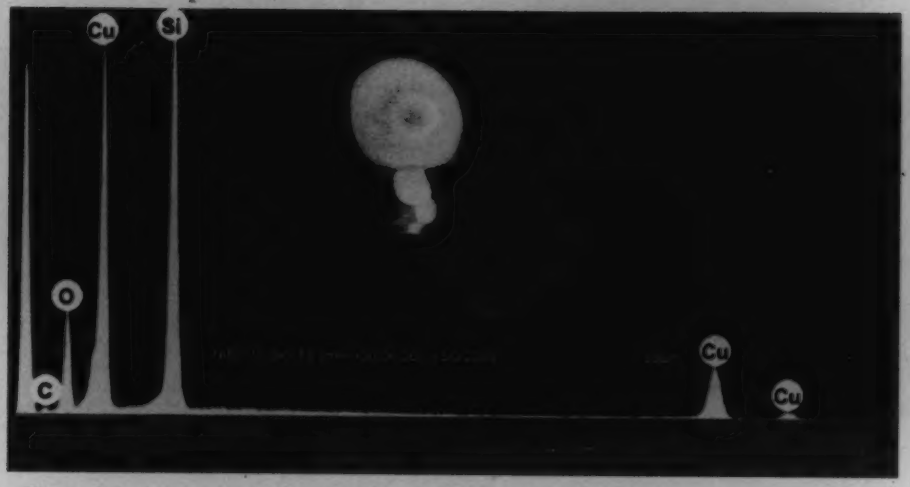

Figure 2.6. Copper-containing structure. SEM image and EDX spectrum of structure found in Zone I containing copper. The carbon comes from post-synthesis surface contamination.

~0.5-1 mm (length of zone down tube axis). This structure forms a ring within the inner circumference of the alumina tube. Nanostructures from this zone are shown in Figure 2.7 and are consistent with literature results.[30] The morphology of the structures in Zone II is similar to that of Zone I in its most downstream region, that is, pin-like structures (with some octopus-like structures) in the size range of 100-500 nm for the tips and 50-300 nm for the base of the nanowires. Similar to Zone I, the nanowires are up to at least 50 μm in length. There are also 30-50-nm diameter nanowires and/or nanoparticle chains among the pin-like structures. Some structures seem to have been converting into the short bar structure that was present in Zone I. Lee et al. do not report the thin nanowires in Zone LII, however, they mention that in the cross-section there are sintered nanoparticle chains and short bars believed to form with extended heating.[30] Though a study was not conducted in the present work on the cross-section of the ridge, electron micrographs were taken of the substrate at points where the ridge broke off and only the pin-like structures were observed. TEM SAED shows that the tips are single crystalline silicon. The SAED for a wire (not shown) shows spots with weaker intensity and possibly polycrystallinity, though the polycrystallinity may arise from both the wire and a tip contributing to the pattern. XRD confirms that Zone II is made of polycrystalline silicon with no texture. EDX confirms the presence of silicon and oxygen only.

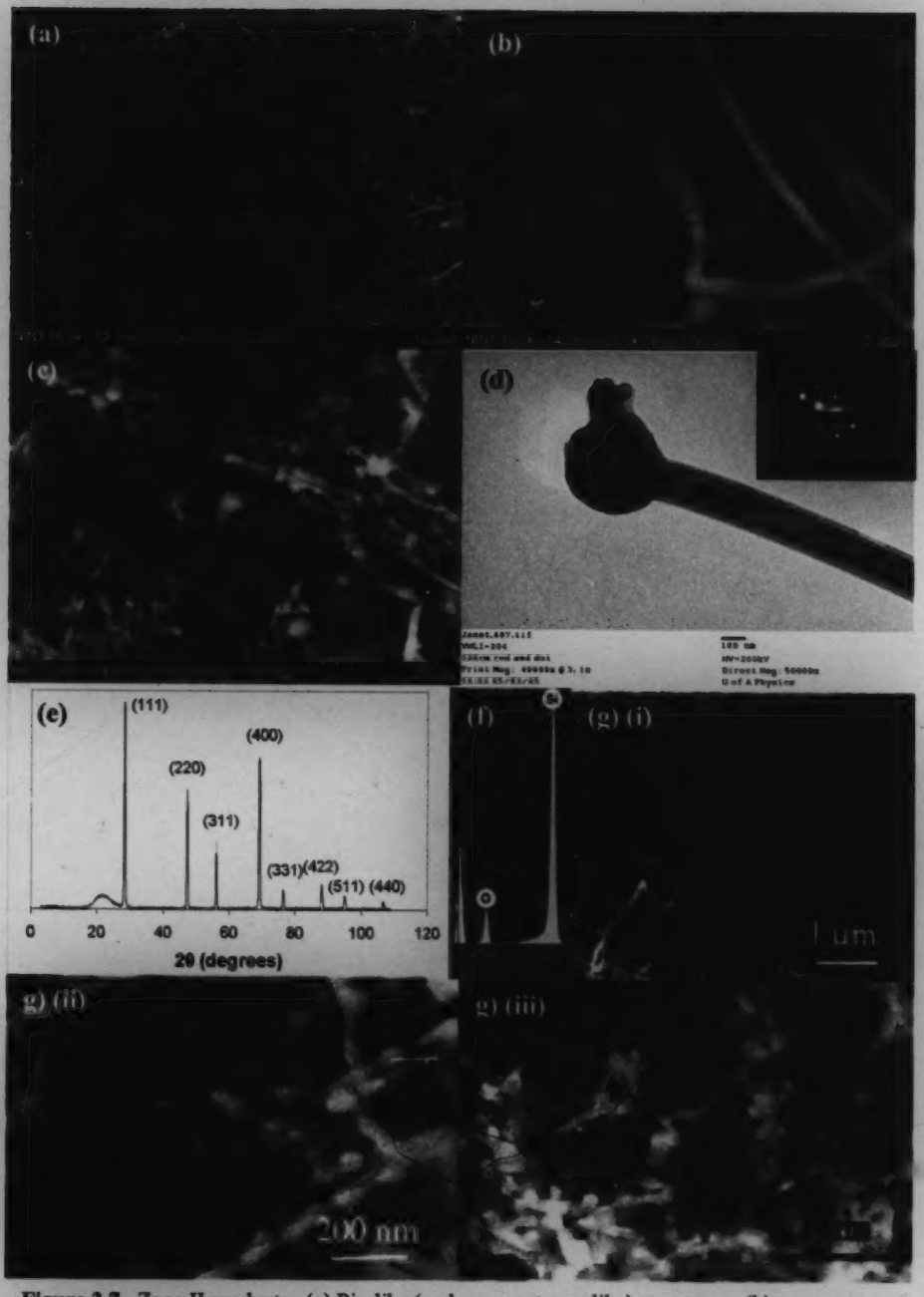

Figure 2.7. Zone II products. (a) Pin-like (and some octopus-like) structures. (b) Nanowires/nanoparticle chains among pin-like structures. (c) Structures converting into short bars. (d) TEM image of pin-like structure showing core-shell structure. Inset is SAED showing tip to be single crystalline (zone axis [111]). (e) XRD spectrum. (f) EDX spectrum. (g) Zone LII products from reference 30. (i) Pin-like structures. (ii) Sintered nanoparticle chains. (iii) Short bars.

2.3.1.3 Zone III

Unlike in literature reports, Zone III cannot be visually distinguished. Lee et al. indicate Zone LIII consists of yellow and pink lines perpendicular to the tube axis grown in a region from 1230°C to 1180°C.[30] The yellow portion is made up of the pin-like structures and the pink of tadpole-like structures. Measurements of their structures reveal that the tadpole-like structures are smaller in diameter than the pin-like structures. Since smaller objects reflect light of smaller wavelength, this would account for the different colours for the different structures present. In the present case, Zone III seems to consist of patches of pin-like structures, blended in with Zone IV, which is composed of nanowires and nanoparticle chains, as shown in Figure 2.8. The tips of the pin-like structures are 50-100 nm in diameter and wire bases are 30-60 nm wide, similar to the smallest pin-like structures in Zone II; Zone III can therefore be seen as an extension of Zone II. Tadpole-like structures are found in one sample that was heated at a lower temperature (~1000°C) for a while (~2 h) before the temperature was finally raised to ~1430°C; however, these were found in Zone I, a more upstream area. These 'tadpoles' have head diameters of 50-200 nm, tail diameters of 30-150 nm at the base, and tail lengths of 500 nm to 4 μm. The dimensions of the tadpole-like structures in Zone LIII are in the lower end of these ranges. Because of the dimensions of Zone III structures, EDX analysis could not be performed on the structures alone. However, previous literature reports indicate that the heads are crystalline silicon with an amorphous silicon oxide sheath, while the tails can be either amorphous silicon oxide or crystalline silicon sheathed with amorphous silicon oxide.

2.3.1.4 Zone IV

Zone IV continues from Zone II, is blended with Zone III, and extends to where the substrate is probably about 1050°C. The material in this zone is characterized by a very thin, delicate, pale yellow, wispy or veil-like appearance. If thin enough and is not a loose mass over the substrate, then over the reflective

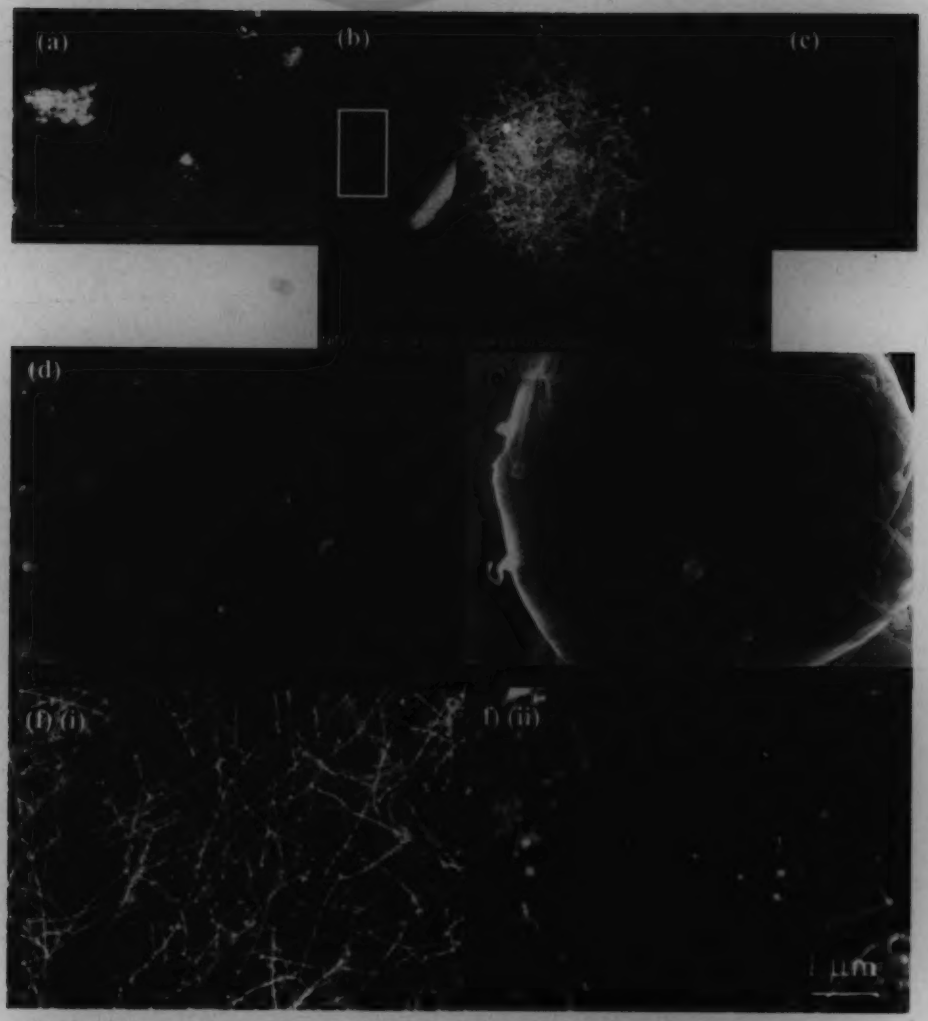

Figure 2.8. Zone III products. (a) Patches of pin-like structures among nanowires and nanoparticle chains. (b) Patch of pin-like structures. (c) Close-up of boxed section in (b). (d) Pin-like structures from experiment in which temperature was held at lower temperature first. Note that the tips start off as smaller particles on the substrate. (e) Tadpole-like structures on the tip of an octopus-like structure in Zone I of said experiment. (f) Zone LIII products in reference 30. (i) Pin-like structures. (ii) Tadpole-like structures.

silicon substrate, it may appear bluish, though the actual material is still yellow (compare (a) and (b) in Figure 2.4). It is reported in the literature that Zone LIV extends from where the substrate is 1180°C to 930°C and consists of a somewhat similar macroscopic product.[30] As stated earlier, the product in Zone IV consists of nanowires and nanoparticle chains, which are aligned in the direction of the gas flow (see Figure 2.9). The diameter of these wires and chains is 10-40 nm,

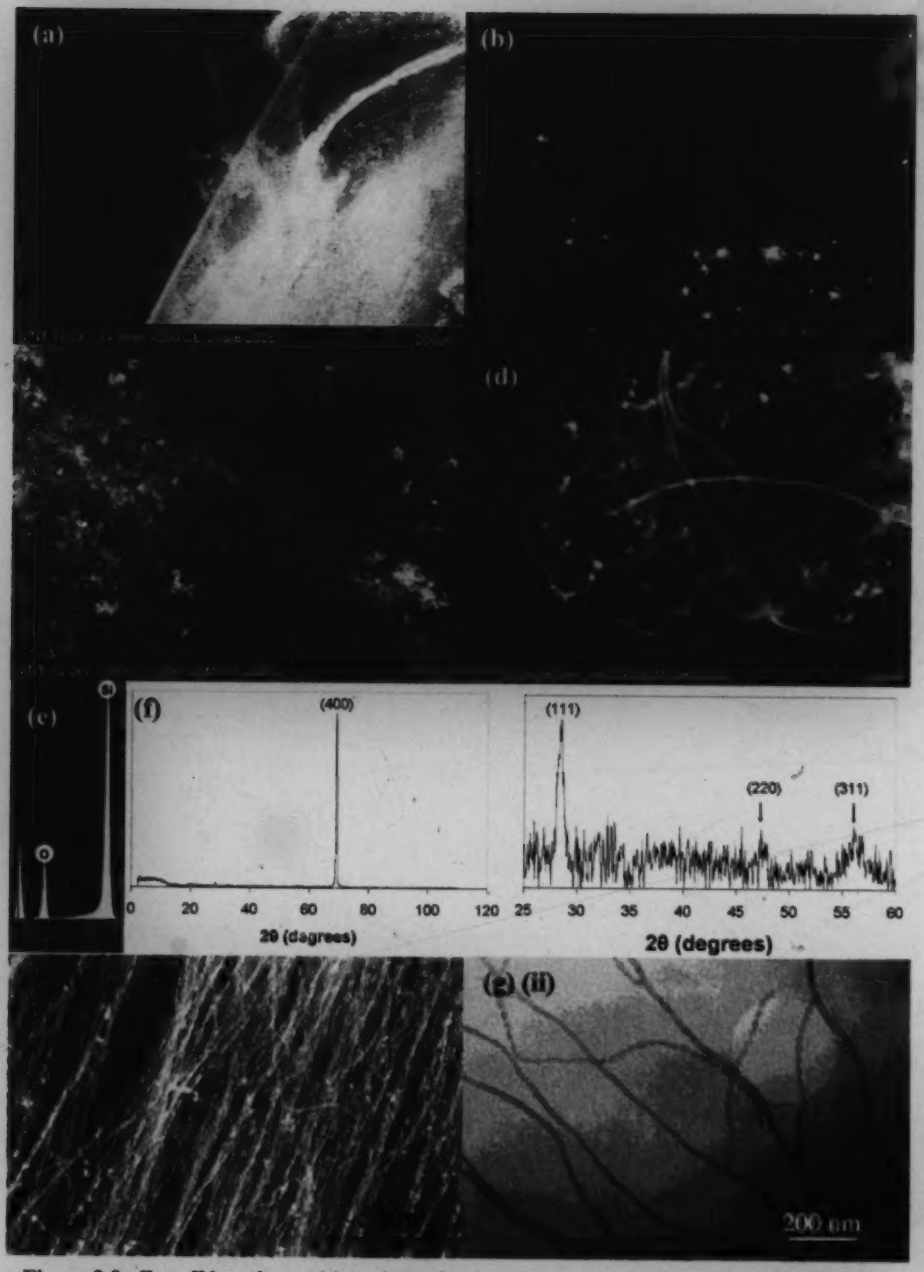

Figure 2.9. Zone IV products. (a) A piece of carbon tape was pressed onto the substrate and viewed under the SEM. Part of the delicate film can be seen to float around. (b) Aligned bundles of the nanowires and nanoparticle chains. (c) SEM image at a higher magnification. (d) Individual smooth nanowires and nanoparticle chains. (e) EDX spectrum. (f) XRD spectrum with close-up of visible peaks (the (400) peak is due to the substrate). (g) Zone LIV products from reference 30. (i) Aligned products. (ii) TEM image of individual nanowires and nanoparticle chains.

similar to that seen in Zone LIV (20-30 nm). The estimated length of these wires and chains may be in the millimetre range. Even though XRD shows only the strongest reflections of silicon due to the small amount of material on the substrate, it shows that it is indeed polycrystalline silicon. EDX shows that only silicon and oxygen are present. We may infer from this data and from the work of others[30] that the structures have a crystalline silicon core sheathed with amorphous silicon oxide, likely a mixture of nanowires and nanoparticle chains. The nanowires are crystalline silicon with an amorphous silicon oxide sheath, while the nanoparticle chains are crystalline silicon nanoparticles that are sheathed with and connected to each other with silicon oxide. It is also very reasonable to assume that there are also bulbous nanowires, nanowires that are in the process of converting into nanoparticle chains, as will be described in the Discussion section. Although literature reports state that nanowires are more dominant towards the lower temperature end of this region and nanoparticle chains towards the higher temperature end,[27] this is not noticeable here. However, towards the cooler end of Zone IV, the product appears roughened, as Zone V products begin to appear (*vide infra*). This roughening may conceal any difference in the dominance of one type of product over the other, since the degree of roughening is severe, thus masking an otherwise smooth or bulbous texture (for nanowires and nanoparticle chains, respectively).

2.3.1.5 Zone V

Zone V is the region where the lowest temperature of deposition occurred, between 1050°C to about 800°C. The temperature range reported for Zone LV is 930°C to 890°C, which is considerably narrower.[30] Upon visual inspection of Zone V, the product appears to be a spongy, caked-on, yellow to brown mass, becoming darker towards the downstream. There is no sharp transition from Zone IV to Zone V. The temperature ranges are given only as a very rough estimation of where a zone may begin or end. Sometimes, a thin yellow 'veil' similar to that seen for Zone IV is present on top of the spongy mass. Though the brown colour

was reported previously, the estimated temperature range is higher than that found in the literature.[30] SEM analysis indicates the veil consists of nanowires (with possibly nanoparticle chains) with a roughened, sometimes almost dendritic, texture (Figure 2.10). These wires are 20-1000 nm in diameter and the average diameter increases downstream. The caked-on mass is a porous, spongy, clustery material grown on top of thick silicon oxide (shown through rings of various colours seen by the naked eye). The mass seems to have grown where the oxide is thickest (few hundred nanometres), as there is a ring of a single colour around the yellow mass (same thickness of oxide at periphery).[e] SEM reveals that the roughening and sponginess become more severe downstream. The spongy material and nanowires appear to consist of chunks adorned with tiny features down to 5 nm (see Figure 2.10d). EDX shows only silicon and oxygen present. XRD reveals the presence of polycrystalline silicon (with no texture) with broad peaks and a large hump due to an amorphous phase. TEM SAED (not shown) confirms low crystallinity. Previous literature reports both the existence of the spongy cluster deposition and aligned, roughened nanowires that widen downstream from about 50 nm to 5 μm as the products become darker in colour.[30,43,44] Based on the similarities of the present products with those previously reported, it is reasonable that the material (spongy deposition and nanowires) found in Zone V is SiO, with traces of crystalline silicon nanoclusters and/or the nanowires and nanoparticle chains from Zone IV, which would also be roughened like that of the pure SiO nanowires. Figure 2.10 shows the nanowires and spongy product as merely two extremes of the same material, since the spongy material often contains short wire-like sections.

2.3.2 Etching of silicon nanowires

Chemical etching of the present nanomaterials proved to be challenging. One successful attempt occurred when an entire substrate was immersed in 5% HF, according to etching procedure (1). Some of the nanowire/nanoparticle chain

[e] The thickness of silicon dioxide can be estimated by its colour when the thickness is at least ~50 nm. Ellipsometry proved to be unreliable as there was some spongy deposition on top.

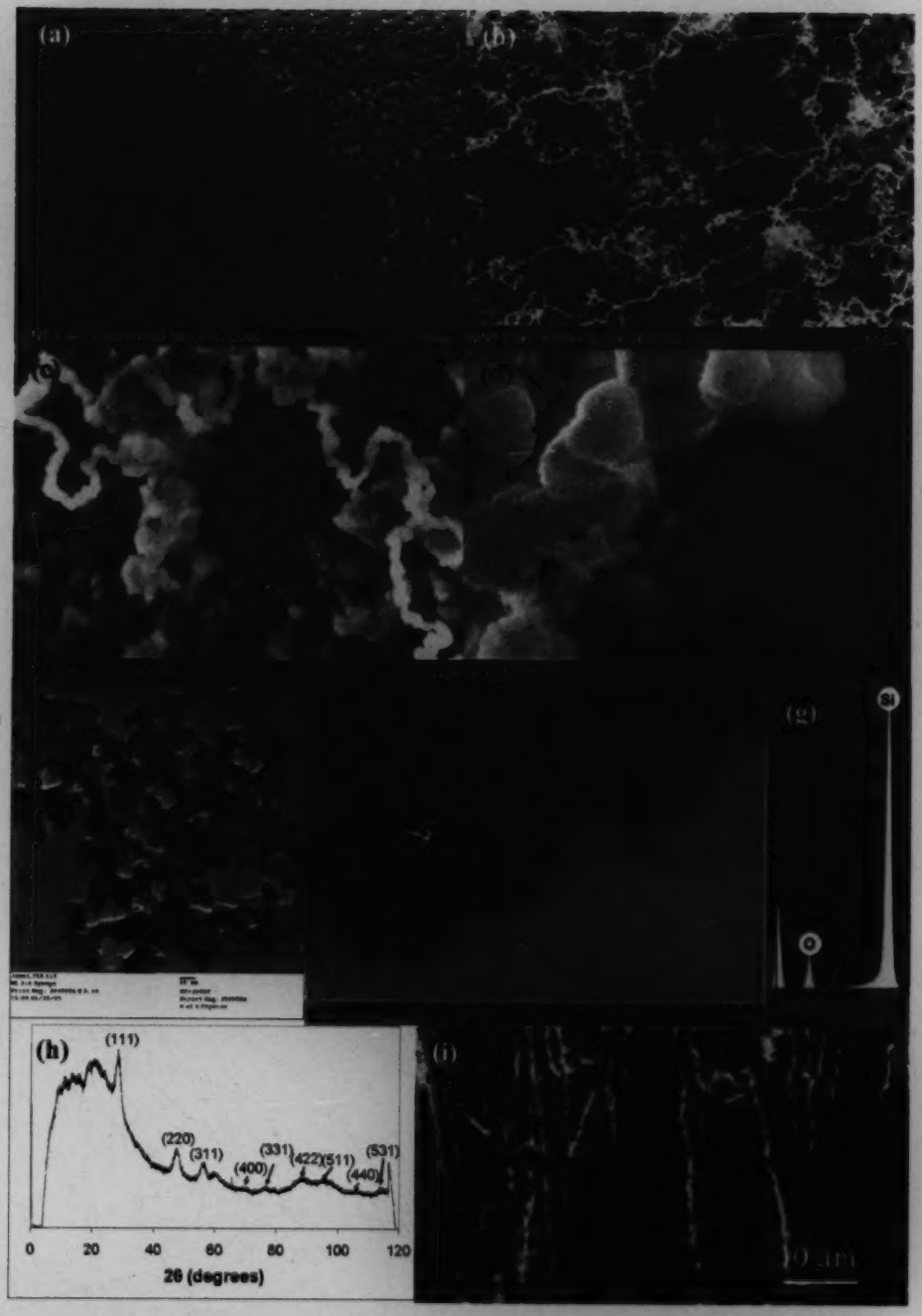

Figure 2.10. Zone V products. (a) Overview. The top right corner shows more aligned features. (b) and (c) Spongy and wire-like features at different magnifications. (d) Products on TEM grid. The spongy features are manifest as both large (chunky) and small features. (e) TEM image. (f) Bright-field STEM image showing tiny features. (g) EDX spectrum. (h) XRD spectrum. (i) Aligned SiO nanowires from reference 30.

film from Zone IV delaminated in the ethanol dip-rinse and was drawn out by pipette and drop-coated directly onto a silicon substrate (without pentane rinse). The resulting FTIR spectrum is depicted in Figure 2.11a, showing the silicon

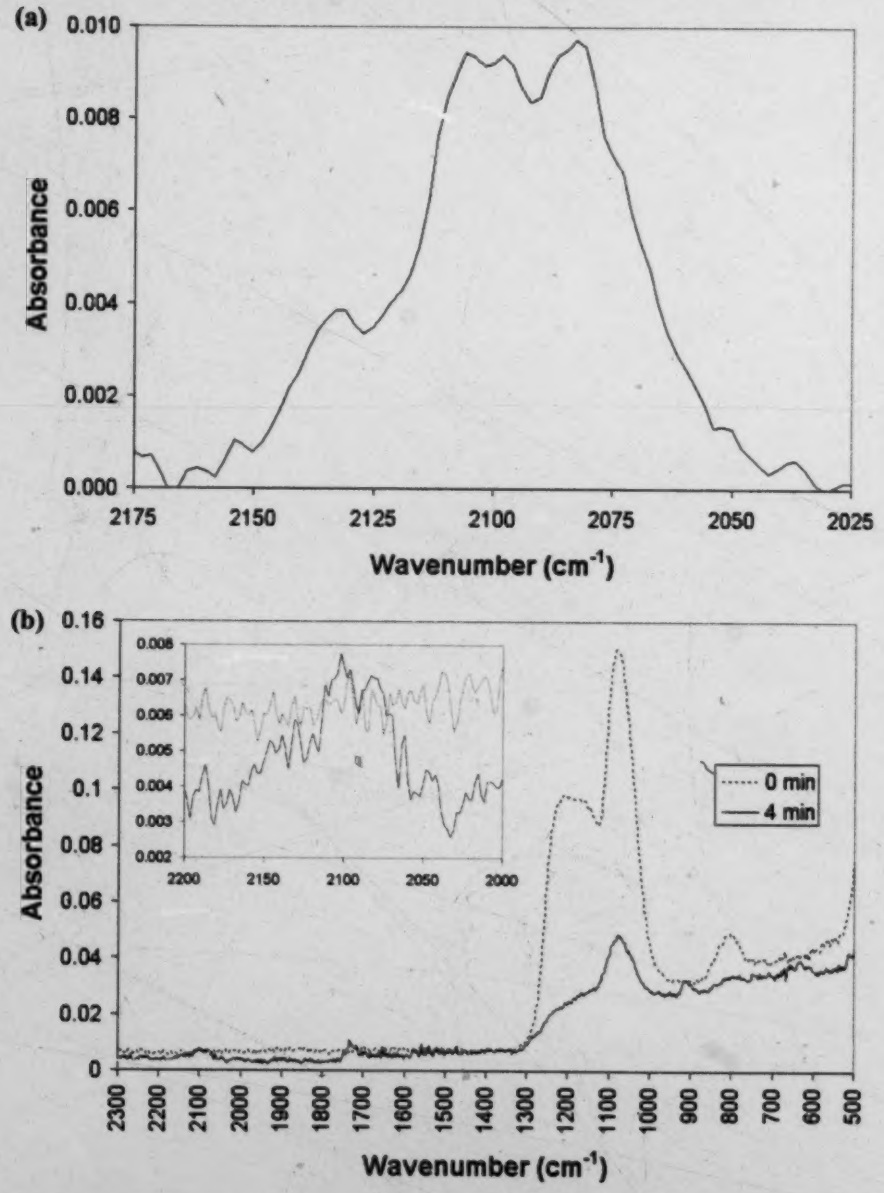

Figure 2.11. FTIR spectra of etched products. (a) An entire substrate was immersed. Diffuse reflectance mode was used. (b) Spectra obtained before and after a substrate was etched with 1:1 49% HF:EtOH vapour, plotted on a common scale. Normal transmission mode was used. Inset shows a close-up of the spectral region between 2200 and 2000 cm^{-1}.

hydride stretch, confirming the hydride termination expected upon oxide etching. Other attempts with this procedure were not successful and it was unclear why this particular case succeeded. Etching procedure (4) seemed to be the most effective overall and most facile of the different routes. An example of a successful attempt resulted from etching Zone IV of an as-grown substrate with 1:1 49% HF:EtOH vapour. The resulting FTIR spectrum is shown in Figure 2.11b after etching for 4 min. After etching for an additional 2 min, then another 4 min, the spectrum did not noticeably change.

The pertinent vibration modes of the spectra are as follows. The silicon hydride (SiH_x, x=1-3) stretching frequencies are centred around ~2100 cm^{-1},[66] shown in both spectra after etching. The frequencies from 1300-1000 cm^{-1} can be attributed to silicon oxide (SiO_x) species.[67,68] The ~915 cm^{-1} mode can be assigned bending modes of silicon dihydride (SiH_2)[67] or monohydride (SiH). The modes from 700-600 cm^{-1} can come from a few sources: SiH and SiH_2 deformation modes and Si-Si stretch mode.[67] In Figure 2.11b, the intensities of the modes associated with the oxide species decrease while the modes associated with SiH_x species appear during etching.

2.3.3 Photoluminescence

Zone IV products from some samples were tested using the spectrophotometer. No photoluminescence was detected. At best, other samples gave off a faint red emission when viewed under ultraviolet light at 254 nm in very dim lighting conditions. When an excitation wavelength of 365 nm was used, visible emission was virtually non-existent. The red emission is expected from other reports involving nanocrystalline silicon.[68,69]

2.4 Discussion

2.4.1 Growth mechanism

Before delving into a discussion of the growth mechanism, it is helpful to consider some of the issues involved in the synthesis and characterization.

The products obtained in the present series of experiments are necessarily difficult to analyze due to a large sample-to-sample variation. Parameters include the position of the alumina tube (with respect to the furnace); the configuration of the substrates and their position with respect to the tube; the amount, distribution, position, and degree of oxidation of the SiO reagent; how well the tube was purged (factors are time and flow rate); the heating schedule; the hold temperature; period of time at hold temperature; and the cooling schedule. In the current experiments, some of these parameters were varied in an attempt to determine optimal conditions. Other parameters, such as positioning of the various components, were relatively constant, but, due to the nature of the experiment, it is very well possible that even small differences, which are difficult to eliminate, may translate into large variations in the products. In some cases, even when the parameters of a particular experiment were repeated, the results differed significantly. In particular, the yield changed, as determined by visual inspection and mass measurements. The temperature ranges in the current work are very rough estimations, because the thermocouple (TC) measurement is sensitive to the thermocouple tip distance from the heating element. This factor may also errantly make two runs appear similar when the TC readings are the same but the TC tip-element distances are different. Thus, it is difficult to say how well the temperature ranges of the different zones in the current work compare to those in reference 30. Overall, there were many possible factors which caused the differences among the experimental runs and deviations from the products of other workers. As mentioned earlier, the presence of a spatial temperature gradient and a gradual increase and decrease in temperature during heating and cooling, respectively, could lead to different products being present in

the various zones, even though there may have been a dominant product in a particular zone.

The products, especially in Zone IV, were particularly delicate and were sometimes blown off during the preparation of samples for SEM.[f] This also may be a source of error as products from different zones may be blown into other zones, though it does not seem likely to be a large source of error, as secondary products make up a very small proportion of the products and appear to be integrated with the primary products (see, for example, the discussion of fine nanowires attached to the octopus-like and pin-like structures in Zones I and II).

The nanowires, especially the type found downstream of Zone II, are particularly difficult to view at high magnification (e.g., 80 000X). This was because the nanowires nucleate at one end and the rest of the wire is not attached to the substrate. Because of their lightness and the vacuum, the nanowires could move. Thus, many images at high magnification were blurry due to this and/or due to the difficulty in finding the right parameters to view the nanowires (e. g., working distance, accelerating voltage).

As a result of the different equipment and parameters used, the temperature gradient in the current project was steeper compared to that of Lee and others.[30] If the temperature gradient was shallower, either both spatially and/or temporally, then perhaps Zone III would be better defined and would contain the tadpole-like structures.

The metal found in a few samples arises from trace contaminants in the SiO reagent. The structures found with metal were probably grown through the VLS mechanism, as it is expected that the VLS mechanism is operative as well.[27] In addition to the VLS mechanism, it is important to note that the growth mechanism described in the Introduction applies to Zone IV and does not apply as readily to the other zones. The following discussion will attempt to describe some aspects of the mechanisms operative in these other zones as well.

---

[f] Samples are blown to ensure that products do not come off in the vacuum.

2.4.1.1 Zones I, II

The silicon monoxide reagent vaporizes when heated and is carried downstream to a cooler region, where the substrate is located. Though not specifically investigated in the present work, it is expected that, in Zones I and II, the reagent deposits as large particles on the substrate surface, which correspond to the clumps that are present, as reported by others as well.[29] (The deposition of these large particles will be discussed in more detail later.) At least some of the spheres from which nanowires grow form directly on these large SiO particles, which were probably deposited onto the substrate in a solid state while the furnace was still cool. Other spheres may come directly from small vapour particles (when the furnace was hotter), as postulated earlier in the Introduction (for Zone IV growth). As the experiment continues and small particles of reagent are deposited, it is possible that a direct phase separation from the large particles occurs (mechanism unclear) and the nanowires grow out of the large particles. As in the VLS mechanism, there is likely a molten droplet on which reagent deposits and nanowires precipitate out.[30] Like in the VLS mechanism, the precipitation is likely to depend on the composition, temperature, and size of droplet, the last of which is related to temperature anyway (*vide infra*). However, there are some important differences in this analogy.

(1) In the VLS mechanism, the wire is made of the semiconductor, while the tip is composed of both the metal catalyst and the semiconductor. In the mechanism applicable for nanostructures in Zones I and II grown through the OAG method, the elements present in both the tips and the wires are the same, silicon and oxygen, albeit not necessarily in the same proportion.

(2) In the VLS mechanism, the wires have a uniform diameter throughout their lengths or most of their lengths. In the OAG method, the tip grows as the experiment wears on. This affects the instantaneous diameter of the wire that precipitates out; hence, the nanowires are tapered. Figure 2.8d shows that the particles on the substrate are indeed smaller than the tips with tapered wires. Thus, both the tip and the wire grow at the same time. The tip grows up to some maximum size determined by the deposition temperature (which

increases at the beginning of the experiment), while the wire diameter depends on the temperature indirectly through the tip size and possibly directly on the temperature through some other relation. (The reason for the uncertainty in maximum size of the nanowires arises from the nanowires being one-third to a half of the tip size towards the downstream [e. g., 100-nm tip with 50-nm wire base], while the ratio can be much smaller towards the upstream [e. g., 7-μm tip with 1.3-μm wire base].) The deposition temperature determines the size of the structures: since smaller particles have a lower melting point, the products decrease in size with decreasing temperature.[27]

(3) In the VLS mechanism, only one wire grows out from each tip. In the OAG method, the octopus-like structure is very common, in which several wires emanate from a single tip. At the attachment point to the tip, the diameters of the nanowires are usually about the same, since the diameter of a nanowire is dependent on the size of the tip out of which it grows.

The process of tip and wire growth is illustrated in Figure 2.12. It appears that the tip rises up from the surface of the large reagent particle or from the substrate itself as the nanowire grows. Thus, the initial wires are anchored at one end. As the tip enlarges, it is able to support the growth of more wires. (The higher the temperature, the more molten the tip and the larger the tip. The more molten the tip, the more absorptive it is. The larger the tip, the more space it has for more wires.) These new wires that grow then have a free end. However, in practice, it is very difficult to find these free ends, of which some are shown in Figure 2.13a. When the tapered end could be found, it was usually attached to the substrate or to another nanowire. If it was attached to the substrate, then it was likely the initial wire. If there was more than one nanowire from the same tip attached to the substrate, or if the tapered end was attached to another nanowire, then the postulated reasons for this are (1) the nanowires are quite flexible, as indicated by their curvature; (2) this flexibility allows them to impinge on other nanowires or the substrate, whatever surface that is available to it, and (3) the high temperature of the synthesis enables the nanowire ends (high curvature) to be reactive enough to fuse to other nanowires or the substrate, though it is unlikely

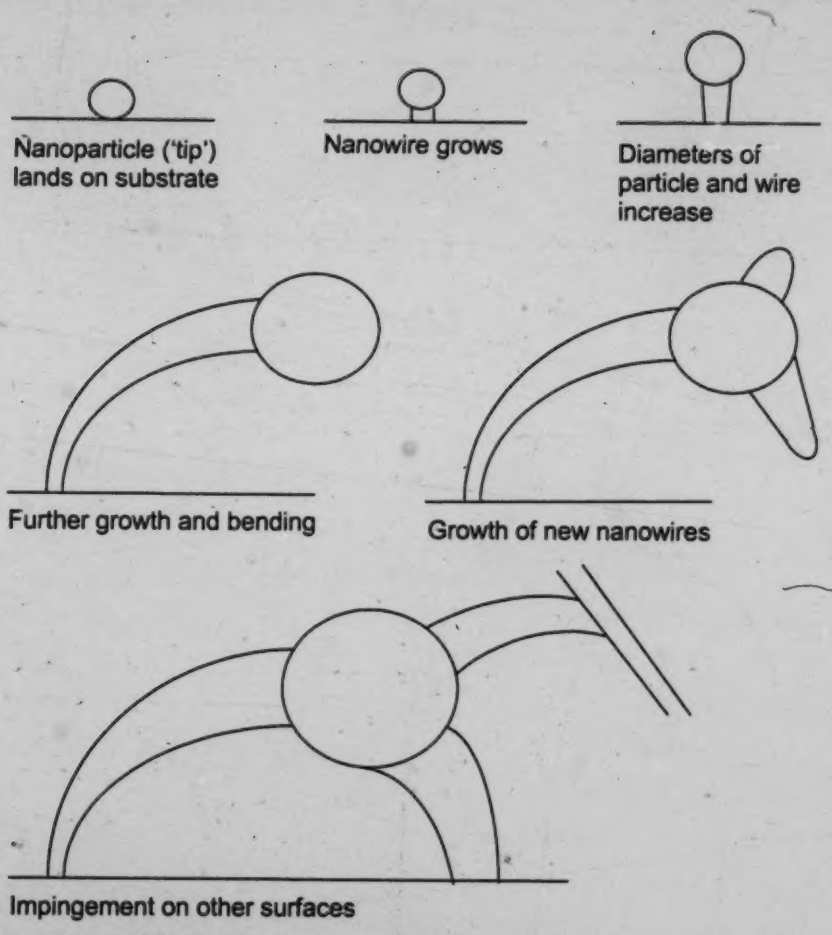
Nanoparticle ('tip') lands on substrate
Nanowire grows
Diameters of particle and wire increase
Further growth and bending
Growth of new nanowires
Impingement on other surfaces

Figure 2.12. Growth sequence of octopus-like structure.

that the impinged surfaces are very reactive themselves, as the silicon oxide sheath prevents lateral growth of the nanowires. Sometimes, a particle nucleates on another nanowire, and this also causes the tapered end to be attached to another nanowire (see Figure 2.13 and Figure 2.14). It is unclear whether a tapered end has impinged onto a nanowire or the nanowire nucleated there, except in cases in which an impinging end is larger than the wire to which it is attached (see Figure 2.13b).

Due to the high temperature, especially in the upstream area of Zone I, the tips from which the nanowires grow are often disordered shapes, as they are more liquid-like. As the tip is particularly reactive at high temperatures, more wires can nucleate and apparently even seamlessly fuse with the particle to create

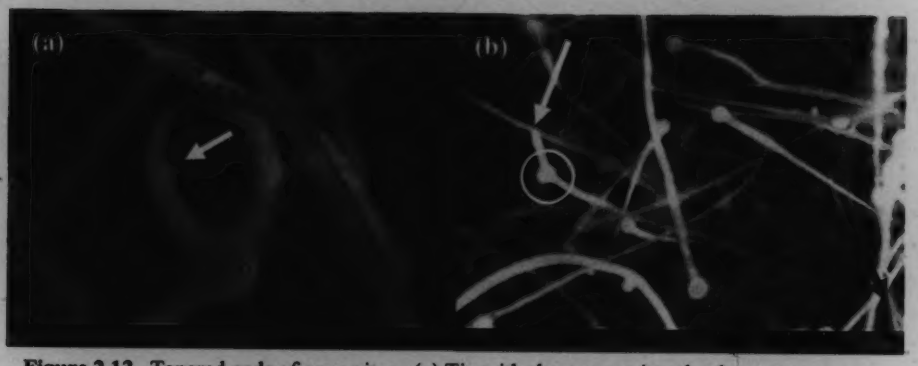

Figure 2.13. Tapered ends of nanowires. (a) Tip with short nanowires that have not impinged on other surfaces. The arrow points to a nanoparticle nucleation that has landed on the nanowire but which has not grown into a nanowire itself yet. (b) The black arrow points to the tapered end of a nanowire, located where the circled tip originally landed. The white arrow points to where a new nanowire from the same tip has impinged. The impinged nanowire is thinner than the impinging nanowire.

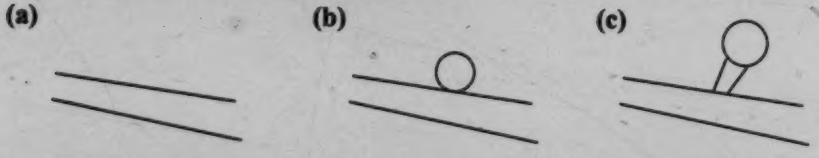

Figure 2.14. Nucleation on a nanowire. (a) Bare nanowire. (b) Round tip lands on nanowire. (c) Nanowire grows out from tip and is anchored to original nanowire, lifting tip off from surface of the original nanowire.

different shapes, like the structure shown in Figure 2.5e. The flower-like structure in Figure 2.5d is really an octopus-like structure with many wires growing out of it. In some cases, the wires cover the tip such that the tip can no longer be seen. There are also numerous instances of bifurcation and coalescence of nanowires, some of which are also shown in Figure 2.5d.

It is interesting to note that many of the tips are facetted with a hexagonal shape (Figure 2.15), which was also previously observed.[30] The SAED in Figure 2.7d shows that the tip is single crystalline. Thus, it is very likely that each tip is single crystalline, even for those that are not facetted, as the particular tip used for SAED was not clearly facetted. Facetting likely results from the structure trying to achieve a more thermodynamically stable state, its Wulff body.[70,71] The Wulff theorem states that the equilibrium shape of a crystal is constructed by erecting normals from an origin to all possible crystal faces such that the length of each normal is proportional to the surface free energy of the corresponding face. The inner envelope of the planes perpendicular to the normals is the crystal shape

Figure 2.15. Facetted tips. Clearly facetted tips are circled.

that minimizes the surface free energy for a given volume at a given temperature. The hexagonal shape of the silicon tips is consistent with the shape predicted by Wulff construction.[7] At high temperature, it is more facile to achieve this state as atoms can diffuse more easily. This is also evident in the fact that the nanowires (from at least Zone LIV) are bound by the stable {111} and {100} faces and are thus also facetted.[32] Nanowires synthesized via the VLS mechanism have a similar hexagonal cross-section.[7] Facetting of the tips may affect the position on the tip where the nanowires grow, especially since different crystal faces have different stabilities and the nanowires may grow in a dominant direction. One group found that their nanowires predominantly grow in the <112> or <110> direction.[32] However, another group found that their nanowires grow in the <111> direction through the OAG method.[72] (The <111> direction is the dominant growth direction in VLS growth above a certain wire diameter, even when the nanowire does not nucleate on a surface at all.[6,7]) The difference in dominant growth directions suggests that a dominant growth direction may involve other factors besides the thermodynamic stability of the enclosing planes.

We now return to the subject of SiO particle deposition. The appearance of Zone I is quite clumpy, with each clump apparently consisting entirely of nanostructures (it is unclear how an entire clump converts into nanostructures). There are also long nanowires (~200 nm thick) which extend between the clumps, as shown in Figure 2.16. It has been proposed that the nanowires grow out of a clump, and then a part of that clump gets blown away to a different spot, stretching the nanowires across the expanse between the original and newly

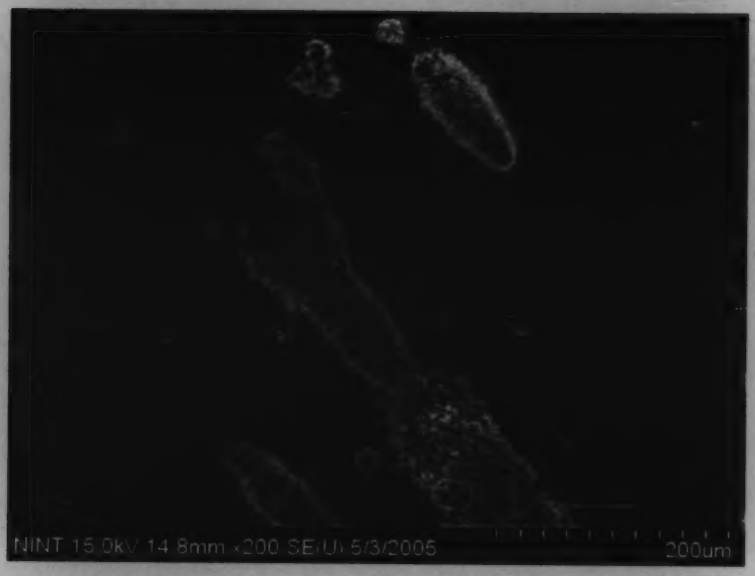

Figure 2.16. Zone I clumps. SiO deposits as clumps on which nanostructures are grown. Wires extend between clumps.

formed islands.[29] It seems unlikely that most of the nanowires outside a clump would extend to another if this were not so. These nanowires are probably Zone-IV-type deposits formed during the heating stage, since the clumps were deposited in a more solid state. Besides the clumpy appearance of Zone I, more evidence of nanowires growing out of the clumpy particles can be found by examining the remaining SiO reagent (Figure 2.17). This reagent appears macroscopically as chunks of slightly compacted powder, lighter brown in colour than the unreacted powder, with the outer surfaces of the chunks bluish, and whitish or yellowish if heated extensively. The leftover SiO reagent has the same products as Zone I, that is, octopus-like, pin-like, and disordered structures, and long nanowires about ~100-200 nm thick in the bluish areas. These products are merely larger due to the higher temperature. The brownish areas have simply a roughened texture or less formed (more disordered) products, because these areas are less reacted. At low magnification under the variable-pressure SEM, the chunks have a fuzzy growth, which actually consists of nanostructures. Though the whitish and yellowish areas were not examined, these are probably areas where there is more product formation due to extended heating, as the lighter colour indicates a higher ratio of SiO_2 to SiO.[30] XRD shows that the leftover

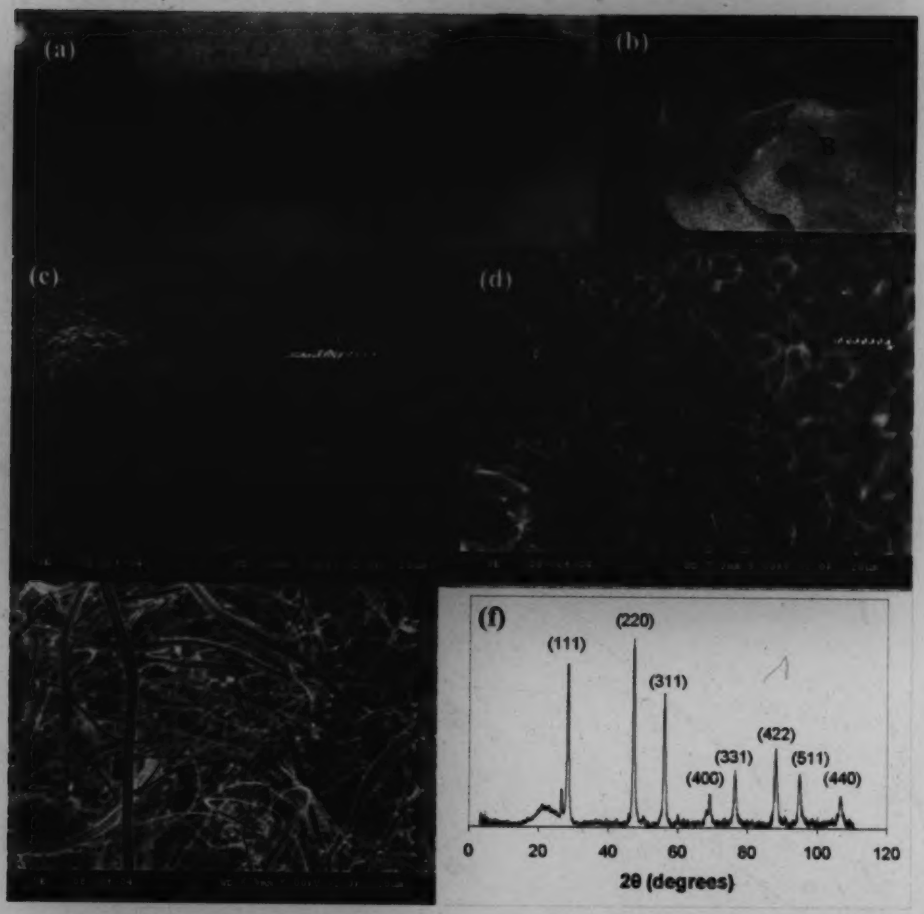

Figure 2.17. Leftover SiO reagent. (a) Optical photograph. (b) Large SiO particle. The light area is slightly fuzzy due to growth. (c) Unreacted surface, which may be found in the area labelled A in (b). (d) Structures formed where there was more reaction. (e) Octopus-like and pin-like structures, which may be found in the area labelled B in (b). (f) XRD spectrum.

clumps are polycrystalline silicon with a large amount of amorphous material (the unreacted SiO). The polycrystalline peaks are broader compared to those of Zones I and II, also indicative of the less developed structures.

As mentioned before, the colours of Zones I and II are different even though they have similar structures. Some insight may be gleaned from examining the unexposed side of substrates from experiments in which a stacked configuration was used. Because the reagent particle flow sometimes had slight access to the unexposed side, product deposition occurred there. The colour of the products here varies from grey to red-brown to orange to yellow to green to

blue to purple as one views the substrate from upstream to downstream, as shown in Figure 2.18. Under the SEM, the products are similar to the octopus-like and pin-like structures and short bars of Zones I and II but are progressively smaller from upstream to downstream. This is reasonable considering the above discussion concerning the size reduction as the environment gets cooler and the fact that smaller objects reflect light of smaller wavelength. Therefore, this accounts for the clumps in Zone I becoming more yellow with smaller nanostructures as the temperature decreases and the yellow ridge-like structure of Zone II containing smaller nanostructures than Zone I. It is as yet unclear as to why there is such an abrupt colour transition from grey to yellow on the exposed surface and why Zone II forms a ridge much higher than the clumps of Zone I. More insight may be gained if there is a shallower temperature gradient, as it may be possible to see a broader range of colours and a more gradual increase in the height profile on the exposed side.

The short bars obtained in Zones I and II start out as the usual octopus-like and pin-like structures, oriented in random directions. It appears that through extended heating, they fuse together.[30] Because the original structures touch each other, the fused structures have only short wire-like sections and are no longer

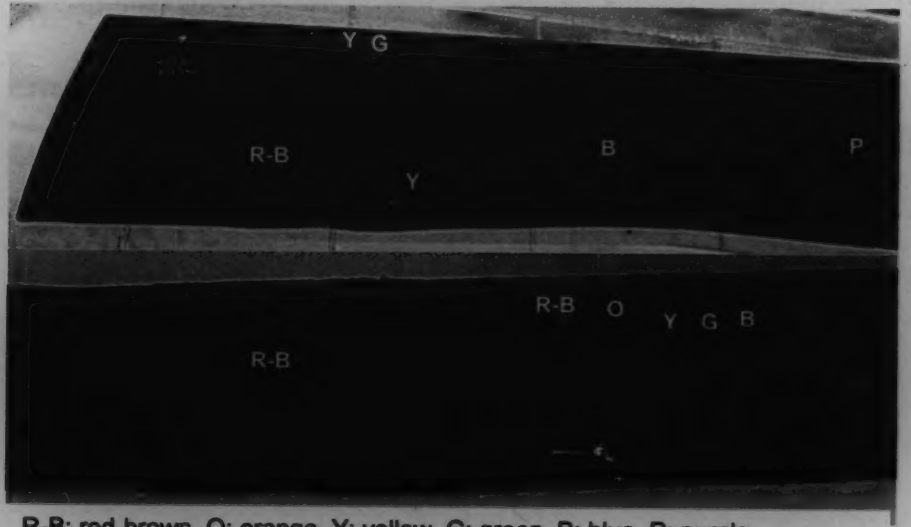

R-B: red-brown, O: orange, Y: yellow, G: green, B: blue, P: purple

Figure 2.18. Substrate surfaces showing spectrum of colours.

nanowires on the order of tens of microns long. Previous literature reports that there are also sintered nanoparticle chains, another result of the high temperature synthesis.[30] These chains demonstrate the spheroidization mechanism taking place (*vide infra*).

As mentioned earlier, there are nanowires 20-200 nm thick that are found in Zones I and II. There are also certain protrusions on the spheres which taper very sharply, some with these nanowires growing out of them, others which are probably nucleations without further growth yet (see Figure 2.19). As some of these nanowires are in the same size range as those in Zone IV, it is quite possible that these nanowires nucleated and grew there as the furnace cooled down and these zones experienced the temperature range conducive to Zone IV growth. This is also evidenced by the many protrusions without the nanowires (still in nucleation stage) and by the nanowires not being the primary product. These protrusions may also be the source of the tadpole-like structures found in the one particular sample.

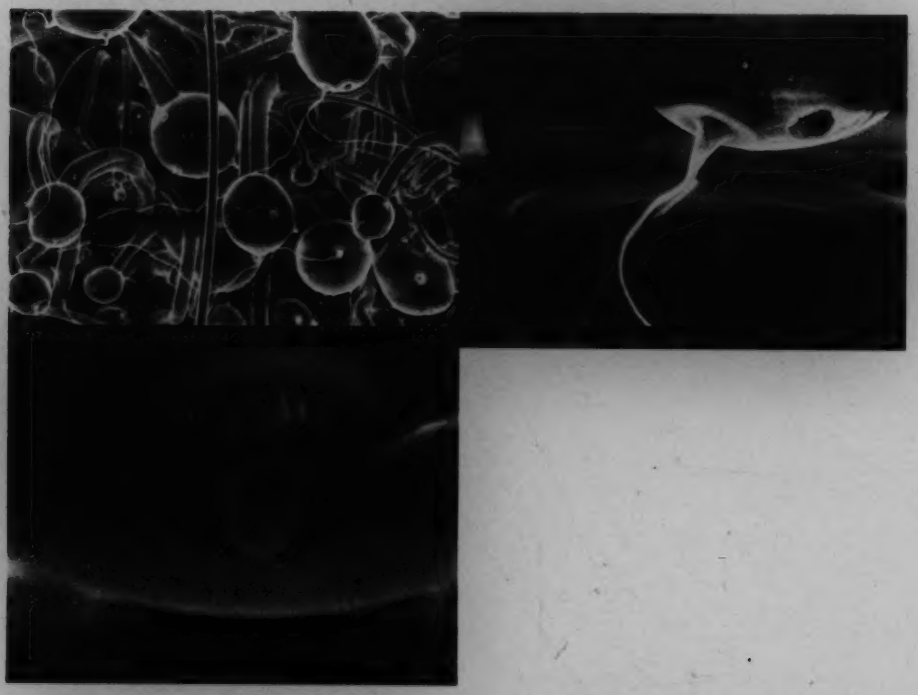

Figure 2.19. Protrusions on Zone I tips. Fine nanowires grow out of many of them. These may also be found in Zone II.

2.4.1.2 *Zone IV*

The mechanism proposed for the growth of the nanowires and nanoparticle chains is a vapour-solid mechanism in which the reagent converts from the vapour form directly into a solid with no liquid intermediate, as the diameter should vary with the temperature in the case of a liquid intermediate.[27] To account for the different morphologies (e. g., nanowires, nanoparticle chains), a spheroidization mechanism, based on the Rayleigh mechanism,[73,74] was proposed (see Figure 2.20).[27] This mechanism is based on the structure reducing its silicon-silicon oxide interfacial energy by converting into spheres. The nanowires convert into nanoparticle chains, then to tadpole-like structures, eventually to separate spheres as the temperature increases. The size and separation of the particles in the chains increase as the temperature increases as well. This temperature requirement is probably related to diffusion. In the present study, support for the vapour-solid deposition mechanism is evident in the nanowires and nanoparticle chains being about the same size. However, tadpole-

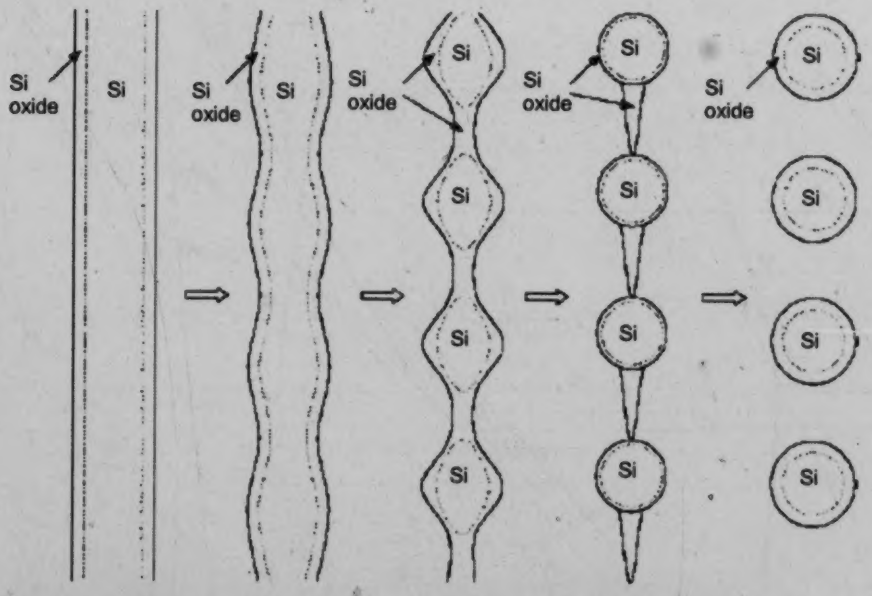

Figure 2.20. Spheroidization mechanism. The spheroidization mechanism explains the transition from smooth nanowire to bulbous nanowire to nanoparticle chain to chain of tadpole-like structures to separate nanoparticles. (Adapted from reference 27.)

like structures are absent and it is difficult to say for certain that, at the downstream end of Zone IV, there is a higher proportion of smooth nanowires or even chains with smaller nanoparticle separation distance. As stated earlier, the roughening of the products (described below) may account for the lack of transparency in this matter. Others have suggested other mechanisms for the growth and range of morphologies.[75-77]

It is worth noting that spheroidization is not the complete explanation. It explains why the silicon core breaks up; however, if fails to provide insight into why the nanoparticles in the chains are not always spheres. Most of the nanowires are facetted (the {111} and the {100} planes are the most stable) and when they break up into particles, they remain facetted, as polyhedral shapes have been found, evidenced by cross-sections of rectangular and triangular shapes.[35] This phenomenon is probably related to the stability of the enclosing faces, as the structures attempt to attain a thermodynamically preferred shape (Wulff body). Other workers indicate the spheroidization mechanism is not satisfactory for the formation of these structures and are currently investigating the underlying mechanism.[35]

2.4.1.3 Zone V

Zone V was the coolest region where there was product deposition. It appears that initially the SiO reacted with residual oxygen to form SiO_2, up to a few hundred nanometres thick. The equation describing the oxide formation is given as follows.

$$SiO + \tfrac{1}{2} O_2 \rightarrow SiO_2 \qquad (3)$$

This oxide could not have been due to residual oxygen reacting with the substrate. Tests without the reagent powder confirmed that a thermal oxide would preferentially form in the hottest region and is considerably thinner than what was observed in experimental runs with SiO powder. Probably what occurred was the temperature was not hot enough for the disproportionation reaction to occur to form Si-SiO_x core-shell structures, so SiO merely reacted with the residual

oxygen to form the stable, saturated SiO_2,[g] and when there was not enough oxygen, the SiO reagent particles deposited as SiO nanostructures. This would explain why the yellow mass grew on top of where the oxide was thickest: based on the local conditions (factors may include gas-phase kinetics, heat transfer, etc.), this was the place most favourable for any sort of oxide deposition, whether SiO_2 or SiO. The SiO reagent particles would have reacted with the residual oxygen in the other zones as well; however, it was hot enough, so disproportionation still occurred to form the core-shell structures. Instead of a thick oxide on top of the substrate in these zones, there was probably more oxygen incorporated into the oxide sheath of the nanostructures, with the sheath having a ratio of O:Si closer to 2, being a thicker oxide, or both.

These structures in Zone V have some semblance of nanowires. However, only a fraction of these grew as distinct nanowires. Many of the structures that nucleated became spongy or rough at an early stage of growth. Roughening is also evident on the surface of the (long) nanowires. This may be caused by the temperature of the substrate being cooler in this region. In fact, it may be so cool that the SiO reagent particles, in many cases, condense and deposit randomly rather than at the tip of the nanowires. It is harder for the SiO particles to travel far enough to reach the tip of the nanowire before the temperature is too cool for them to stay in vapour form and/or the stability of different surfaces available are nearly the same. Thus, the few nanowires that are able to grow longitudinally are roughened and many structures just simply do not become nanowires at all. However, the spongy material does have short wire-like sections that, only when agglomerated, appear spongy, and, hence, there may be local points of higher reactivity. Others have also observed this type of spongy material and attribute it to the SiO depositing as cluster particles and not being at a high enough temperature to disproportionate into Si and SiO_2 phases.[43] It is also very possible that many of the nanowires that were found here actually nucleated in an area more upstream, such as in Zone IV or the transition region between Zones IV and

[g] The bond enthalpies for Si-O (for equation 2) and O-O (for equation 3) are 799.6±13.4 kJ/mol and 498.36±0.17 kJ/mol, respectively. These values are for gaseous diatomic species at 298 K.[78]

V, as some of the nanowires in Zone IV appear to be this type of rough nanowire and not the smooth nanowire or bulbous nanoparticle chain type. Some of the nanowires formed in Zone V are not as rough, indicating that these nanowires may have started out with a smooth surface, and then, as the experiment proceeded, SiO reagent particles impinged on them randomly, roughening them. As stated before, there is a slight crystallinity in this zone, so some of the growth is probably Zone IV type growth, as Zone IV products exhibit crystallinity. Since the transition is gradual, it is plausible that some of the Zone IV growth continued into Zone V and merely roughened and became more SiO-like in character.

The roughening due to impingement of SiO particles occurred in other regions but to a lesser degree. Some examples are shown in Figure 2.21 from Zone II. If there is enough random impingement, the local 'densified' thickness of the nanowire may be affected, as it is very probable that nanowires of Zone V are thickened this way, as the spongy deposition increases and the earlier deposition densifies. The random impingement in zones other than Zone V may have occurred during the (heating and) cooling stages of the experiment, as the regions upstream of Zone V would have experienced the lower temperature at which Zone V product forms. Evidence of this occurring during cooling may be seen in that there are no spongy products beneath smooth products and there are smooth products underneath spongy products. Observation of this is by looking through spaces between products at the top (see Figure 2.22). An interesting possible result of the cooling is that there are thin, roughened nanowires in

Figure 2.21. Impingement of SiO particles. (a) Entire spongy masses formed. (b) Individual nanostru ctures are roughened.

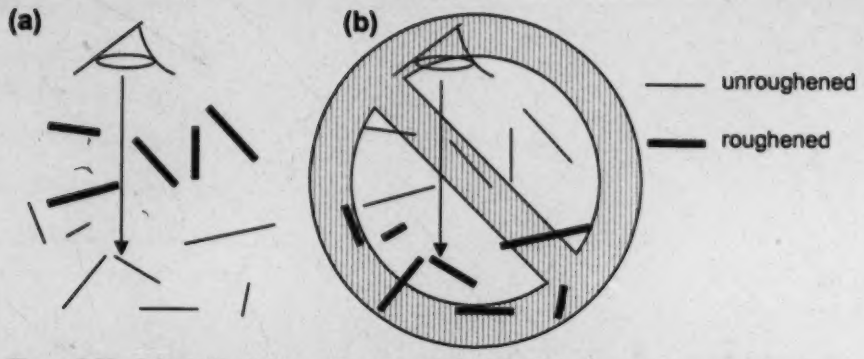

Figure 2.22. Schematic of observation of roughened products. (a) Roughened products are observed to be on top of unroughened products, as the products underneath can be seen through spaces between the top products. (b) Roughened products are not seen underneath unroughened products.

Zones I and II, arising from nanowire growth similar to Zone IV then roughening like that seen in Zone V. In addition, the product of Zone V appears to have the largest temperature range conducive to its growth as compared to the products of other zones.

2.4.2 Etching of silicon nanowires

The products of interest that were being etched were mostly of Zones II and IV. It was initially thought that Zone IV consisted of thin, crystalline silicon nanowires which could be used in electronic applications. However, upon closer inspection, it appeared that many of the wires were actually bulbous, indicative of silicon nanoparticle chains or wires in the process of converting into them. Also, because the chains (and wires) were so thin, it was difficult to etch the products without completely etching them away,[h] otherwise the products that were not etched away were so scarce that a signal in the FTIR spectrometer could not be detected. The total yield of all the products from the vapour-phase synthesis was tens of milligrams, with the bulk of this mass in Zones I, II, and V and very little in Zone IV. Others also had difficulty in achieving a high yield in the etching step.[79] The method of etching with a vapour of HF[80] was more successful;

[h] The etch rate of n-type, 2 Ω·cm Si(111) in 48% HF is 0.3 Å/min.[2] Though this may appear to be slow, the effect of an etchant may be enhanced in nanoscale systems.

however, the SiH_x modes were weak and there was still evidence of oxide present. It is unclear whether this oxide was from the original synthesis or is from post-etching oxidation or a combination of both, as oxidation may be enhanced for nanoscale systems as compared to bulk systems. Furthermore, these vapour-etching experiments were performed on the as-grown substrates, so the nanowires were still not separated from the original substrate. It is possible that separation of nanowires through a dispersion, followed by drying of the solvent (either evaporation of the entire vessel or drop-coating the dispersion onto a substrate) and etching with HF vapour would work. This seems reasonable as some of the products were dispersed through crushing and sonication and since the vapour-etching of the as-grown products on the original substrate showed some success, although achieving a high yield from this composite procedure may still prove challenging. However, it was decided at this point to characterize the nanowires by drop-coating the dispersion onto a substrate and performing atomic force microscopy (AFM) on them before performing any more etching experiments. Also, it was decided that perhaps the products of Zone II may be better since they were more robust (thicker) and abundant. A short while later, another method of producing silicon nanowires (described in the next chapter) was used instead.

2.4.3 Photoluminescence

There were limited studies involving photoluminescence. Some products from Zone IV were examined using the spectrophotometer and the spectrum showed no photoluminescence or the signal was otherwise too weak to be observed. One factor may be that the instrument parameters may not have been optimized. The faint red emission under the UV lamp for some samples indicates that a photoluminescence spectrum should be possible to obtain, yet it also indicates that optimization is necessary. It is reasonable that the red emission would only be faint. Most of the products were not small enough that light emission due to quantum confinement could occur, as quantum confinement effects are significant only when the characteristic dimension of a nanostructure is

less than the Bohr radius, which is ~5 nm for silicon.[69] The minimum size of the products observed in Zone IV was about ~10 nm. It is reasonable to expect that the crystalline core of some products is small enough to exhibit quantum confinement, enabling a faint red emission of as-grown products to be seen, but they certainly do not comprise a significant proportion. The low yield compounded with the dilution effect of the dispersion may have resulted in the photoluminescence signal being too weak to be observed, if the instrument parameters were not optimized.

2.5 Conclusion

The vapour-phase, oxide-assisted method of growing silicon nanowires from SiO was used to grow a variety of products, which were comparable to those previously described by others. The products appear to be Si-SiO_x core-shell octopus-like structures, pin-like structures, nanowires, and nanoparticle chains; and SiO nanowires and spongy deposition. The octopus-like and pin-like structures were likely grown through a process analogous to the VLS mechanism. Si nanowires and nanoparticle chains likely grow through a vapour-solid process, with spheroidization responsible for their morphology. SiO nanowires and spongy cluster deposition were probably formed from SiO depositing directly without disproportionation. Other aspects of the growth processes were investigated, including impingement of SiO reagent throughout the different zones and examination of the leftover SiO reagent to reveal growth on large SiO particles.

Etching experiments were attempted, of which the most successful route was the etching with HF vapour.

There was evidence that photoluminescence occurs, though it may have depended on the experimental run and a photoluminescence spectrum may only be possible to obtain if the instrument parameters are optimized.

2.6 References

(1) Semiconductor Industry Association. *2005 Annual Report: 2020 Is Closer Than You Think;* Paulus, J., Ed.; San Jose, CA, 2005.

(2) Madou, M. J. *Fundamentals of Microfabrication: The Science of Miniaturization*, 2nd ed.; CRC Press: New York, 2002.

(3) Buriak, J. M. *Chem. Rev.* **2002**, *102*, 1271.

(4) Liu, G.-Y.; Xu, S.; Qian, Y. *Acc. Chem. Res.* **2000**, *33*, 457.

(5) Wagner, R. S.; Ellis, W. C. *Appl. Phys. Lett.* **1964**, *4*, 89.

(6) Morales, A. M.; Lieber, C. M. *Science* **1998**, *279*, 208.

(7) Wu, Y.; Huynh, L.; Barrelet, C. J.; Bell, D. C.; Lieber, C. M. *Nano Lett.* **2004**, *4*, 433.

(8) Carim, A. H.; Lew, K.-K.; Redwing, J. M. *Adv. Mater.* **2001**, *13*, 1489.

(9) Chung, S.-W.; Yu, J.-Y.; Heath, J. R. *Appl. Phys. Lett.* **2000**, *76*, 2068.

(10) Zhang, X.-Y.; Zhang, L.-D.; Meng, G.-W.; Li, G.-H.; Jin-Phillipp, N.-Y.; Phillipp, F. *Adv. Mater.* **2001**, *13*, 1238.

(11) Westwater, J.; Gosain, D. P.; Tomiya, S.; Usui, S.; Ruda, H. *J. Vac. Sci. Technol. B* **1997**, *15*, 554.

(12) Trentler, T. J.; Hickman, K. M.; Goel, S. C.; Viano, A. M.; Gibbons, P. C.; Buhro, W. E. *Science* **1995**, *270*, 1791.

(13) Tilke, A.; Blick, R. H.; Lorenz, H.; Kotthaus, J. P. *J. Appl. Phys.* **2001**, *89*, 8159.

(14) Tsutsumi, T.; Ishii, K.; Hiroshima, H.; Kanemaru, S.; Suzuki, E.; Tomizawa, K. *Jpn. J. Appl. Phys.* **2002**, *41*, 4419.

(15) Peng, K.; Yan, Y.; Gao, S.; Zhu, J. *Adv. Mater.* **2002**, *14*, 1164.

(16) Peng, K.; Wu, Y.; Fang, H.; Zhong, X.; Xu, Y.; Zhu, J. *Angew. Chem. Int. Ed.* **2005**, *44*, 2737.

(17) Ono, T.; Saitoh, H.; Esashi, M. *Appl. Phys. Lett.* **1997**, *70*, 1852.

(18) Kamins, T. I.; Williams, R. S.; Chen, Y.; Chang, Y.-L.; Chang, Y. A. *Appl. Phys. Lett.* **2000**, *76*, 562.

(19) Niu, J.; Sha, J.; Yang, D. *Physica E* **2004**, *24*, 278.

(20) Holmes, J. D.; Johnston, K. P.; Doty, R. C.; Korgel, B. A. *Science* **2000**, *287*, 1471.

(21) Wang, N.; Tang, Y. H.; Zhang, Y. F.; Yu, D. P.; Lee, C. S.; Bello, I.; Lee, S. T. *Chem. Phys. Lett.* **1998**, *283*, 368.

(22) Zhang, Y. F.; Tang, Y. H.; Wang, N.; Yu, D. P.; Lee, C. S.; Bello, I.; Lee, S. T. *Appl. Phys. Lett.* **1998**, *72*, 1835.

(23) Wang, N.; Zhang, Y. F.; Tang, Y. H.; Lee, C. S.; Lee, S. T. *Appl. Phys. Lett.* **1998**, *73*, 3902.

(24) Wang, N.; Tang, Y. H.; Zhang, Y. F.; Lee, C. S.; Lee, S. T. *Phys. Rev. B* **1998**, *58*, R16024.

(25) Shi, W. S.; Peng, H. Y.; Zheng, Y. F.; Wang, N.; Shang, N. G.; Pan, Z. W.; Lee, C. S.; Lee, S. T. *Adv. Mater.* **2000**, *12*, 1343.

(26) Zhang, Y. F.; Tang, Y. H.; Lam, C.; Wang, N.; Lee, C. S.; Bello, I.; Lee, S. T. *J. Cryst. Growth* **2000**, *212*, 115.

(27) Peng, H. Y.; Pan, Z. W.; Xu, L.; Fan, X. H.; Wang, N.; Lee, C. S.; Lee, S. T. *Adv. Mater.* **2001**, *13*, 317.

(28) Fan, X. H.; Xu, L.; Li, C. P.; Zheng, Y. F.; Lee, C. S.; Lee, S. T. *Chem. Phys. Lett.* **2001**, *334*, 229.

(29) Zhang, Z.; Fan, X. H.; Xu, L.; Lee, C. S.; Lee, S. T. *Chem. Phys. Lett.* **2001**, *337*, 18.

(30) Pan, Z. W.; Dai, Z. R.; Xu, L.; Lee, S. T.; Wang, Z. L. J. *Phys. Chem. B* **2001**, *105*, 2507.

(31) Ma, D. D. D.; Lee, C. S.; Lifshitz, Y.; Lee, S. T. *Appl. Phys. Lett.* **2002**, *81*, 3233.

(32) Li, C. P.; Lee, C. S.; Ma, X. L.; Wang, N.; Zhang, R. Q.; Lee, S. T. *Adv. Mater.* **2003**, *15*, 607.

(33) Teo, B. K.; Sun, X. H.; Hung, T. F.; Meng, X. M.; Wong, N. B.; Lee, S. T. *Nano Lett.* **2003**, *3*, 1735.

(34) Baumer, A.; Stutzmann, M.; Brandt, M. S.; Au, F. C. K.; Lee S. T. *Appl. Phys. Lett.* **2004**, *85*, 943.

(35) Sun, X. H.; Wong, N. B.; Li, C. P.; Lee, S. T.; Sham, T. K. *J. Appl. Phys.* **2004**, *96*, 3447.

(36) Ma, D. D. D.; Lee, C. S.; Au, F. C. K.; Tong, S. Y.; Lee, S. T. *Science* **2003**, *299*, 1874.

(37) Peng, H. Y.; Wang, N.; Shi, W. S.; Zhang, Y. F.; Lee, C. S.; Lee, S. T. *J. Appl. Phys.* **2001**, *89*, 727

(38) Niu, J.; Sha, J.; Yang, D. *Physica E* **2004**, *23*, 131.

(39) Gole, J. L.; Stout, J. D.; Rauch, W. L.; Wang, Z. L. *Appl. Phys. Lett.* **2000**, *76*, 2346.

(40) Zhang, Y. F.; Tang, Y. H.; Peng, H. Y.; Wang, N.; Lee, C. S.; Bello, I.; Lee, S. T. *Appl. Phys. Lett.* **1999**, *75*, 1842.

(41) Wang, N.; Tang, Y. H.; Zhang, Y. F.; Lee, C. S.; Bello, I.; Lee, S. T. *Chem. Phys. Lett.* **1999**, *299*, 237.

(42) Tang, Y. H.; Zhang, Y. F.; Wang, N.; Lee, C. S.; Han, X. D.; Bello, I.; Lee, S. T. *J. Appl. Phys.* **1999**, *85*, 7981.

(43) Zhang, Y. F.; Tang, Y. H.; Wang, N.; Lee, C. S.; Bello, I.; Lee, S. T. *J. Cryst. Growth* **1999**, *197*, 136.

(44) Lee, S. T.; Zhang, Y. F.; Wang, N.; Tang, Y. H.; Bello, I.; Lee, C. S. *J. Mater. Res.* **1999**, *14*, 4503.

(45) Lee, S. T.; Wang, N.; Lee, C. S. *Mater. Sci. Eng. A* **2000**, *286*, 16.

(46) Zhang, R. Q.; Lifshitz, Y.; Lee, S. T. *Adv. Mater.* **2003**, *15*, 635.

(47) Sun, X. H.; Tang, Y. H.; Zhang, P.; Nafel, S. J.; Sammynaiken, R.; Peng, H. Y.; Zhang, Y. F.; Wong, N. B.; Lee, S. T. *J. Appl. Phys.* **2001**, *90*, 6379.

(48) Zhang, Y. F.; Liao, L. S.; Chan, W. H.; Lee, S. T. *Phys. Rev. B* **2000**, *61*, 8298.

(49) Tang, Y. H.; Zhang, Y. F.; Peng, H. Y.; Wang, N.; Lee, C. S.; Lee, S. T. *Chem. Phys. Lett.* **1999**, *314*, 16.

(50) Zhang, R. Q.; Zhao, M. W.; Lee, S. T. *Phys. Rev. Lett.* **2004**, *93*, 095503.

(51) Zhang, R. Q.; Chu, T. S.; Cheung, H. F.; Wang, N.; Lee, S. T. *Mater. Sci. Eng. C* **2001**, *16*, 31.

(52) Li, C. P.; Sun, X. H.; Wong, N. B.; Lee, C. S.; Lee, S. T.; Teo, B. K. *Chem. Phys. Lett.* **2002**, *365*, 22.

(53) Teo, B. K.; Li, C. P.; Sun, X. H.; Wong, N. B.; Lee, S. T. *Inorg. Chem.* **2003**, *42*, 6723.

(54) Li, C. P.; Sun, X. H.; Wong, N. B.; Lee, C. S.; Lee, S. T.; Teo, B. K. *J. Phys. Chem. B* **2002**, *106*, 6980.

(55) Sun, X. H.; Peng, H. Y.; Tang, Y. H.; Shi, W. S.; Wong, N. B.; Lee, C. S.; Lee, S. T. *J. Appl. Phys.* **2001**, *89*, 6396.

(56) Sun, X. H.; Li, C. P.; Wong, N. B.; Lee, C. S.; Lee, S. T.; Teo, B. K. *J. Am. Chem. Soc.* **2002**, *124*, 14856.

(57) Sun, X. H.; Li, C. P.; Wong, N. B.; Lee, C. S.; Lee, S. T. *Inorg. Chem.* **2002**, *41*, 4331.

(58) Zhou, X. T.; Zhang, R. Q.; Peng, H. Y.; Shang, N. G.; Wang, N.; Bello, I.; Lee, C. S.; Lee, S. T. *Chem. Phys. Lett.* **2000**, *332*, 215.

(59) Zhang, Y. F.; Tang, Y. H.; Zhang, Y.; Lee, C. S.; Bello, I.; Lee, S. T. *Chem. Phys. Lett.* **2000**, *330*, 48.

(60) Sun, X. H.; Wong, N. B.; Li, C. P.; Lee, S. T.; Kim, P. S. G.; Sham, T. K. *Chem. Mater.* **2004**, *16*, 1143.

(61) Sun, X. H.; Sammynaiken, R.; Naftel, S. J.; Tang, Y. H.; Zhang, P.; Kim, P. S.; Sham, T. K. *Chem. Mater.* **2002**, *14*, 2519.

(62) Wong, T. C.; Li, C. P.; Zhang, R. Q.; Lee, S. T. *Appl. Phys. Lett.* **2004**, *84*, 407.

(63) Meng, X. M.; Hu, J. Q.; Jiang, Y.; Lee, C. S.; Lee, S. T. *Appl. Phys. Lett.* **2003**, *83*, 2241.

(64) Kolb, F. M.; Hofmeister, H.; Scholz, R.; Zacharias, M.; Gosele, U.; Ma, D. D.; Lee, S. T. *J. Electrochem. Soc.* **2004**, *151*, G472.

(65) Yao, Y.; Li, F.; Lee, S. T. *Chem. Phys. Lett.* **2005**, *406*, 381.

(66) Ito, T.; Kiyama, H.; Yasumatsu, T.; Watabe, H.; Hiraki, A. *Physica B* **1991**, *170*, 535.

(67) Gupta, P.; Colvin, V. L.; George, S. M. *Phys. Rev. B* **1988**, *37*, 8234.

(68) Stewart, M. P.; Buriak, J. M. *J. Am. Chem. Soc.* **2001**, *123*, 7821.

(69) Canham, L. T. *Appl. Phys. Lett.* **1990**, *57*, 1046.

(70) Blendell, J. E.; Carter, W. C.; Handwerker, C. A. *J. Am. Ceram. Soc.* **1999**, *82*, 1889.

(71) Herring, C. *Phys. Rev.* **1951**, *82*, 87.

(72) Shi, Y.; Hu, Q.; Araki, H.; Suzuki, H.; Gao, H.; Yang, W; Noda, T. *Appl. Phys. A* **2005**, *80*, 1733.

(73) Lord Rayleigh (Strutt, J. W.) *Proc. Lond. Math. Soc.* **1878**, *10*, 4.

(74) Nichols, F. A.; Mullins,, W. W. *Trans. Metall. Soc. AIME* **1965**, *233*, 1840.

(75) Cheng, S.-W.; Cheung, H.-F. *J. Appl. Phys.* **2003**, *94*, 1190.

(76) Cheng, S.-W.; Cheung, H.-F. *Appl. Phys. Lett.* **2004**, *85*, 5709.

(77) Zhou, J. F.; Han, M.; Liu, M. D.; Song, F. Q.; Wan, J. G.; Chen, Y. F.; Wang, G. H. *J. Cryst. Growth* **2004**, *269*, 207.

(78) *CRC Handbook of Chemistry and Physics*, 86th ed.; Lide, D. R., Ed.; CRC Press: New York, 2005.

(79) Sham, T. K.; Naftel, S. J.; Kim, P. S. G.; Sammynaiken, R.; Tang, Y. H.; Coulthard, I.; Moewes, A.; Freeland, J. W.; Hu, Y. F.; Lee, S. T. *Phys. Rev. B* **2004**, *70*, 045313.

(80) Létant, S. E.; Sailor, M. J. *Adv. Mater.* **2000**, *12*, 355.

3 Metal nanostructures on semiconductor substrates

3.1 Introduction

Nanostructures and nanomaterials are being intensely studied due to their potential utility in a wide variety of applications and to further fundamental scientific knowledge. One class of nanostructures is metal nanoparticles, since they possess very interesting electrical and optical properties, which depend on their size and shape.[1-10] The current interest in working with metals on semiconductors lies in the fact that the feature sizes of electronics are becoming increasingly small;[11] thus, smaller and smaller metal interconnects and electrodes on the semiconductor substrate are needed. It is therefore necessary to develop procedures that allow tailoring of size and morphology of metal nanostructures on both elemental and compound semiconductor substrates.

Through solution-phase procedures, a variety of metal nanostructures have been produced with different metals, sizes, and shapes. Among these are cubes,[6,12,13] multipods,[12,14] disks and plates of various shapes,[7-9,12,15-17] rods,[1,12,18] wires,[19-21] and spheres,[18] as well as others.[6,10,13,22] However, research on metal nanostructures produced through electrochemical deposition is just burgeoning.

Metals have long been considered to be contaminants in semiconductor processing.[23] Trace amounts of metal ions in etching solutions have led to metal deposition (and substrate oxidation), deteriorating the quality of the substrate. Now research groups and industry[24] have turned to electrochemical deposition as a possible route to the metallization of semiconductors (*vide infra*). Compared to other processes, such as sputtering and chemical vapour deposition (CVD), electrochemical deposition is relatively simple, facile, versatile, and inexpensive with respect to both equipment and materials.[25] Conformal coverage,[26] thick layers (high throughput),[25] and patterned substrates[27,28] can be achieved through different procedures. Besides thick films, electrochemical deposition is being utilized to synthesize films of round nanoparticles and clusters[3,29-36] and dendritic[37,38] structures, as well as rods.[4,39]

The term electrochemical deposition encompasses several different techniques. Electrolytic deposition involves applying an external electrical current to plate a metal from a metal salt solution onto a working electrode, enabling the working electrode to be a substrate that remains intact. Electroless deposition does not involve an external current; rather the electrochemical reaction occurs spontaneously.[25]

Electroless deposition is a more general term for three different specific processes: autocatalytic, substrate-catalyzed, and galvanic displacement (immersion plating) processes, as illustrated in Figure 3.1. The autocatalytic process[25] typically involves various substances, such as the metal salt, reducing agent, pH adjuster, and other bath additives. Once deposited, the reduced metal serves as a catalyst for further deposition. In the substrate-catalyzed process,[25] the substrate acts as the catalyst for the deposition of metal, also in the presence of the metal salt and an external reducing agent. When the substrate becomes completely coated with the deposit, deposition can no longer occur. The galvanic process,[25] however, precludes the need for an external reducing agent as the substrate acts in this role. The substrate provides its bonding electrons from its valence band to reduce the metal ions, in the process becoming oxidized. As long as the oxidized substrate ions can penetrate through the deposited metal film or the electrons can transfer through the formed oxide, the process may continue.

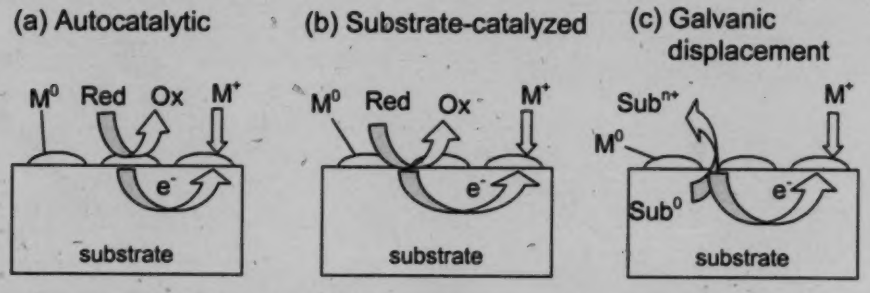

Figure 3.1. Electroless deposition processes. (a) Autocatalytic deposition in which the reduced metal serves as the catalyst for further reduction by the external reducing agent. (b) Substrate-catalyzed deposition in which the substrate serves as the catalyst for reduction by the reducing agent. (c) Galvanic displacement in which the substrate serves as the reducing agent and becomes oxidized. (Adapted from reference 25.)

However, the oxidation products may not always be a hindrance, as oxidation may occur far from the site of metal deposition.

The current work concerns the galvanic displacement process, chosen because it involves the simplest type of bath composition. Various deposit/substrate combinations may be achieved by combining different half-cell reactions, as shown in Table 3.1.[23] If the half-cell combination (complete reduction-oxidation reaction) has a positive potential, then the reaction may proceed. Metals with a reduction potential higher than that of hydrogen will tend to deposit on the substrate. If the reduction potential is lower than that of hydrogen, then hydrogen gas evolution will predominate over metal deposition unless certain conditions are changed; for example, nickel may deposit on silicon in alkaline solutions.[40]

Galvanic displacement follows the general reactions outlined below:

Reduction $M^{n+} + ne^- \rightarrow M^0$,

Oxidation $Sub \rightarrow Sub^{m+} + me^-$,

where M is a metal and Sub is a substrate, which may be a metal, semiconductor, or insulator.[25] In this study, metals include gold, silver, and platinum. Semiconductor substrates include silicon, germanium, gallium arsenide, and indium phosphide. (The case of silver on silicon will be discussed further below.)

Table 3.1. Reduction potentials

Reduction half-cell reaction	Reduction potential (V vs. SHE)
$Au^{3+} + 3e^- \rightarrow Au$	1.42
$Pt^{2+} + 2e^- \rightarrow Pt$	1.18
$Ir^{4+} + 4e^- \rightarrow Ir$	0.93
$Pd^{2+} + 2e^- \rightarrow Pd$	0.83
$Ru^{2+} + 2e^- \rightarrow Ru$	0.80
$Ag^+ + e^- \rightarrow Ag$	0.79
$Rh^{3+} + 3e^- \rightarrow Rh$	0.76
$Cu^{2+} + 2e^- \rightarrow Cu$	0.34
$Re^{3+} + 3e^- \rightarrow Re$	0.30
$Ge^{4+} + 4e^- \rightarrow Ge$	0.12
$2H^+ + 2e^- \rightarrow H_2$	0
$Ni^{2+} + 2e^- \rightarrow Ni$	-0.23
$SiF_6^{2-} + 6H^+ + 4e^- \rightarrow Si + 6HF$	-1.20

This report describes various sizes and morphologies of metal deposits obtained using simple procedures and bath solutions. The products are primarily characterized by scanning electron microscopy (SEM) and energy dispersive X-ray (EDX) analysis. For the Ag on GaAs samples, X-ray diffraction (XRD) and open-circuit potential (OCP) measurements were performed to gain insight into the growth mechanism.

The special case of silver on silicon was actually used to produce silicon nanowires. As outlined in the previous chapter, silicon nanowires are a potentially important type of nanoelectronic building block. The synthesis used is a modified literature preparation.[41-43] The basic procedure is to immerse a silicon substrate into a warm bath of hydrofluoric acid (HF) and silver nitrate ($AgNO_3$). (Although there may be subtle effects associated with the substrate orientation and nature and level of doping, the reaction still proceeds in the same manner.) Nanowires are produced as illustrated in Figure 3.2. Silver clusters are deposited and the silicon underneath them is oxidized to insulating silicon dioxide (SiO_2).[44] HF etches the silicon dioxide, causing the silver deposits to sink into the substrate.

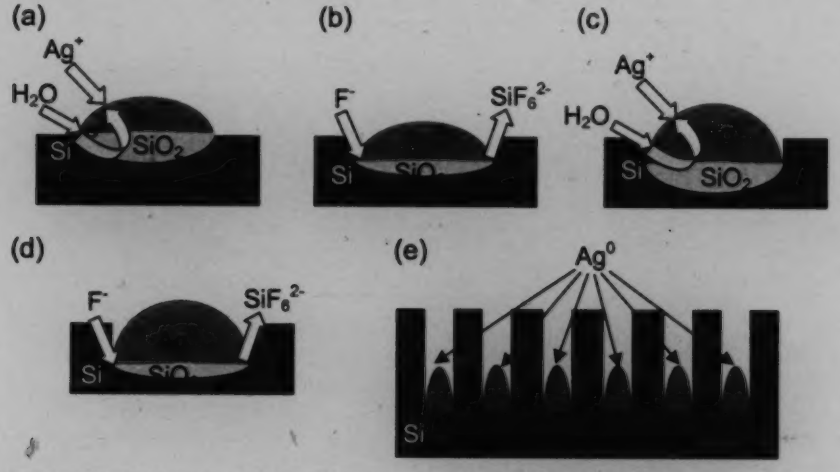

Figure 3.2. Etching mechanism of silicon nanowires. (a) Ag cluster deposits on the Si substrate and SiO_2 forms underneath the deposit. (b) SiO_2 is etched by HF, leading the Ag deposit to sink into the substrate. (c) The Ag deposit grows bigger and the substrate underneath becomes oxidized again. (d) The new SiO_2 formation becomes etched, causing the Ag to sink even farther. (e) As the cycle repeats, the deposits continue to sink, leaving unetched parts of the substrate standing. Unclear, however, is how the deposits develop into dendrites. (Adapted from reference 44.)

The silver clusters grow larger and develop into dendrites, while the silicon underneath the deposits gets oxidized to silicon dioxide. Again, the silicon dioxide then undergoes etching by HF, leading the deposits to sink farther. This cycle continues. As the deposits sink, they leave unetched (or less etched) parts of the substrate standing. Note that this is in contrast to the previously proposed mechanism in which standing nanowires were *preserved* by the silver dendrites.[41] The actual case is that if dendrites are found on the nanowires, these nanowires were simply less etched and the dendrites have not sunk as much. The deposits have been reported to be found at the interface of the bulk substrate and wires/pillars in an experiment controlled to avoid dendrites. The HF is necessary as silicon dioxide is a solid electrical insulator and prevents electron transfer to reduce the silver ions. Thus, this is a simultaneous galvanic displacement and etching process.

The chemical equations[44,45] that describe the process are given below.

Reduction	$Ag^+ + e^- \rightarrow Ag$
Oxidation	$Si + 2H_2O \rightarrow SiO_2 + 4H^+ + 4e^-$
Etching	$SiO_2 + 6HF \rightarrow SiF_6^{2-} + 2H^+ + 2H_2O$
Overall	$4Ag^+ + Si + 6HF \rightarrow 4Ag + SiF_6^{2-} + 6H^+$

The products were characterized by SEM, EDX, and XRD. Etching experiments to refine and hydride-terminate the nanowires were also attempted; however, these proved to be unfruitful.

3.2 Experimental

3.2.1 Materials

3.2.1.1 Reagents for substrate preparation and cleaning

All water used was deionized (DI) water from a Barnstead NANOpure Diamond purifier (resistivity=18 MΩ·cm). Sulphuric acid (H_2SO_4) (96-98%, ACS grade) was purchased from EMD Chemicals. Hydrogen peroxide (H_2O_2) (30%) was supplied by J. T. Baker. Hydrochloric acid (HCl) (36.5-38.0%, ACS

grade) was purchased from EMD Chemicals. Hydrofluoric acid (HF) (49%, CMOS grade) was obtained from J. T. Baker. Ammonium hydroxide (NH_4OH) (28.0-30.0%, Finyte grade) was supplied by J. T. Baker. Nitric acid (HNO_3) (68.0-70.0%, ACS grade) was obtained from Anachemia.

3.2.1.2 Bath reagents and additives

Hydrogen tetrachloroaurate(III) trihydrate ($HAuCl_4 \cdot 3H_2O$) (≥99.9%) was purchased from Aldrich. Silver nitrate ($AgNO_3$) of minimum 99.0% purity, ACS grade, was supplied by EM Science for use in the silicon nanowire/silver dendrite synthesis. Silver nitrate of 99.9995% purity was purchased from Strem Chemicals for use in all other experiments. Silver sulphate (Ag_2SO_4) (98%, ACS grade) was purchased from Strem Chemicals. Sodium tetrachloroplatinate(II) hydrate ($Na_2PtCl_4 \cdot xH_2O$) (42.44% Pt) was purchased from Strem Chemicals. Sodium dodecylsulphate (SDS) (ion pair chromatography grade) was obtained from Fluka Chemika. Hydrobromic acid (HBr) (48%, ACS grade) was purchased from Anachemia. Hydrochloric acid, sulphuric acid, and hydrofluoric acid are the same as above. 1-Butyl-3-methylimidazolium tetrafluoroborate (BMT) (≥97%) was supplied by Fluka Chemika.

3.2.1.3 Semiconductors

Indium phosphide (InP) wafers ((100) orientation, n-type, sulphur-doped, 0.001 Ω·cm) were obtained from CrystaComm. Small InP pieces were cut and sonicated in acetone and methanol for 10 min each and then dried with a nitrogen (N_2) stream. Each wafer piece was then placed in 100 mL of 1:1 49% HF:H_2O for 10 min to etch the native oxide, followed by dipping into 5 beakers of DI water for 2 min each and drying with N_2.

Gallium arsenide (GaAs) wafers ((100) orientation, n-type, 0.001 Ω·cm) were purchased from ITME. Small pieces were cut and sonicated in acetone and methanol for 10 min each and then dried with N_2. To etch the native oxide, each piece was then placed into a solution of 4:1:100 H_2SO_4 (96-98%):H_2O_2

(30%):H_2O for 2 min, then 1:3 HCl (36.5-38.0%):H_2O for 2 min. The wafer was then dipped into 5 beakers containing DI water for 2 min each and dried with N_2.

Germaninum (Ge) wafers ((100) orientation, p-type, gallium-doped, 0.018-0.036 Ω·cm, 500-μm thickness) were purchased from Umicore. The wafer pieces were degreased in an ultrasonic methanol bath for 10 min, in boiling dichloromethane for 10 min, and then in an ultrasonic methanol bath for 10 min again. Each piece was placed into a 1:4 NH_4OH (28.0-30.0%):H_2O solution for 5 min to etch the native oxide. After etching, the wafers were thoroughly rinsed with DI water and dried with N_2.

Silicon (Si) wafers ((100) orientation, n-type, phosphorus-doped, 0.5-1 Ω·cm) were obtained from Silicon Quest International. Small pieces were cut and sonicated in acetone and ethanol for 10 min each and rinsed with DI water. The pieces were then put into dilute HF solution (1-2%) for 10 min to etch the native oxide. No rinsing was required as the next step involved etching in HF.

3.2.2 Synthesis procedure

3.2.2.1 Metal deposition

In dark lighting conditions, the cleaned (degreased and etched) substrate of approximate size 4 mm × 4 mm was placed in a vessel containing an aqueous solution of the metal salt and any applicable bath additive, either an acid or surfactant, diluted to 10 mL. After the set reaction time, the substrate was removed and dipped in DI water and methanol and dried using N_2.

3.2.2.1.1 Au on InP

Samples were prepared using 9×10^{-4} mol/L $HAuCl_4$ and an acid on InP(100) substrates as described above. When H_2SO_4 was used, the reaction time for a 0.1% acid solution was 1 h, and for 2% 30 min. For HBr, the reaction times for 0.1% were 1 h and 24 h, and for 2% 30 min and 24 h. Experiments with HCl

were performed in a likewise manner as for HBr, except that trials at 2% were done at 30 min and 3 h.

3.2.2.1.2 Pt on InP

Samples were prepared with 9×10^{-4} mol/L Na_2PtCl_4 and H_2SO_4 on InP(100) substrates as described above for a reaction time of 1 h. H_2SO_4 concentrations were 0.4%, 1%, and 2%.

3.2.2.1.3 Ag on InP

Samples were prepared on InP(100) with 9×10^{-4} mol/L $AgNO_3$ and 2% H_2SO_4 for reaction times of 1 h and 3 h, and 10^{-3} mol/L $AgNO_3$ with no acid for 1 h and 3 h.

3.2.2.1.4 Ag on GaAs

These samples on GaAs(100) were prepared with concentrations of 10^{-5} mol/L, 10^{-4} mol/L, and 10^{-3} mol/L of $AgNO_3$ for reaction times of 10 min and 30 min. Samples prepared with 10^{-3} mol/L were prepared with reaction times of 1 h, 3 h, and 21 h also. Some samples were prepared with 10^{-3} mol/L Ag_2SO_4 for reaction times of 30 min and 1h.

3.2.2.1.5 Ag on Ge

Samples were prepared with 10^{-3} mol/L $AgNO_3$ and a surfactant on Ge(100) substrates. One sample was prepared with 200 μL of BMT for 3 h. Other samples were prepared with SDS with concentrations of 10^{-3}, 3.0×10^{-2}, 5.0×10^{-2}, and 8.0×10^{-2} mol/L for a reaction time of 3 h, and 10^{-3} and 2×10^{-3} mol/L for a reaction time of 24 h.

3.2.2.2 Si nanowires and Ag dendrites (Ag on Si)

3.2.2.2.1 Etching synthesis

The cut pieces of Si(100) were placed in a warm bath (~50°C) of 5 mol/L HF (~10%) and 0.02-0.04 mol/L $AgNO_3$ for 1 h. The polytetrafluoroethylene (PTFE) or polypropylene (PP) container was covered with a PTFE block or loose PP lid in order to avoid excessive evaporative losses without overpressurizing the system. After synthesis, the samples were rinsed with an excess of water and laid to air dry on absorbent pads.

3.2.2.2.2 Etching refinement

After peeling off the loose silver dendrite film, samples were dispersed in ethanol either by sonicating scrapings from the substrate or sonicating the substrate itself. Because SEM revealed much silver deposition in the dispersions of early trials, in later trials the mixture was discarded after 5 min of sonication, followed by sonicating the substrate further in fresh ethanol for 10-15 min. To the resulting dispersion was then added 1-4% HF and 10-26% HNO_3 to etch down the size of the wires and to separate large pillars or belts into nanowires. The mixture then went through cycles of centrifugation, supernatant removal, and sonication in fresh water/ethanol in order to rinse the product. Because of the HNO_3, the wires have an oxide coating. In order to etch this coating and to generate a hydride-terminated surface, the wires were etched in 5% HF alone. The product then went through a rinsing procedure similar to that for rinsing out HF/HNO_3. After the final sonication, a drop from the dispersion was drop-coated onto a piece of silicon wafer and a Fourier-transform infrared (FTIR) spectrum was taken (with the bare silicon wafer as background). The details on the FTIR spectrometer and conditions are provided in the previous chapter.

3.2.3 Characterization

3.2.3.1 Scanning electron microscopy (SEM)

Characterization by SEM was performed on the Hitachi S-4800 with conditions provided in the previous chapter.

3.2.3.2 Energy dispersive X-ray spectrometry (EDX/EDS)

EDX analysis was performed with the Oxford Instruments Inca x-sight detector built into the SEM. Conditions are as described in the previous chapter.

3.2.3.3 X-ray diffractometry (XRD)

Powder XRD was conducted on the Bruker AXS D8 Discover and Inel XRG 3000 with conditions as described in the previous chapter.

3.2.3.4 Open-circuit potential (OCP) measurements

Open-circuit potential measurements were performed on a PAR 263A potentiostat from Princeton Applied Research with Pt and Ag/AgCl as the auxiliary and reference electrodes, respectively. A copper wire was attached to the GaAs(100) substrate with nickel paste such that the connection made no contact with the solution. The substrate was immersed in DI water for 100 s, after which $AgNO_3$ was added to make the final concentration 10^{-3} mol/L. The OCP was measured for 500 s after the salt addition. The three test cases included an as-cut substrate, a substrate with unexposed edges, and a substrate with unexposed edges and half of its surface abraded with sandpaper. The samples with no edges were prepared by covering the edges and back of the substrate with epoxy. The scratching on the third sample was used to increase surface area.

3.3 Results and Discussion

3.3.1 Au on InP

3.3.1.1 Results

When gold was deposited on InP(100) using H_2SO_4 as a bath additive, regular and semi-regular polyhedral shapes were obtained (see Figure 3.3a, c). These shapes included triangular and hexagonal plates, five-fold twinned structures, and rods, among others. There were also irregularly shaped particles that were facetted. The sizes of these particles were about 100-150 nm. There was rather uncontrolled deposition at local defects such as scribe lines or edges, as the deposition here was either agglomerated clusters or spikes or dendrites (see Figure 3.3b). For the sample prepared with 0.1% acid for 1 h, there was sparser deposition compared to that prepared with 2% acid for 30 min. The sample with

Figure 3.3. Au on InP with H_2SO_4. (a) Regular polyhedral shapes obtained with 0.1% acid for 1 h. (b) Same conditions as for (a) but at substrate defect (local cathode) near the edge. (c) Regular polyhedral shapes obtained with 2% acid for 30 min. The particle density is higher, causing coalescence of particles. (d) Same conditions as for (c) but close to edge (global cathode).

higher acid concentration also had more deposits near the edges due to a global cathodic effect (see Figure 3.3d), as opposed to only the spiky deposition obtained at local defects for the one at lower acid concentration. (The edges and corners of the substrate are collectively a global cathode, while the centre is a global anode.)

When the acid was changed to 0.1% HBr, the deposition consisted of disordered shapes with dense, spiky deposition at local defects. At a deposition time of 24 h (see Figure 3.4a), there was simply more deposition and etching as compared to 1 h. EDX confirms that the deposition is gold (Figure 3.4b). When the concentration was changed to 2% for 30 min, regular and semi-regular polyhedral shapes appeared with sizes similar to those found for H_2SO_4. In Figure 3.5, there can be seen icosahedra, decahedra, pentagonal prisms (elongated decahedra), cuboctahedra, truncated tetrahedra, and hexagonal and triangular plates. Again, local defects promoted uncontrolled growth consisting of spikes, similar to that seen in Figure 3.3b. When the reaction was allowed to proceed for 24 h, the particles in the centre of the substrate increased in size and began to coalesce, though their original shapes can often still be distinguished, as shown in Figure 3.6a. The deposition at local defects was thickened and began to smooth out due to coalescence (Figure 3.6b, c).

When the acid was changed to 2% HCl, the deposition was similar to that obtained with 2% HBr. Polyhedral shapes were seen at 30 min in larger quantity

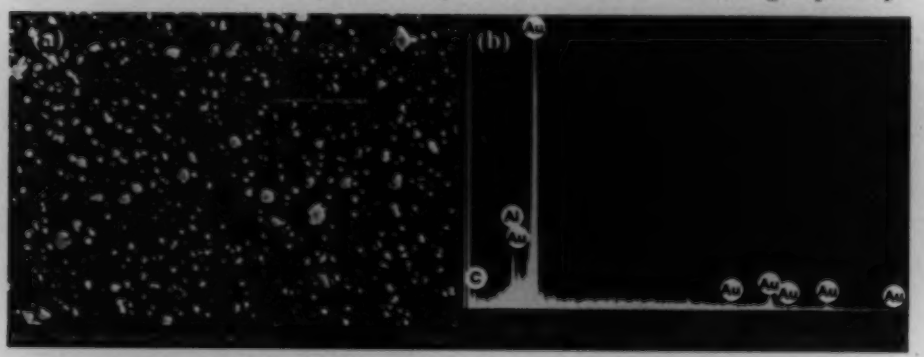

Figure 3.4. Au on InP with 0.1% HBr for 24 h. (a) The particles are irregularly shaped and there is extensive etching. (b) EDX spectrum taken of metal deposition overhanging the substrate edge; hence, there is no In or P signal. The C and Al signals come from the carbon paste and aluminum stub used in SEM preparation.

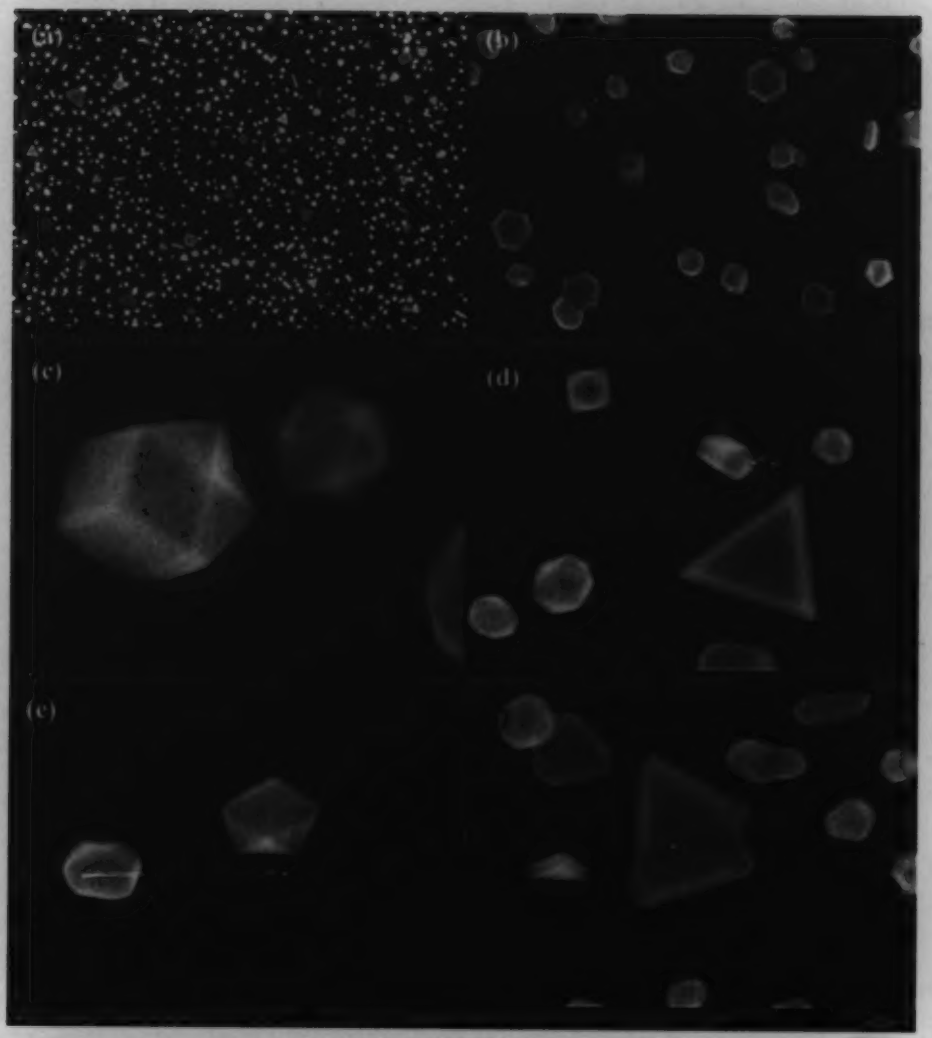

Figure 3.5. Au on InP with 2% HBr for 30 min. (a) and (b) Overall surface showing the various particles at different magnifications. (c) A pentagonal prism (or elongated decahedron) (left) and an icosahedron (right). (d) Five-fold twinned structures, a cuboctahedron (top left), and a triangular plate. (e) Decahedron (right). (f) 'Triangular plate' with a lateral twin (centre of image). Other facetted, irregularly shaped particles may also be seen throughout the images.

and there were larger particles and coalescence at 3 h. At a concentration of 0.1%, there was less deposition as compared to HBr at the same concentration. When the reaction time increased, there did not appear to be any deposition (except at locally active sites [defects]), but there was a lot of etching.

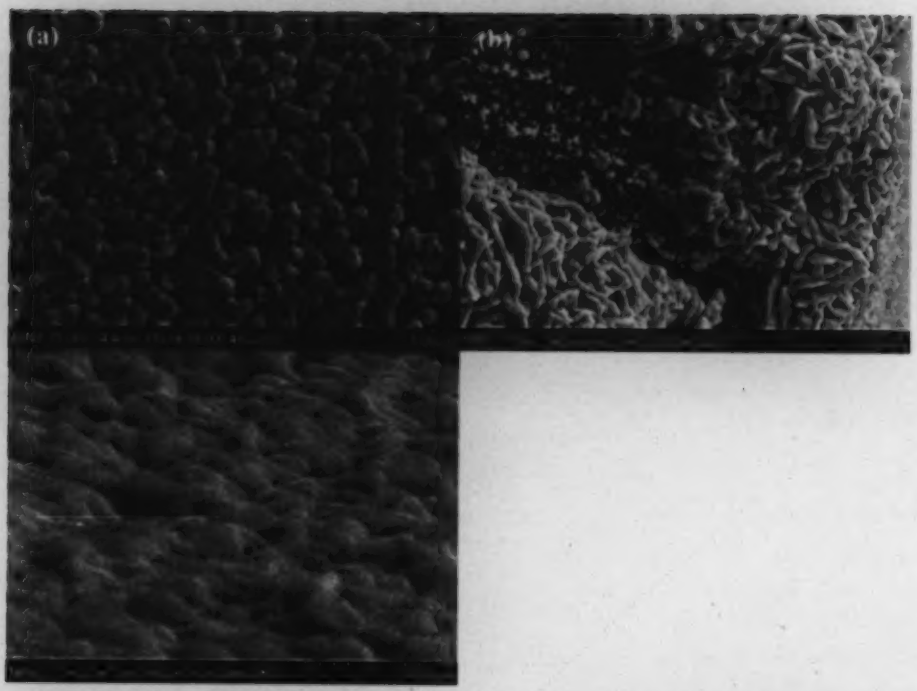

Figure 3.6. Au on InP with 2% HBr for 24 h. (a) Coalescence of particles in the centre of the substrate. (b) Thick, spiky deposition at the edge. (c) Coalesced, partially smoothed film at a corner.

3.3.1.2 Discussion

The results of the gold particle deposition on indium phosphide closely resemble those previously reported.[46] Though not studied in detail, it appears that the effect of 0.1% H_2SO_4 after 1 h is similar to that of 2% H_2SO_4 after 30 min, except that the former case had sparser deposition.

When 2% HBr or HCl were used as additives, the resulting products were similar to those obtained with H_2SO_4, except there were fewer products obtained with HBr than with HCl. The amount of deposition was more similar to 0.1% H_2SO_4 after 1 h than to 2% H_2SO_4 after 30 min. This was also noted previously.[46] When the reaction time increased, products began coalescing together, though the original shapes were still evident. When 0.1% HBr or HCl was used, there was mostly etching. When the reaction time was 24 h for HCl, the etch pits were larger than those obtained with HBr and there was less metal deposition (as compared to both 0.1% HCl for 1 h and 0.1% HBr for 24 h), consistent with a

faster rate of reaction seen with HCl: what deposition there was had detached due to copious etching. Previously reported experiments indicated that the relative rates of deposition for the hydrogen halides is HF>HCl>HBr,[46] suggesting a slower reaction rate as the strength of the acid increases (for hydrogen halides). It is peculiar that a concentration of 2% for H_2SO_4, HCl, and HBr produces similar structures, while at 0.1%, H_2SO_4 and HBr/HCl produce different results.

The OCP experiments performed in a previous literature report[46] show similar behaviour in different acids (H_2SO_4, HF, H_3PO_4) of the same concentration and that the nucleation occurs within the first 100 s of deposition; thereafter, deposition consists of particle growth. The report concludes that this similarity in OCP behaviour is consistent with the similarity in particle size within and among samples. This would explain the similarity in particle size in this series of experiments as well.

We will now discuss the appearance for the myriad of shapes that were obtained. Lofton and Sigmund noted that even though there were so many synthesis methods in the literature, the same shapes appeared among them, and some syntheses produced a variety of shapes as well.[47] They explained these results as a consequence of twinning in conjunction with the stability of the close-packed {111} planes of the face-centred cubic (FCC) structure. We note here that the regular decahedron and icosahedron consist of 5 and 20 tetrahedra, respectively, in a twin relationship, albeit in a strained structure;[47,48] the tetrahedron is bound by the stable {111} faces. The truncated tetrahedron and the hexagonal and triangular plates have tabular faces of the {111} orientation. There were also cuboctahedra, cubes whose truncated corners are of {111} orientation or, conversely, octahedra with truncated corners of {100} orientation (the regular octahedron has eight {111} faces). There were facetted rods (needles) and other particles as well. These shapes and related shapes were seen previously by others for gold and other transition metals.[6,20,21,47-61] With the exception of the cuboctahedron and its final shape of the regular octahedron, this plethora of shapes all have at least one twin.[60] It is known that gold, silver, and silver halides have a lower stacking fault energy than most metals (47 ± 7 erg/cm^2 for bulk gold

and 19±3 erg/cm^2 for bulk silver).[47,62,63] The ease of twinnability of a material is related to a low stacking fault energy[62] and, furthermore, the stacking fault energy in the vicinity of a coherent twin is only a fraction of the stacking fault energy in the bulk.[64]

Nuclei may contain twins in order to maximize the {111} faces or they may develop twins soon after nucleation.[47-65] It is well known that twins cause re-entrant grooves (A in Figure 3.7) to appear in the growing particle, enabling further deposition, while ridges (B in Figure 3.7) inhibit deposition.[47,65-69] Even though the twin plane, flat faces, and the planes of the ridges and grooves are all of {111} orientation, the groove grows the most rapidly, as the atoms depositing in the groove are stabilized by the presence of more surrounding atoms.

This ridge-groove geometry accounts for the presence of triangular and hexagonal plates, since the edges consist of close-packed lines of atoms (accounting for the hexagonal or triangular geometry) and the edges grow much faster than the flat faces parallel to the twin plane (accounting for the plate geometry). In order for growth to continue indefinitely on a particular edge, the

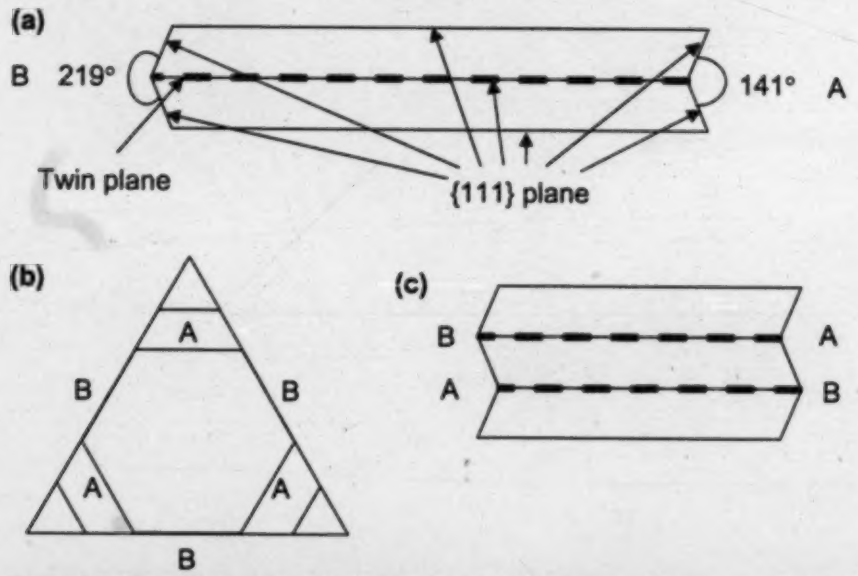

Figure 3.7. Re-entrant grooves in twinning. (a) A single twin causes three re-entrant grooves (A) to be present on alternating sides of a hexagon (in (b)), eventually causing it to fill out to a triangle (usually truncated tetrahedron for a single twin). The ridges (B) inhibit growth. (c) Two twin planes enable growth on all six sides so that the hexagon can grow very large. (Adapted from reference 47.)

edge must be regenerated by adjacent edges. A plate with an odd number ($2n$-1) of parallel twins becomes a triangular plate, since one set of sides (having n re-entrant grooves) grows faster than the other set (having n-1 re-entrant grooves) (see Figure 3.7b).[47,69] The faster-growing sides grow themselves out of existence, since the slower-growing sides cannot regenerate these faster-growing sides quickly enough. Thus, only the three slower-growing sides remain to form a triangle. Singly and triply twinned particles seem to be the most common for this class. A singly twinned particle results in a triangular plate if the twin is in the middle[67] and in a truncated tetrahedron (like a thick plate) with a twinned slab on its base if the twin is not equidistant from the two tabular faces.[68] A particle with an even number of parallel twins ends up as a hexagonal plate, as each set of alternating sides regenerates the other set, causing all six sides to grow equally quickly.[69] However, the most common number of twins for this class of particles is two.[68] The different contrast (in electron microscopy) at the edges of these plates reflects the presence of the grooves and ridges or the slanted sides in the case of a truncated tetrahedron. It should be noted that, because the development of some of the particles obtained was arrested, some of the particles with a hexagonal outline would have ended up being a triangular plate or truncated tetrahedron.

For the regular polyhedral structures (icosahedra, decahedra), re-entrant grooves at the vertices grew out, leaving the radial edges and axis points to be slow-growing B-type ridges.[47] After the particle has filled out to its final regular polyhedral shape, all faces grow at the same rate. Due to the lattice strain in these structures (72° between the tetrahedra [at least on average] vs. $\cos^{-1} \frac{1}{3} \approx 70.5°$ in an unstrained structure), these structures cannot grow very large like the plates.[47,48] However, the appearance of these shapes is likely, since the twinning and stacking fault energies are low, and the twinning energy and lattice strain can be compensated by the gain in stability due to the close-packed faces (for a small particle size).[47]

Although the ends of most of the rods cannot be seen face on, at least some of them are elongated decahedra. (An elongated decahedron is a

decahedron with a [flat-ended] pentagonal prism sandwiched between its two pentagonal pyramids.) Again, because of the strained five-fold symmetry, the diameters of the elongated decahedra cannot be very large. The growth of the elongated decahedra and other various one-dimensional structures can be accounted for by twinning, though some of the precise mechanisms need corroboration.[47,68]

Other facetted structures present may also be accounted for by twinning, with some types occurring more frequently than others.[47,68]

It is unclear as to why different acids or different acid concentrations have different effects on the number, size, and shape of particles. A factor to be considered is the solubility of the oxidation products in the acid. Since the process is galvanic displacement, the oxide may hinder the electrodeposition process if not dissolved into the bath solution. This is evidenced by the reaction stopping after 30 min if no acid is present.[46] The acid and concentration may also affect the relative growth rates of the different crystal faces, leading some shapes to be more thermodynamically driven than kinetically driven, and vice versa.[58,60]

Some other workers have noted regular polyhedral shapes of metal nanoparticles deposited on single crystal substrates via high vacuum methods.[49,50] Because these particular particles have an epitaxial relationship with the substrate, it may be possible that the particles grown in the present experiment also have an epitaxial relationship based on the atomic spacing of the contacting planes (both substrate and particle) and the interfacial energy. (The substrates in the present case may have an oxide layer regrown before placement into the salt bath; however, it is reported that silver particles evaporated onto Si(100) with native oxide have an epitaxial relationship with the substrate after annealing.[70])

3.3.2 Pt on InP

3.3.2.1 Results

There was very little deposition of platinum on InP(100). No platinum appeared in the EDX spectrum for deposition with 0.4% H_2SO_4. There was

deposition mostly only at defect sites when the concentration increased to 1% (Figure 3.8a). When the concentration increased to 2%, there were many dendritic structures on the surface (Figure 3.8c); however, EDX analysis indicates that there is no platinum in these structures, only indium and phosphorus and, in the bright areas, oxygen as well. Thus, it is likely that the bright areas are an oxide and the dark areas are where the oxide had peeled off of the substrate. The only piece of metal deposition to be found was a coiled nanowire, shown in Figure 3.8d.

3.3.2.2 Discussion

There was no significant deposition when trying to deposit platinum onto indium phosphide. Only defect sites were electrochemically active enough to allow deposition in the presence of 1% H_2SO_4. At 2%, there appears to be much

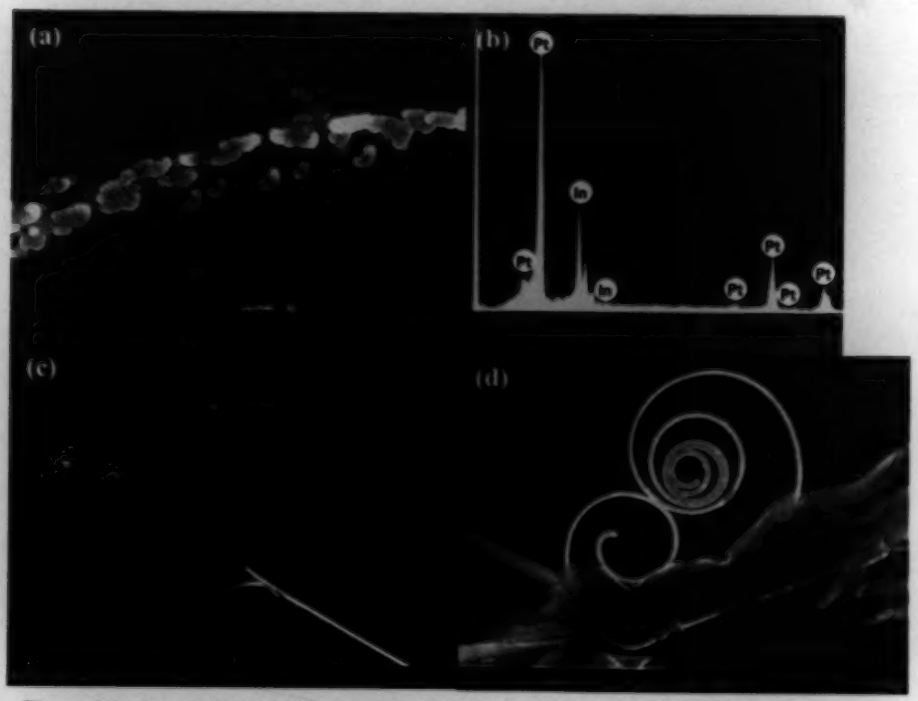

Figure 3.8. Pt on InP with H_2SO_4 for 1 h. (a) Platinum particles obtained with 1% acid. (b) EDX spectrum of Pt particle obtained with 1% acid. (c) Dendritic structure obtained with 2% acid. No platinum was found in this structure. (d) Platinum coil partially under oxide (2% acid).

substrate oxide formation, indicated by the shiny dendritic structures or their dark 'footprints,' which did not have as much oxygen. As for the platinum deposition, this could indicate one of several scenarios. (1) There was substantial platinum deposition initially, which then peeled off because either (a) platinum is perhaps not adherent to InP or (b) it formed on top of oxide and the oxide peeled off. (2) There simply was not much deposition at all. Compared to gold, it is expected that there would be less metal deposition, as the reduction potential of Pt^{2+} is lower than that of Au^{3+}. However, given the data, it is impossible to say what occurred and therefore more trials will have to be performed. Even if there is little deposition, there may still exist conditions (e. g., with a different acid or salt or concentration) that allow platinum to deposit more readily, as there is more silver deposition than platinum on indium phosphide with the particular platinum and silver salts chosen (*vide infra*), even though the reduction potential of Ag^{+} is lower than that of Pt^{2+}. The platinum nanowire coil may have been the result of deposition at a scratch. For example, the particles in Figure 3.8a appear to be deposition at a scratch. With a higher acid concentration, they may coalesce more quickly and form a continuous nanowire. If indeed some of the oxide desorbs and causes the deposited platinum to desorb with it, then we should not expect much platinum deposition to remain. The nanowire then has probably already desorbed and, due to strain effects, coiled up. (The strain may also be responsible for the desorption.) By coincidence, it somehow got wedged between partially desorbed oxide and the substrate.

3.3.3 Ag on InP

3.3.3.1 Results

When silver was deposited on InP(100) in the presence of 2% H_2SO_4, there was sparse deposition of particles that increased in both size (1 μm to up to 2 μm) and areal density as the reaction time increased from 1 h to 3 h (Figure 3.9a). When no acid was present, the particles were considerably smaller at a few tens to hundreds of nanometres (Figure 3.9b). When the reaction time increased

from 1 h to 3 h for no acid, there was less deposition and more etching. The less deposition observed may be due to the greater extent of etching, causing the deposition to not adhere. Though most of these particles were irregularly shaped, quite a few of them were plates of semi-regular shape. Figure 3.9c shows a truncated triangular shape. The EDX spectrum in Figure 3.9d confirms that the particles are composed of silver.

3.3.3.2 Discussion

In the presence of 2% H_2SO_4, there was sparse deposition of mostly irregularly shaped particles, with some particles showing a degree of order, since they were triangular or truncated triangular. When no acid was used, the particles were smaller, demonstrating the effect of an external acid, as was noted previously for gold on indium phosphide.[46] Since there were some particles with

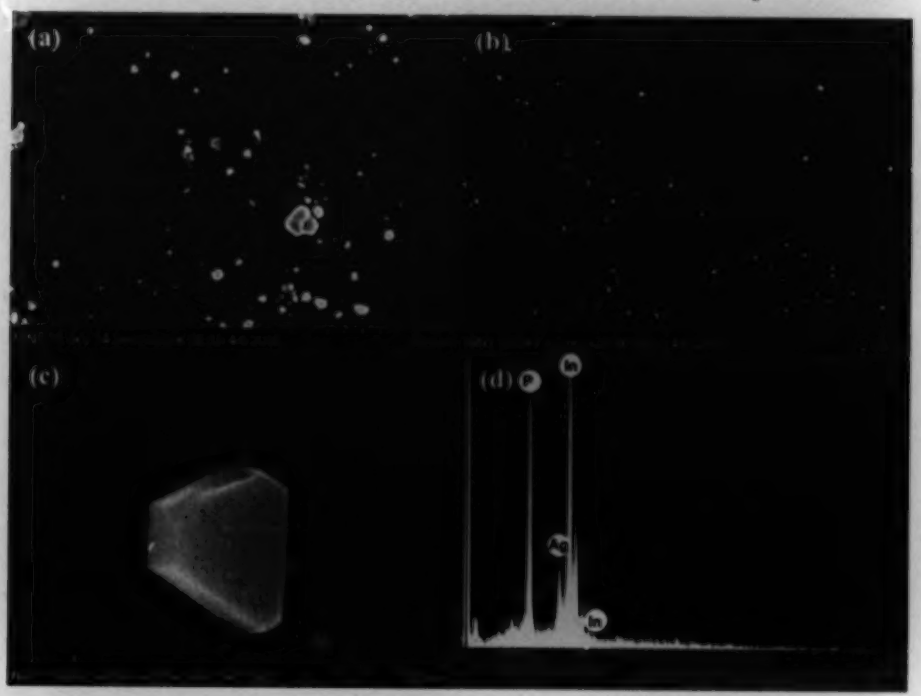

Figure 3.9. Ag on InP. Reaction time of 1 h. (a) With 2% H_2SO_4. At a reaction time of 3 h, there is a higher particle density. (b) With no acid. At a reaction time of 3h, there are fewer particles and more etching. (c) Truncated triangular plate (with 2% H_2SO_4). (d) EDX spectrum of a silver particle. The In and P signals come from the substrate.

a regular or semi-regular shape, it may be possible to form deposition like that obtained with gold by changing the parameters such as concentration of acid, type of acid, etc. Like platinum, it is expected that there would be less deposition than there was with gold based on the reduction potential.

3.3.4 Ag on GaAs

3.3.4.1 Results

At a concentration of 10^{-5} mol/L of $AgNO_3$, there was minimal deposition of silver onto GaAs(100). The texture of the substrate as seen under SEM was similar to that of the bare substrate that had undergone only the cleaning treatment (see Figure 3.10a). When the concentration increased to 10^{-4} mol/L, small particles (30-40 nm) can be seen at the centre of the substrate, being loosely templated by the texture of the underlying substrate. At the edges and corners of

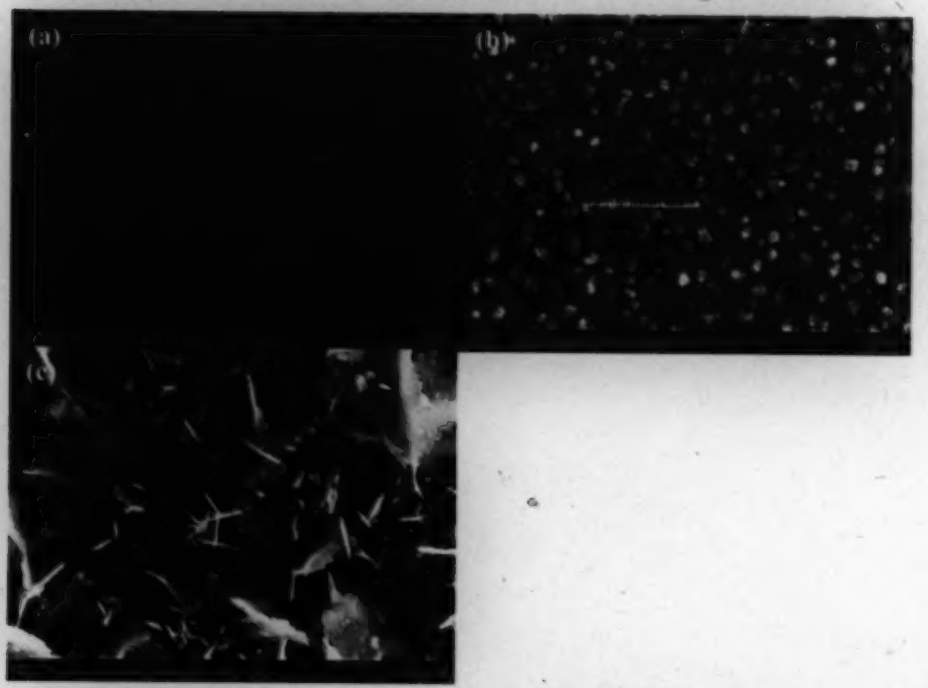

Figure 3.10. Ag on GaAs with very dilute $AgNO_3$. (a) Slight deposition on otherwise the texture of the unreacted substrate, obtained with 10^{-5} mol/L salt solution for 30 min. (b) Particulate deposition obtained with 10^{-4} mol/L for 30 min. (c) Plates at corner of substrate obtained with 10^{-4} mol/L for 10 min.

the substrate, these particles become plates, becoming larger as one progresses towards the edge. These plates may be up to 1 μm in size and are shown in Figure 3.10c. As the reaction time increased from 10 min to 30 min for both concentrations, there was slightly more deposition in both size of particles (50 nm for 10^{-4} mol/L, see Figure 3.10b) and overall coverage. The plates for the concentration of 10^{-4} mol/L also became slightly larger.

With a salt concentration of 10^{-3} mol/L for 10 min, the plates covered the whole substrate, not just the edges and local defects. As shown in Figure 3.11, many of the plates actually stood up perpendicularly to the substrate. Again, there was a higher concentration at the edges and corners and the plates became larger as well. The plates were about 10-20 nm thick, as seen in Figure 3.12. For a reaction time of 10 min, the plates in the centre were about 200 nm wide and had dispersed among them small particles similar to those present at lower concentrations. The width grows to about 500 nm at the corners. However, for a reaction time of 30 min (see Figure 3.13), the substrate was overall less densely

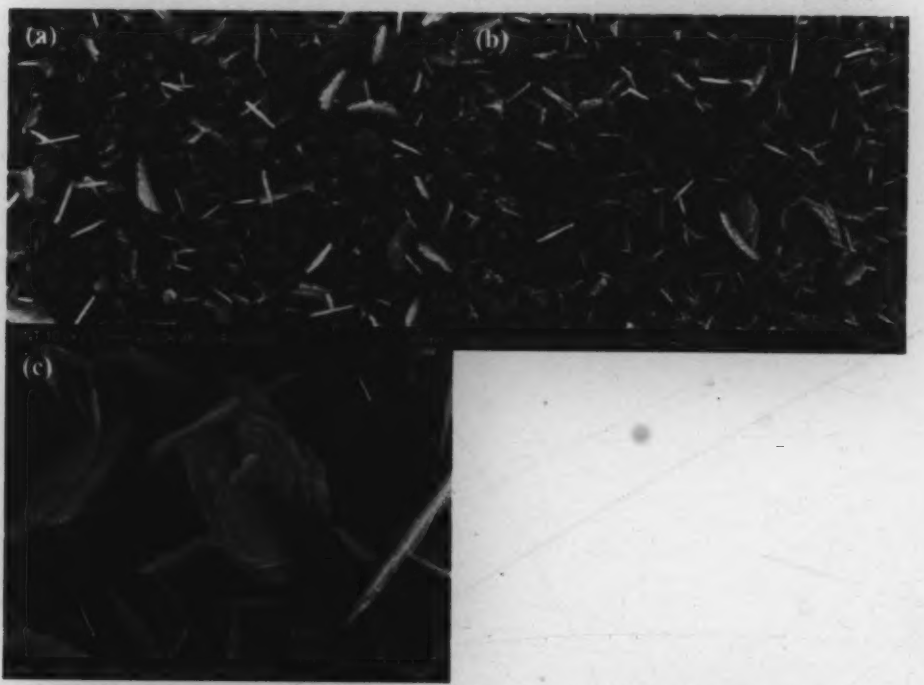

Figure 3.11. Ag on GaAs with 10^{-3} mol/L $AgNO_3$ for 10 min. (a) Plates in centre of substrate. (b) More plates at edge of substrate, virtually covering whole surface. (c) Larger plates that become stacked at corner of substrate.

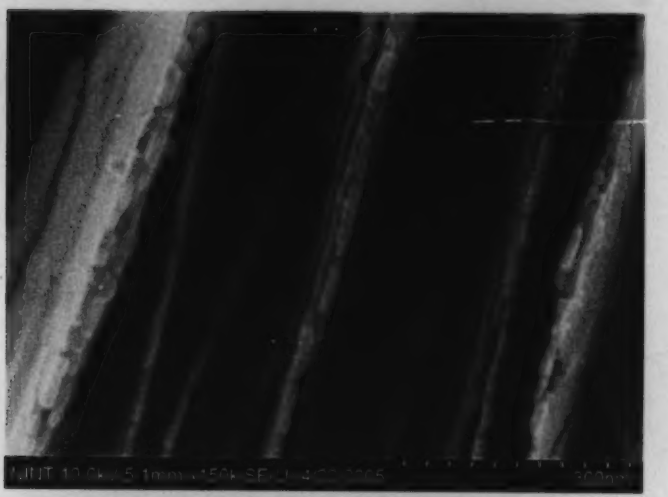

Figure 3.12. Thickness of Ag plates. The plates range from 10 to 20 nm thick. This particular image comes from a sample grown for 30 min with purging of the bath beforehand.

covered but had large stacks of plates in various configurations. Some stacks contained more than 100 plates lined up parallel to each other. These structures were several microns large with plates of 1-2 μm (plate aspect ratio ~100). At the edges of the substrate, these structures had larger plates, though sometimes the edge had structures with sizes only gradually increased from the centre to the edge. An EDX spectrum (Figure 3.13f) shows that the stacks are composed of silver.

As the reaction proceeded for 1 h (Figure 3.14), the structures became even larger with densely packed plates and extremely complex motifs, with what appeared to be small plates caved in at the end of the structure to form a flower-like pattern (Figure 3.14d). Some structures were smaller, depending on the local activity of the site. In the middle of the substrate, the overall 'background' between these structures (and apparently on which they sit) consisted of particles similar in size and coverage to those formed at low concentrations. However, towards the edges and corners, the particles gave way to plates. Furthermore, the large structures decorated the very edge as shown in Figure 3.15.

When the reaction was allowed to proceed for 21 h, the structures that formed were very large, often interconnecting each other (Figure 3.16a, b). These networks could extend hundreds of microns across the substrate. The height of

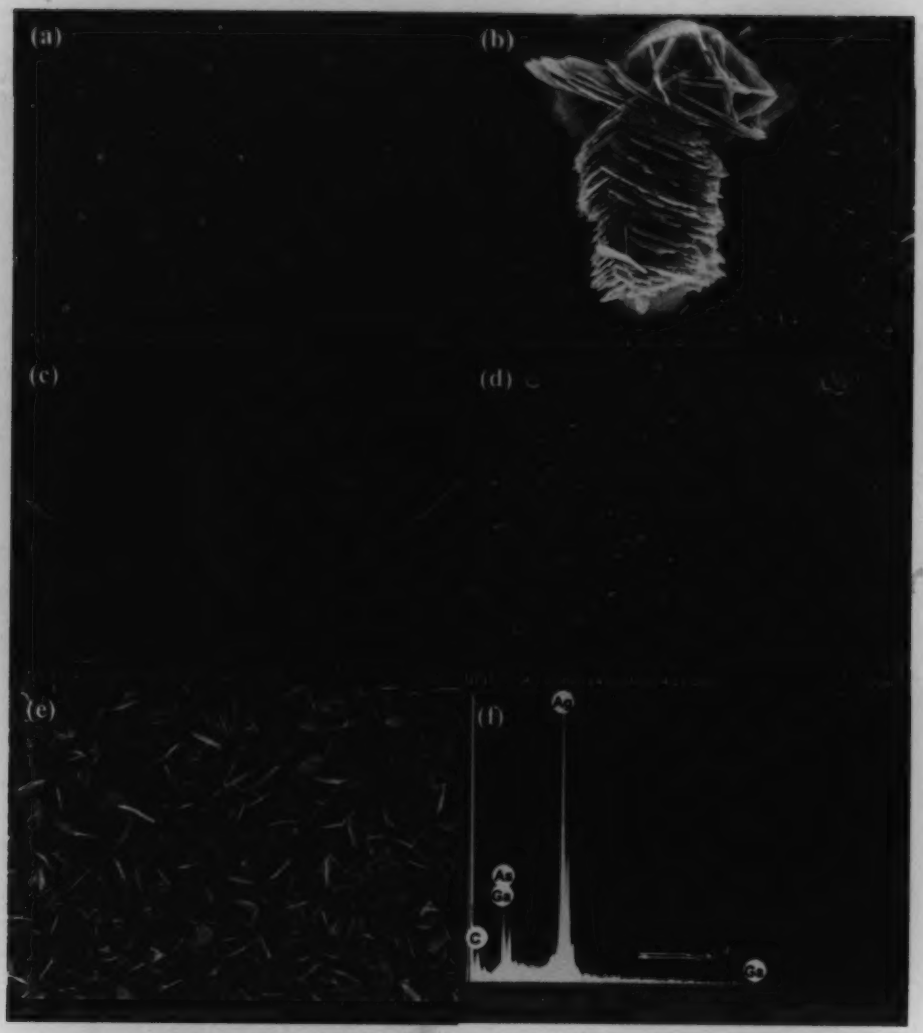

Figure 3.13. Ag on GaAs with 10^{-3} mol/L $AgNO_3$ for 30 min. (a) to (c) are taken from the centre of the substrate. (a) Overview. (b) Stacked-plate structure that is one of the 'particles' seen in (a). (c) Background of smaller plates and particles on which stacked structures lie. (d) Overview towards edge of substrate. (e) Background close to the edge. The edge looking face on is similar. (f) EDX spectrum of stacked-plate structure. The Ga and As signals come from the substrate and the C signal comes from post-synthesis surface contamination.

some of the structures was at least 30 μm, as determined by SEM of the edge with the substrate parallel to the electron beam. The sides of these structures were often plates overlapping each other to form a continuous cover, rather than edges of plates seen at lower reaction times (compare Figure 3.17c with Figure 3.14f). Coalesced masses and scaffolding were also found, as shown in Figure 3.17. The tendency towards a hexagonal shape for the plates is very apparent, though this

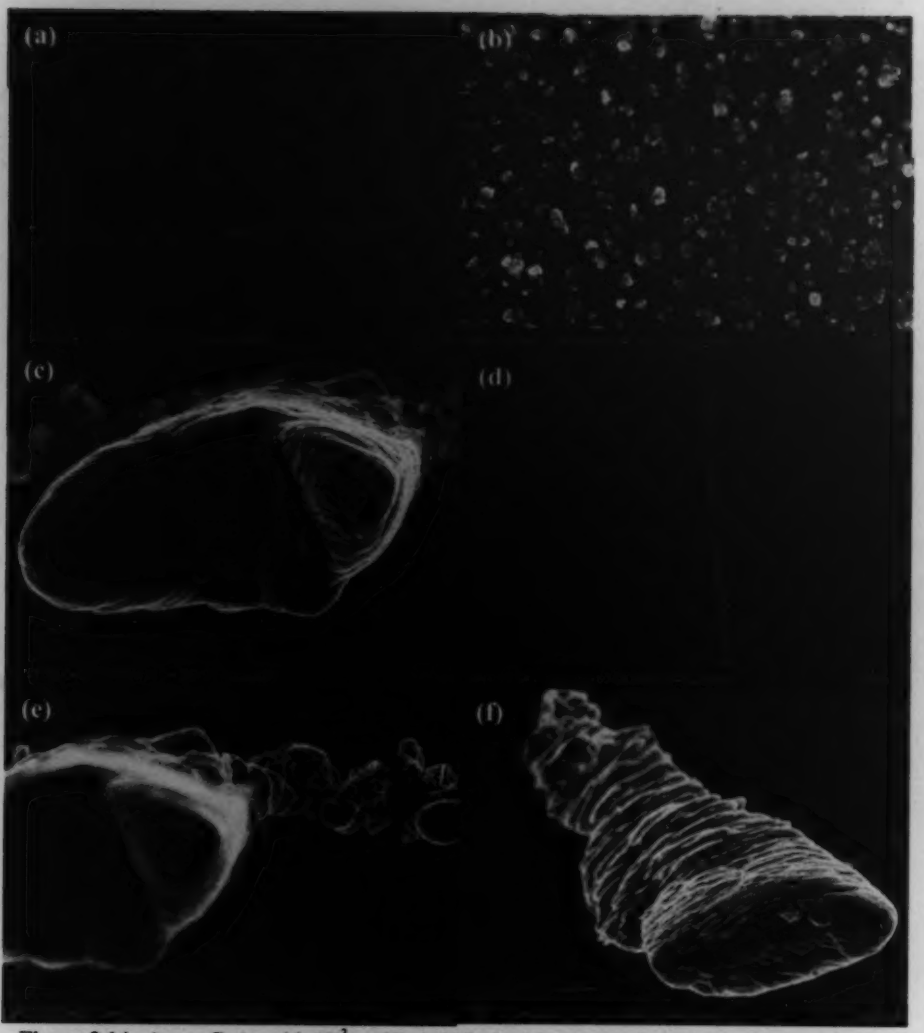

Figure 3.14. Ag on GaAs with 10^{-3} mol/L $AgNO_3$ for 1 h: centre of substrate. (a) Overview of substrate at low magnification. (b) Background on which large structures lie. (c) Large structure indicated in (a). (d) Close-up of boxed section in (c). (e) Smaller structures consisting of similar plates. (f) Large structure showing its side.

effect can also be seen at lower reaction times. On the smooth surfaces (flat plates or coalesced surfaces consisting of bent plates) were found small plates, usually in clusters (Figure 3.16d and Figure 3.17b), as if the smooth surfaces were acting as secondary substrates. The background of the substrate consisted of plates with size 3-5 μm in the centre, gradually diminishing in size towards the edges, finally becoming densely packed particles (see Figure 3.18).

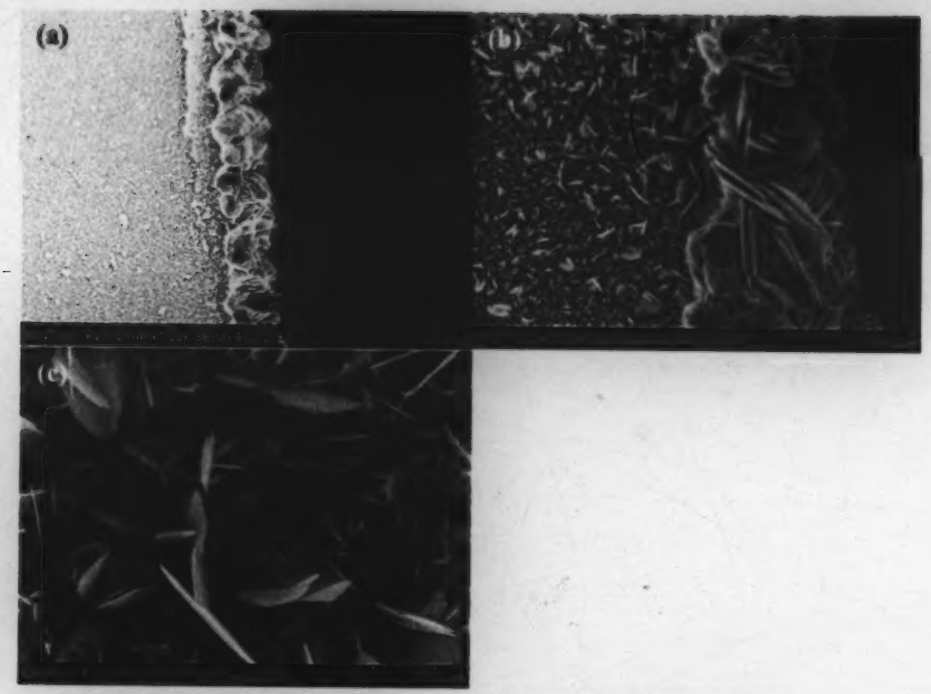

Figure 3.15. Ag on GaAs with 10^{-3} mol/L $AgNO_3$ for 1 h: substrate edge. (a) Edge of substrate. (b) Close-up showing stacks of large plates. (c) Close-up of background.

To investigate the effect of a deoxygenated solution, an experiment was performed in which the metal salt solution was purged with argon for 30 min before the substrate was added. There were single plates that lay flat on the background of sparse particles, in addition to the usual large structures obtained without purging (Figure 3.19a-c). In addition, Figure 3.19d shows that the edges of the large plates are decorated with tiny hexagonal plates (tens of nanometres) after 30 min of reaction. As one progresses from the centre to the edge of the substrate, the particles in the background evolve into plates (Figure 3.19e).

When Ag_2SO_4 was used, the plates still formed but did not arrange themselves in the same way. Most of the product consisted of large flat plates (order of tens of microns, aspect ratio ~1000) that lay flat on a background of smaller plates (Figure 3.20). These flat plates increased in size (individually) and in areal coverage (as a whole) as the reaction time increased. There were some small plates that stood up on the large flat plates and this is more apparent towards the edge of the substrate.

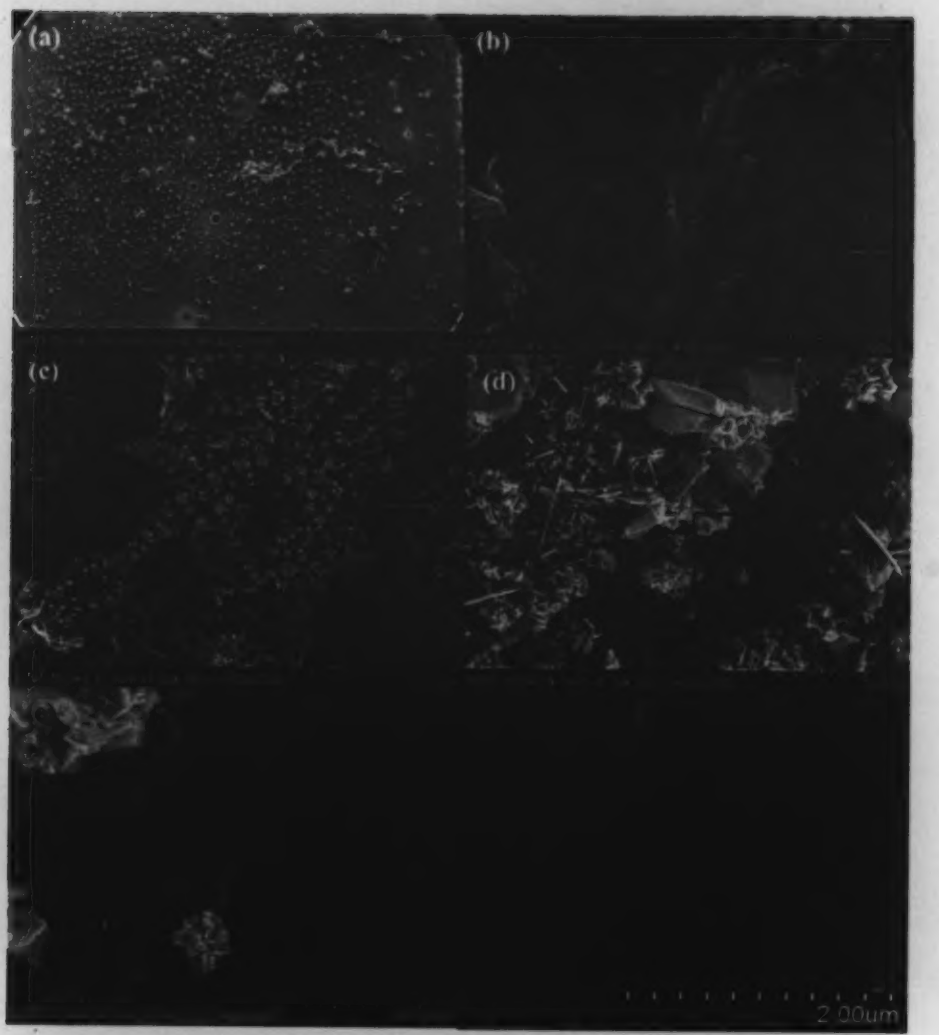

Figure 3.16. Ag on GaAs with 10^{-3} mol/L $AgNO_3$ for 21 h. (a) to (f) Different magnifications. (a) The surface appears to be bumpy. (b) Leaf-like structure. (c) Another large structure. (d) Close-up of boxed section in (c) showing the small features to be clusters of plates in various configurations. (e) Close-up of boxed section in (d) showing plates with hexagonal corners. (f) Close-up of boxed section in (e) showing growth from the edges and slight thickening of plates.

X-ray diffraction patterns were taken of samples prepared with $AgNO_3$ for 10 min and 21 h and with Ag_2SO_4 for 1 h. These spectra, along with those expected for standard samples, are shown in Figure 3.21. For $AgNO_3$, a small amount of both cubic-phase and hexagonal-phase silver can be seen after 10 min. After 21 h of reaction, both phases are seen very clearly, though the peaks of the two phases are not well resolved. These spectra show no discernible texture. In

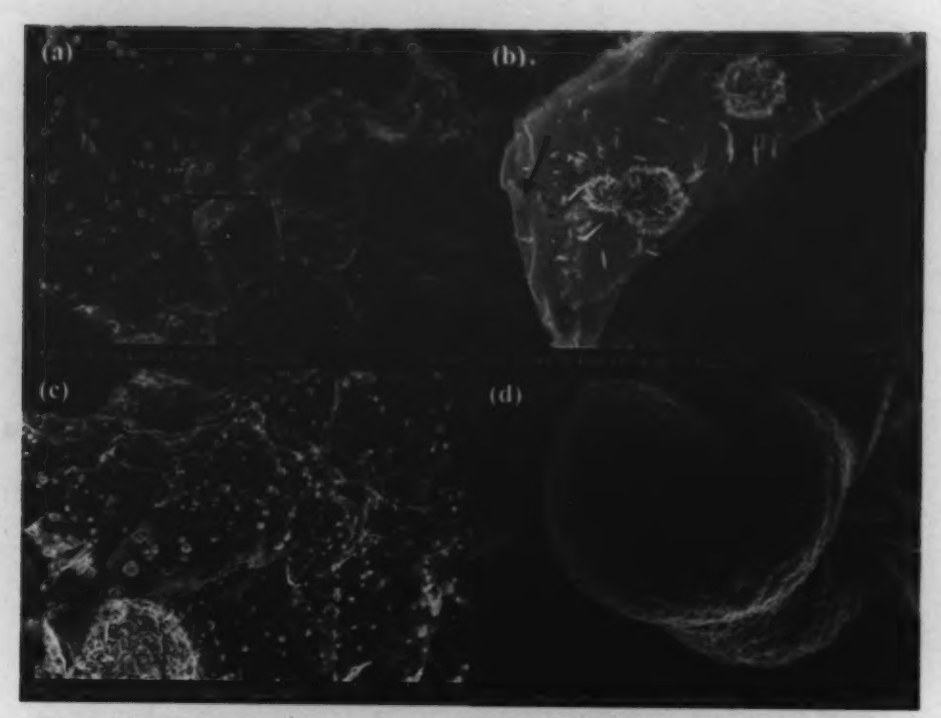

Figure 3.17. Coalescence of Ag plates. (a) to (c) Reaction time of 21 h. (a) Scaffolding structure. (b) Close-up of boxed section in (a) showing some character of individual plates. The arrow points to the edge of a plate. (c) Thickened, bulky mass in which some of the sides may be seen as the faces of coalesced plates and not their edges. (d) Structure consisting of many densely packed plates grown for 1 h, which is likely the precursor to a thickened mass.

contrast, the sample prepared with Ag_2SO_4 displayed a high degree of texture as the cubic-phase (111) peak was much higher than would be expected from a random sample. The two-dimensional XRD pattern also indicated that the contribution for this peak came from an arc next to the GaAs (200) peak. This unequivocally demonstrates that the plates (prepared with Ag_2SO_4) are of (111) orientation, as the plates of the Ag_2SO_4 sample are lying flat against the substrate. The arcing is due to the plates not all being perfectly flat against the substrate but having a distribution of angles with respect to the substrate surface. Open-circuit potential measurements, as shown in Figure 3.22, indicate similar behaviour in all three cases tested, though the exact potential values before and after salt addition were different. The potential jumped about 0.5 V after addition of $AgNO_3$. We will refer to all potentials with reference to the Ag/AgCl electrode. For the as-cut substrate, the potential oscillated around -0.22 V before salt addition and around

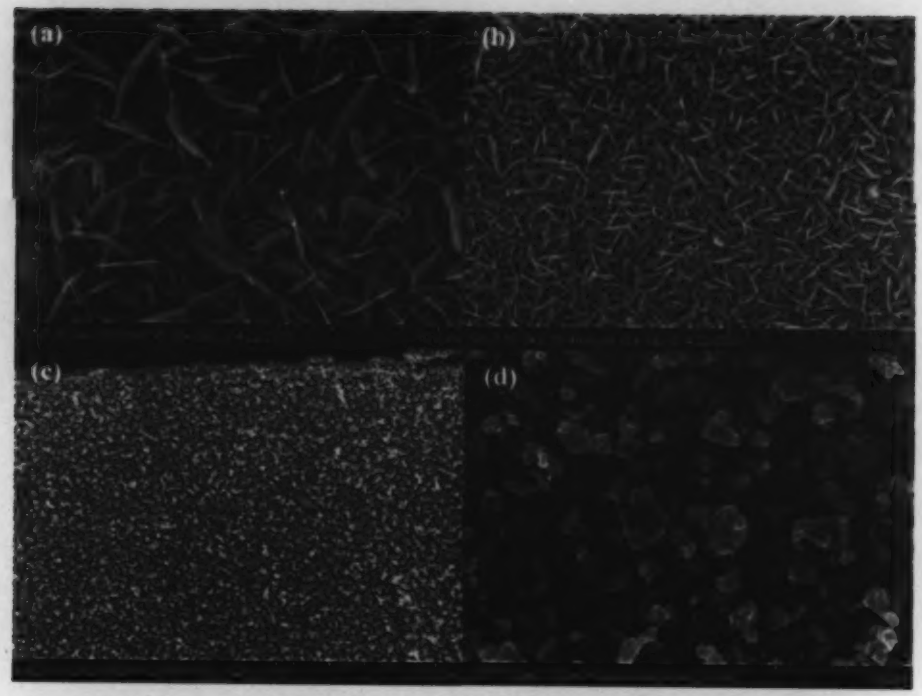

Figure 3.18. Ag on GaAs with 10^{-3} mol/L $AgNO_3$ for 21 h: background. (a) to (c) The texture on which the large structures sit as shown from the centre of the substrate towards the edge for the same magnification. (d) Close-up of texture of (c).

0.26 V after salt addition. The sample with no edges had its potential oscillating about the value -0.24 V before and 0.34 V after salt addition. In the case of the sample with no edges and half its surface scratched, the potential was around -0.31 V before and 0.15 V after salt addition, but these potentials varied more than for the other two cases, besides the oscillations. The oscillations for all the cases had peak-trough heights (twice the amplitude) of about 0.015 V and 0.005 V before and after addition of salt, respectively, and periods of 0.9 s.

3.3.4.2 Discussion

For the silver deposition on gallium arsenide using $AgNO_3$, it appears that the minimum concentration to obtain a reasonable amount of deposit is ~10^{-4} mol/L. At this concentration after 30 min, there is at least deposition of plates around 500 nm at the edges and corners. Small particles deposit in the centre of the substrate. If the time were increased, it may be possible to see these

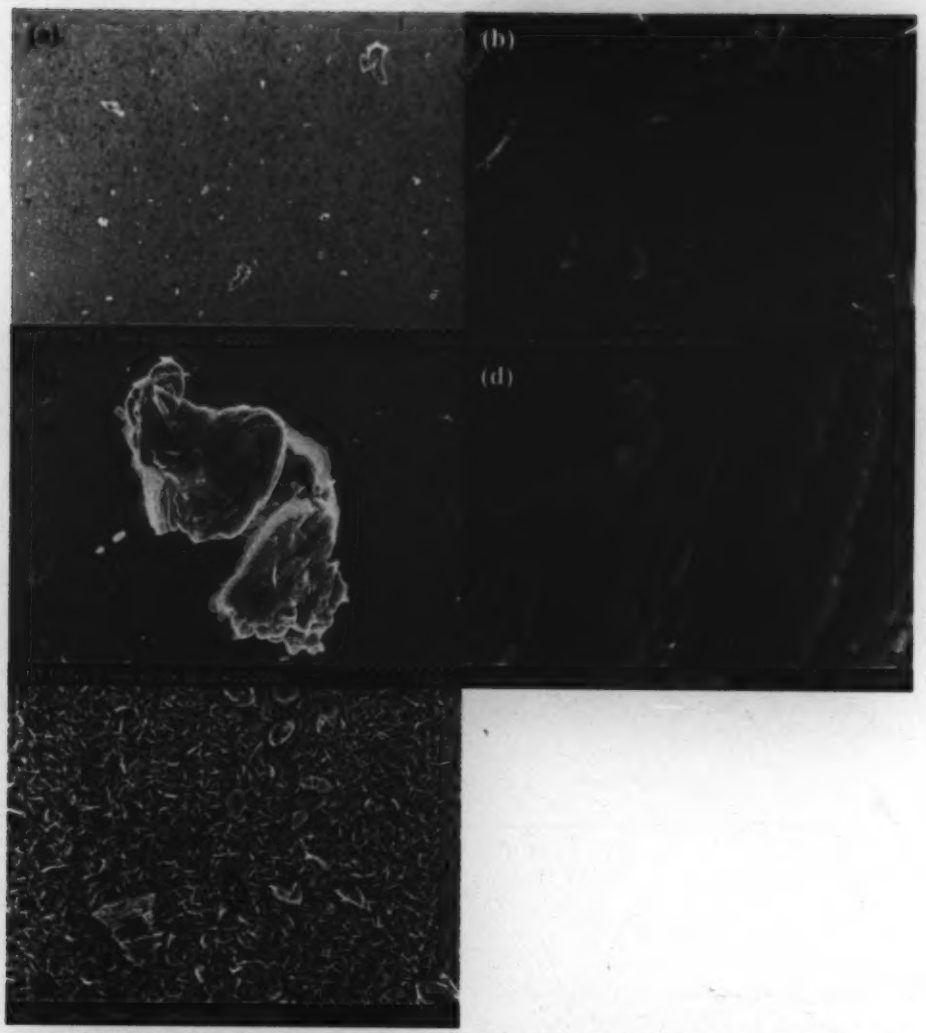

Figure 3.19. Ag on GaAs with pre-purged 10^{-3} mol/L $AgNO_3$ for 30 min. (a) Overview in centre. (b) Close-up of a dark spot in (a), revealing it to be a flat plate. (c) Stacked-plate structure. (d) Edges of plates are decorated with roughly hexagonal shapes. (e) Towards edge of substrate. There are more stacked structures and the background consists of plates (compare with small particles in background of (b)).

particles develop into plates and even stacked structures. (There was some clustering of particles, a possible precursor step to the stacked structures, and it is difficult to say how flat the particles were, i.e., they may have already developed into plates.) At a concentration of 10^{-3} mol/L of $AgNO_3$, the deposition of plates throughout the substrate is rapid and the plates self-assemble into large, beautiful, complex structures after only 30 min. These large structures are probably formed

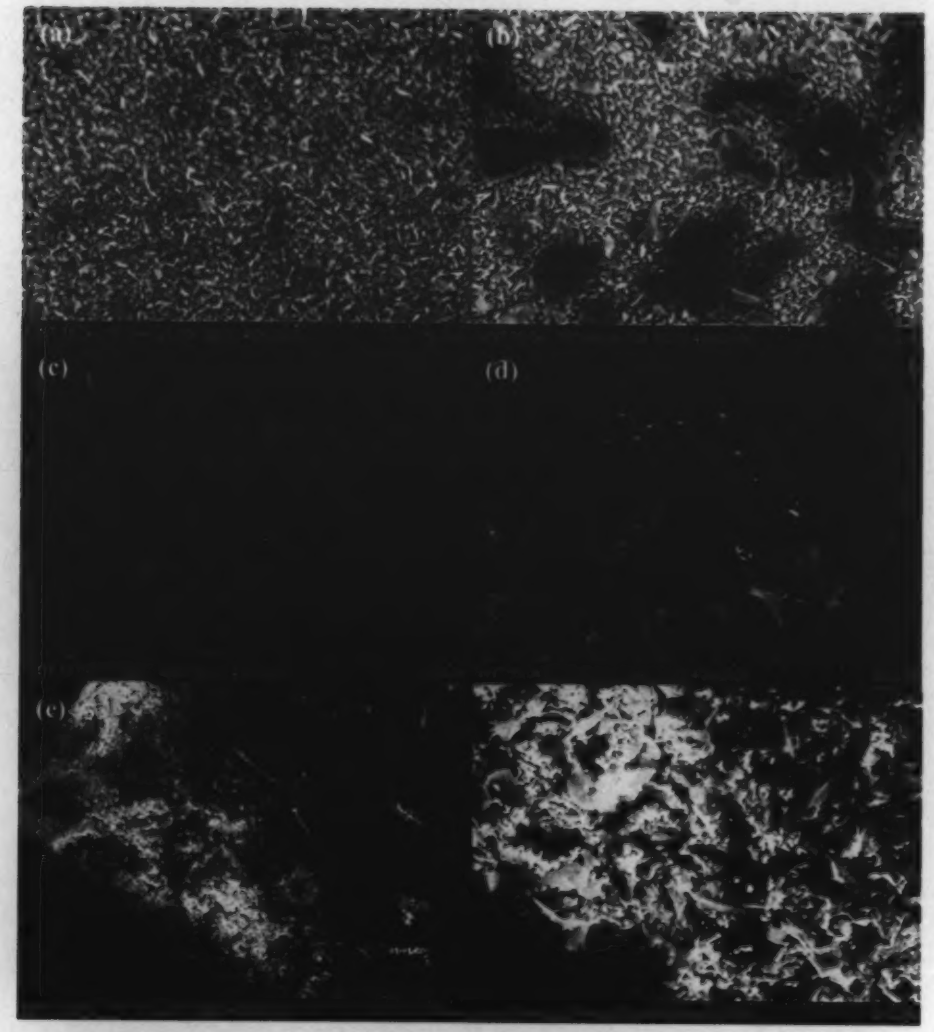

Figure 3.20. Ag on GaAs with 10^{-3} mol/L Ag_2SO_4. (a) and (b) Reaction time of 30 min. (a) Centre of the substrate. (b) Towards the edge of the substrate, showing larger flat structures. (c) to (f) Reaction time of 1h. (c) and (d) Centre of substrate, depicting much larger flat structures than for 30 min. (e) Corner of substrate. The smaller coverage of dark areas indicates the presence of many structures that are not flat but stand up on either the substrate or the flat plates. Smaller features, such as the edges of plates that stand up, appear lighter in the SEM due to charging effects. (f) Close-up of section of (e).

where the local activity of the site is higher, probably due to defects in the wafer. For example, in Figure 3.14a, it was determined by SEM that the structures forming a line did so where the substrate surface was not polished so evenly, indicative of sites of local cathodes. The local anodes would be the surrounding areas, the 'background.' The background consists of mostly plates with some

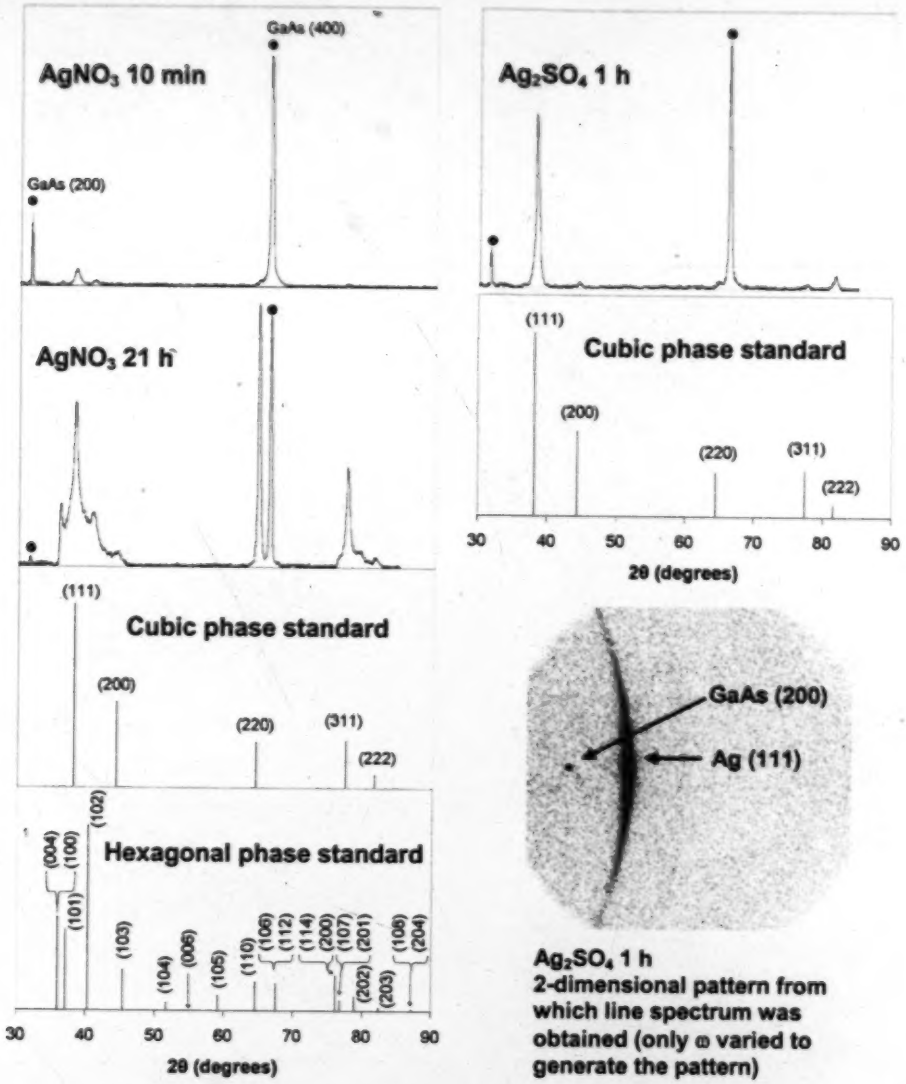

Figure 3.21. XRD spectra of Ag plates on GaAs substrate. The salts and reaction times are indicated. The concentration of the salts was 10^{-3} mol/L. The (006) reflection for the hexagonal phase standard is not visible at this scale but is included for the sake of completion. Circles indicate substrate peaks. Both cubic and hexagonal phases are present with $AgNO_3$ with the cubic phase possibly more dominant. The sample is highly textured with Ag_2SO_4.

particles after 10 min. After 30 min, the background overall appears less densely covered and has deposition that is a clear mix of particles and plates of varying size. After 1 h, it appears similar to that obtained with 10^{-4} mol/L: small, uniform particles evenly distributed. After 21 h, the substrate is again covered with the plates in general (with these plates being larger) and it has *very* large stacked

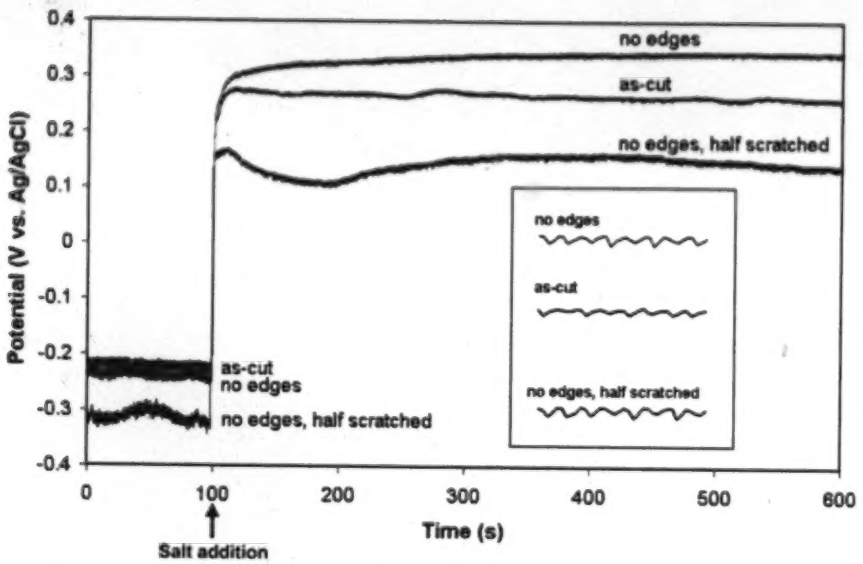

Figure 3.22. Graphs from OCP experiments performed of $AgNO_3$ on GaAs. The jumps in the graphs indicate the addition of the salt to variously prepared substrates. Inset shows the oscillatory behaviour in the graphs after salt addition. The period of the oscillations is about 0.9 s and the sampling period is 0.2 s.

structures. A possible mechanism is some type of Ostwald ripening process wherein the large structures grow at the expense of the small background particles.[71] Afterwards, the background again has even deposition that again grows into plates. This may be a periodic process. A possible reflection of this is that for some deposition times, the particle/plate size and deposition amount increase from the centre of the substrate moving towards the edge, whereas for others, they decrease. Also, in some samples, the edges are decorated with large structures, while in others, they are not (though this may be a consequence of the structures falling off the edge [in the case of Figure 3.18, it is unlikely that there were large structures decorating the edge as there is a gradual diminution of the background plates into particles]). In some samples grown for 30 and 40 min (not shown), there were more plates in the background, but the large structures were not as large as the ones presented here for 30 min and these structures generally consisted of looser clusters of plates. This indicates some sample-to-sample variation, yet may still be indicative of the Ostwald-like ripening process but at a different stage. Others have also noted an Ostwald ripening process for metal

nanoparticles on a conductive substrate.[71] They have also noted that, when compared to water, $AgNO_3$ and acidic solutions enhance the Ostwald ripening (for Ag), while basic solutions inhibit it. Instead of a periodic process, it may be that the Ostwald ripening occurs only until the large structures or its constituent plates reach a certain size, after which everything grows at a more uniform rate. (If this is the case, the Ostwald ripening is more likely to occur up to a certain size of the stacked structures and not the plates, as the plates remain very thin.) It would also be interesting to see if there is a depletion zone (of a certain radius) of the background material surrounding the large structures. Clearly, more trials will have to be done for various reaction times to see a definite pattern and to ensure reproducibility. Electrochemical measurements may give some insight into this phenomenon.

The deposition starts out as small particles and when they reach a size of around 50-100 nm, they have already evolved into plates with highly roughened edges. It is difficult to determine if the particles are flat below this threshold in the SEM. However, since the plate thickness is 10-20 nm, the nucleus is likely stable around this size or a little larger before it rapidly forms into a plate. The plates on the sample prepared with Ag_2SO_4 for 1 h are of the (111) orientation of the cubic phase. This is quite reasonable as plates have a large surface-area-to-volume ratio and the (111) planes are the most stable, being close-packed planes, enabling the surface energy to be minimized.[72] Even though the hexagonal phase is present in the samples prepared with $AgNO_3$, the plates are probably of the close-packed planes (the (004) planes in 3-index notation and (0004) in 4-index notation for hexagonal phase). For simplification, from this point forward, unless otherwise specified, we will use the cubic phase in order to refer to the close-packed planes and its contained lines of atoms. For example, we will refer to the {111} planes when discussing the close-packed planes for both phases and the <110> directions for the close-packed directions for both phases. (The possible issues concerning the coexistence of the two phases will be discussed later.) As the deposition time increases, it is clear that the plates favour a hexagonal or triangular shape or otherwise have edges that appear to be built up of smaller

hexagons or triangles, having corners that are 120° or 60° in angle (see Figure 3.11c, Figure 3.16, and Figure 3.23), corresponding to intersections of <110> lines of atoms (the close-packed lines). The hexagon seems to appear more often than the triangle, probably because atoms at the vertex would be more stable being surrounded by more atoms and/or because of the twinning mechanism as described above (twinning sequences that favour hexagonal shapes may be more likely than those for triangular shapes). Besides a twinning mechanism (more on this later), these (smaller) hexagons and triangles suggest that the plates grow through a dendritic growth mechanism before these shapes fuse together during further growth.

As these plates form, they evolve into complex stacked-plate structures. A

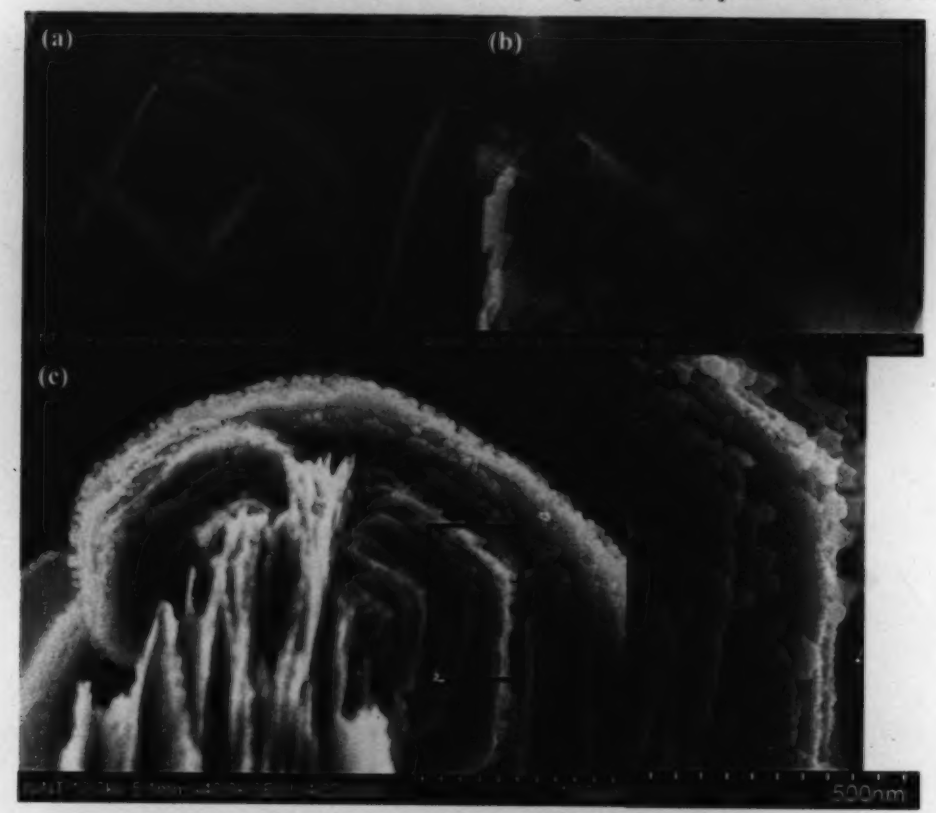

Figure 3.23. Ag plates with 120° and 60° corners. (a) Hexagonal and triangular plates. (b) A large plate with a more complex periphery having 120° and 60° corners (taken from a sample grown with Ag_2SO_4). Note the transparency of the plate. (c) Hexagonal plates taken from a sample in which the bath was purged with argon. (d) Close-up of boxed section in (c) showing the edges of the hexagonal plates to be decorated with smaller hexagons.

scenario of how one set of parallel plates can be in contact with another set of plates parallel to a different direction is described in Figure 3.24. Plane A1 sits on the substrate, then plane B1 nucleates at an (acute) angle α, then plane A2 nucleates at the junction of A1 and B1 parallel to A1 on the side of the junction

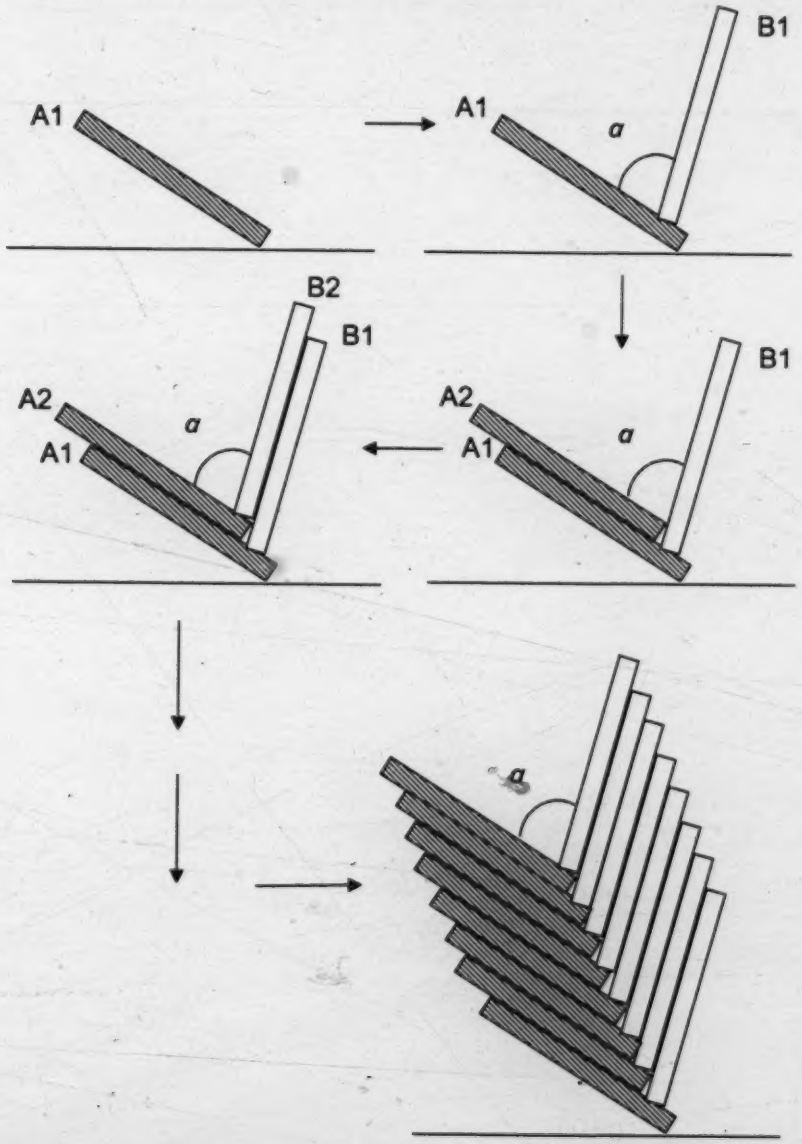

Figure 3.24. Schematic demonstrating successive nucleations. The two sets of plates are in different orientations. New plates nucleate at the junction in either of the two orientations (A-hatched, B-plain).

with angle α, then B2 nucleates on the A2-B1 junction parallel to B1 in a similar fashion, and so on. There exist cases where the two sets do not completely alternate, since the junction is most likely just as active in nucleating A planes as it is for B planes, as the nucleus probably cannot differentiate between the two planes. Actually, it is more likely than not that there is no perfect alternation within a stack. Nucleation can also occur on the obtuse side of the junction (supplementary angle of α or 180°-α).

This angle α is commonly ~70°, as seen from some sample measurements shown in Figure 3.25. The angle $\cos^{-1} 1/3 \approx 70.5°$ is the angle between intersecting {111} planes (in a cubic structure). For large flat plates that are hexagonal, it is also easily seen that new plates nucleate on a line parallel to one of the sides of the hexagon (Figure 3.26). This indicates that the new plates nucleate on <110> or close-packed lines of atoms and that the plate nucleus is probably a continuation of the original plate, until the direction of fast growth is 70.5° to the original plate. Hence, it would be as if the line of atoms is part of two intersecting, close-packed planes. Sometimes, the nucleus remains as a continuation of the original plate and appears as a parallel plate in close contact with the original. At other times, it appears as a totally different parallel plate that is in looser contact with the original. Figure 3.16f shows what appears to be the former case. Figure 3.27 shows a set of plates for which it is rather ambiguous as to which case to which it belongs. There are only three distinct <110> directions on a specific {111} plane and, along each direction, the new plate may grow in

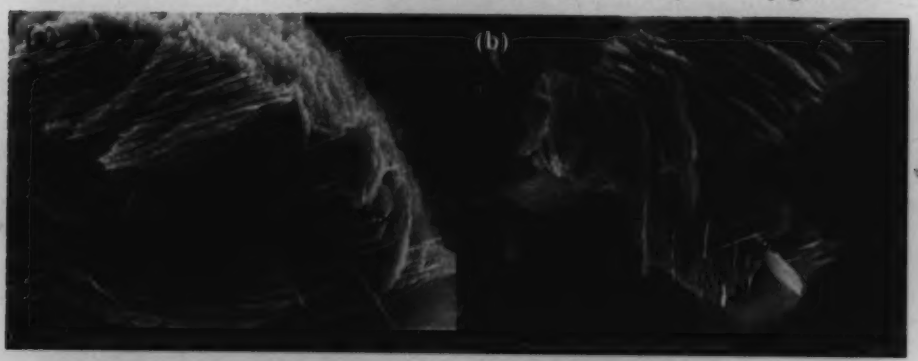

Figure 3.25. Measurements of angle of nucleation of Ag plates. Angles vary within a few degrees of 70.5°, or when measured from the obtuse side, 109.5°.

Figure 3.26. Nucleations of Ag plates parallel to edge of original plate. (b) Close-up of bottom right corner of (a). The indicated edges of the smaller plates are parallel to the indicated edges of the larger plate, with the smaller plates standing up. There are also smaller flat plates in the bottom right corner. Hexagonal and triangular corners are clearly seen in both the large and small plates.

Figure 3.27. Parallel Ag plates. It is unclear if some of the growth are distinct plates or if they are a thickening of other plates.

either of two twinned directions that are 70.5° to the original plate. Thus, there are six possible arrangements for a new plate with respect to the original, besides lying flat against the original. Depending on the arrangement, the overall structure may appear to have its plates caved in due to the many plates standing up on another plate but in different directions (the flower-like patterns in Figure 3.14 and Figure 3.28). In these cases, one would expect the nucleating edges of the plates to impinge on each other at 60°, similar to the situation in Figure 3.26. However, it is difficult to ascertain this in most cases since the original plate is often covered and for the reasons discussed below.

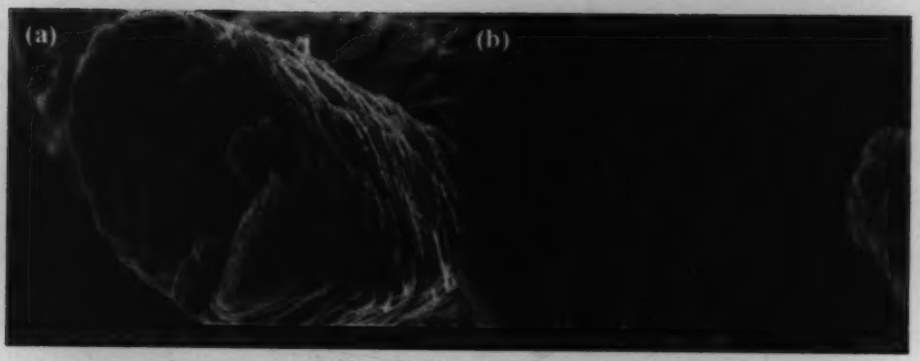

Figure 3.28. Complex structure showing caved-in Ag plates. (b) Close-up of centre of (a).

Though the plates are parallel to {111} and tend to nucleate on each other at ~70.5°, other angles may be found as well. These angles may appear due to impingement, the bending of plates, or for other reasons that are as yet unclear. Although it is often easy to identify junctions that are certainly a result of nucleation (a set of parallel plates in contact with another set of parallel plates), in some cases it is more difficult to distinguish between nucleation and impingement. The plates can bend very easily due to their thinness, since they are 10 to 20 nm thick and are translucent to the electron beam. This bending is more pronounced at higher deposition times. Besides the bending of a plate, it is possible (and possibly more likely) that plates may be forced from their original angle of nucleation, causing a bending of the junction. Though it is unclear how strong a plate adheres to the one on which it has nucleated, another possibility is that a plate can be forced from its original contact point. Possible though unlikely anomalies may include plates of other orientations; for example, the {100} planes are the second most stable in a face-centred cubic structure. (However, stacking faults and twins do not form on {100} planes,[63] making nucleation of new plates unfavorable. Also, reports on metal plates indicate they are of {111} orientation. Nevertheless, further study is needed to definitely rule out the possibility of planes of other orientations.) Another factor compounding the problem of angle measurement is that one really needs to measure the angle between the normals of plates. This is impossible to do on a two-dimensional image except for those plates that are perpendicular to the plane of the image and these are difficult to

find. Some plates are slightly tilted and therefore have a degree of uncertainty. When the plates are perpendicular to the plane of the image, it is impossible to determine if the edges contain hexagonal angles. One can only speculate that at least some of those nucleating at 70.5° do so along a close-packed direction and have corners with hexagonal angles. These complicating factors also affect the angle between impinging plates that have nucleated on the same plate.

As the angle measurement process has inherent error, it may be possible that instead of the 70.5° angle, the angle is 72°, which is the angle between the twin faces in a regular structure consisting of five-fold twins. However, as stated earlier, in a real five-fold twinned structure, the lattice is strained,[47,48] which indicates the unlikelihood of this angle in the case of these plates. In five-fold twinned structures, the twin planes are of {111} orientation. In the absence of a five-fold axis, twinning at {111} planes remains at 70.5°.

X-ray diffraction analysis raises some interesting issues. In the case of deposition with $AgNO_3$, XRD of a sample grown for 10 min shows weak peaks, as the deposition thickness is very thin. These reflections are of both phases of silver, though the cubic phase may be more dominant. (To definitely assign one phase as more dominant than the other, XRD would need to be performed on a standard sample containing equal amounts of both phases so that intensities can be normalized. Alternatively, one may use a sample of each phase, with both samples having the same amount of material and performing XRD with the same parameters. The former case, however, would also make it clear how well-resolved peaks are expected to be in a standard sample and thus a comparison may be made.) After 21 h, the reflections are merely stronger; the structural information remains the same. There are several possible explanations to account for the existence of the two phases and the possible 'smearing' of the peaks together. Note that the thinness of the plates does not appear to be a factor in any peak broadening, as the (111) peak obtained with the Ag_2SO_4 sample has roughly the same width as that of the substrate peak.

(1) There is likely a certain probability that a nucleating plate will be of the hexagonal phase and a certain probability it will be of the cubic phase.

(2) There may be twins and stacking faults of the close-packed planes within the plates. Cubic-phase packing consists of an ABCABC motif, whereas the hexagonal phase an ABAB pattern (see Figure 3.29). An intrinsic stacking fault is one in which an extra plane is inserted into a normal sequence (e. g., ABCABCACBCABC). An extrinsic stacking fault is one in which a plane is missing (e. g., ABCABCBCABC). A twinning sequence may be ABCABCBACBA. Note that if the crystal stopped after the first plane beyond the twin plane with a sequence of ABCABCB, this could be considered as a mere stacking fault. Complex sequences, such as ABCBCACB, are likely to occur as well. These defects may cause the peaks to smear together since the close-packed planes in the hexagonal phase are farther apart than in the cubic phase (larger d-spacing). These sequences may be introduced during growth or they may already be present in the nucleus, in which case, factor (1) is a subclass of factor (2). Likely, twins and stacking faults may be introduced during both nucleation and growth, though in any case, they occur readily as the plates can grow very large (see above in section 3.3.1.2 on Au on InP for twinnability and stacking fault energy).

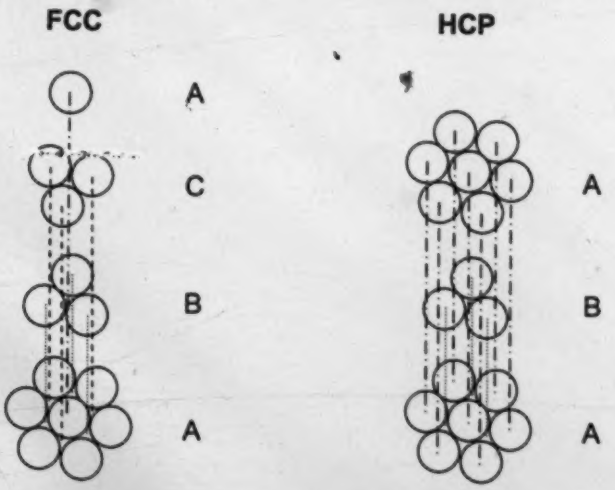

Figure 3.29. Close packing schemes of spheres. The face-centred cubic (FCC) (or CCP=cubic close-packed) lattice is built up in an ABCABC pattern, with the B and C planes occupying holes of different orientation in the A plane. The hexagonal close-packed (HCP) lattice consists of an ABAB pattern in which only one type of hole in the A plane is occupied.

(3) As the plates are not always densely packed, this may contribute to any peak broadening. Again, this would be due to the different d-spacings of the close-packed planes of the two phases.

(4) The effect of (3) is compounded by the plates being thin (tens of close-packed atomic planes), so the boundaries between different plates would make a relatively large volume fraction of a structure compared to the situation if the plates were thicker.

TEM diffraction may be useful in providing further insight into the phase and the nature and degree of crystallinity. High resolution TEM imaging may be helpful as well, especially in viewing the edges to examine the existence of grooves and ridges, as factor (2) is probably the most significant in the appearance of the hexagonal phase and is probably related to the growth rate (see below on discussion of counter ion). There does not appear to be any definite texture within either phase, demonstrating a lack of templating by the GaAs(100) substrate. (GaAs has a zinc blende structure with a lattice constant of 5.65 Å. Ag (cubic phase) is face-centred cubic with a lattice constant of 4.09 Å.)

We will now discuss various aspects of twinning. As mentioned earlier, twins may be introduced during growth. Since a plate can be rather large, a new plane or planes of atoms may deposit as different 'nuclei' in several locations at once. Some of these new growths will continue the correct stacking sequence, while others will not. Thus, not only is the stacking order disrupted, but these new growths will not fuse together properly.[68] Therefore, the crystallinity will be affected both thickness-wise and laterally. Furthermore, new planes may begin to develop before previous ones have been completed.[67,68] These factors lead to the plates not having perfectly smooth faces and also to the roughened and jagged edges. A twin may be introduced in a plane nucleus and thus the nucleus will form an entirely new plate instead of continuing the old plate. It is not clear if a twin needs to be present in the new nucleus or if it would simply develop a twin later during its growth, after which growth rapidly ensues (not necessarily parallel to the old plate). This dilemma is illustrated in Figure 3.30a. The new plate (plate I) forming on a close-packed line can be in one of two twinned directions

and is 70.5° with respect to the original. If the new nucleus has a twin, the edge of one of its variants will be a continuation of the old plate (in the original or twinned/faulted sequence) and the other variant will be completely incoherent with the old plate. The coherent variant and the substrate form a re-entrant groove with an angle of 70.5°. The other variant and the substrate form a groove of 109.5°. However, because of incoherence, it may not necessarily be considered a re-entrant groove; this will depend upon the line of atoms at the junction. If another plate (plate II) is now formed at the acute side, it will fit perfectly if it does not have a twin. However, with one twin, there is again an incongruity. Moreover, not every edge will have a re-entrant groove. This problem is easily solved, however, by considering only doubly twinned plates (Figure 3.30b), as this model accounts for the plates growing very large and having a hexagonal shape. Another necessary result of the twinning is that, because twin boundaries may be considered as grain boundaries, each plate is not actually single crystalline in the strictest sense. For whatever as-yet unknown reason, unlike the synthesis of Au on InP, the silver nanostructures formed are exclusively plates. Also, the Au particles were generally separated, while these Ag plates formed densely.

As mentioned earlier, the growth mechanism may be somewhat dendritic. In addition to the overlapping hexagons and triangles that eventually join together within a plate, the leaf-like structures formed after 21 h are also suggestive of a dendritic mechanism. A dendritic or related growth mechanism is not

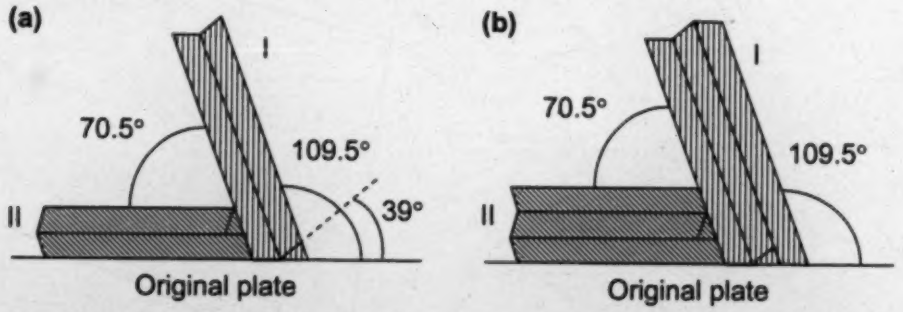

Figure 3.30. Twinning of new plates. (a) Scenario showing newly formed plates with single twins. This situation poses some problems with respect to growth and congruity (the angle of 39° indicates that the close-packed plane on the edge of the particular crystal variant will not meet coherently with the original plate). (b) Scenario showing newly formed plates that are doubly twinned. This situation accounts for the large size and hexagonal shape of the plates.

unreasonable considering that growth is rapid and the plates have a preferred way of nucleation and growth (specific planes at specific angles and on specific lines).[73] Others have also described dendritic growth as related to twinning.[67]

It is interesting to note that the structures start off as clusters then stacks of plates and not a thickened mass. The stacked plate structure may be so prevalent because of the slow growth of the flat faces in comparison to the rapid rates of nucleation and of growth at the plate edges due to twinning. The merged, thickened masses and scaffolding seen in Figure 3.16 and Figure 3.17 are a result of eventual coalescence at long deposition times, not initial growth. Figure 3.17d shows a structure with densely packed plates formed after 1 h. It is not difficult to envision the plates coalescing into a thickened mass with its edges smoothed out. As stated earlier, since the plates have a certain thickness, it then appears that there is a certain nucleation size (probably approximately its thickness or larger) before the plate will grow rapidly in some fast-growth directions within a {111} plane, eventually stabilizing to a hexagonal shape. Since the {111} planes are the most stable, after nucleation, a plate does not thicken at all or only does so very slowly (possibly mostly during the coalescence stage). The plates also have edges that are aligned with each other, either so that the plates in a stack are about the same size or each successive plate has a slightly different size. The bottom portion of Figure 3.25b shows that each of the two sets of plates have plates of the same size tilted against the same imaginary plane, while the top portion of the image shows each successive plate to be of a slightly different size, with the overall shape of the stack being a smooth bell. Another defect worth mentioning is the non-dense packing of plates. However, in many cases, plates may only appear to not pack densely at the edges of the structures as the plates grow and begin to bend.

When the $AgNO_3$ plating bath was sparged with argon for 30 min before the substrate was introduced, the stacked structures were rather similar; however, the edges of the plates were decorated with small hexagons that are discontinuous with the rest of the plate. There are also many large plates lying flat against the substrate. It has been reported that oxygen (and chloride) etches twinned

structures at their twin boundaries in favour of growth of single crystals.[61] However, it is difficult to say for certain if there is any size difference in the structures or plates compared to samples prepared without purging. More experimental work is needed to draw any conclusion for this matter. Further experimentation may also include adding Fe^{2+} or Fe^{3+}, as Fe^{2+} is reported to react with adsorbed oxygen and Fe^{3+} is a known etchant for noble metals.[74]

When the salt was changed from $AgNO_3$ to Ag_2SO_4, there were no more large structures observed. The background consisted of the expected plates in random orientations, but on top of these plates were large plates lying (roughly) parallel to the substrate. When the deposition time increased, these flat plates became much larger, virtually covering the entire surface. There was minimal deposition on top of these flat plates, except at the edges and corners of the substrates, probably due to the global cathodic nature of the edges and corners. This suggests that, besides twinning and stacking faults, the counter ion plays a role in growth. It appears that the sulphate ion is adsorbed more strongly to silver compared to nitrate. The effect is that it disables nucleation of other plates on these flat plates, meanwhile these plates grow very large laterally. (The thickness of the plates did not appear to be affected by sulphate adsorption.) This greater adsorption is likely due to the greater charge on the sulphate ion compared to the nitrate ion. Though it is unknown what the relative amounts of deposition are for the two ions (the 2:1 mole ratio of Ag^+ in the salts would also have to be accounted for), it seems possible that the sulphate lowers the overall growth rate as compared to nitrate, since a slower growth rate may enable the large plates to be exclusively of the cubic phase and to lie flat against the substrate. The lack of the hexagonal phase suggests fewer defects such as twins and stacking faults; however, twins would still be needed to grow the large plates through re-entrant grooves. Because of the possibly slower growth rate, there may be templating by the GaAs substrate. This may be explained as follows. A bed of small plates is present beneath the large plates, but there exists the possibility that the large plate starts off being in contact with the substrate and, during growth, the entire plate or just the newly formed portion of it is forced away from the substrate as the growth

front collides with other plates. However, it should also be noted that the prostrate position of the plates may be due to the plates falling over from a more upright position, unlike the stacked structures that were able to form stable towers.

Open-circuit potential measurements were performed to provide insight into the growth mechanism. The jump in the potential for all three cases upon addition of $AgNO_3$ indicates much electrochemical activity at the surface, that is, the reduction of Ag^+ and the oxidation of the substrate. Afterwards, the steady potential reveals steady, continuous growth of the particles for the first 500 seconds. The final potentials indicate the reactivity of the wafers, as dictated by their surface areas: the 'no edges' wafer had the least negative potential because it had the least surface area, the 'no edges, half scratched' wafer had the most negative potential because it had the most surface area. The potentials before salt addition, however, did not show the same trend, but this may be due to sample-to-sample variation, which may be related to factors such as the oxygen content of the baths.

The origin of the oscillatory behaviour in the OCP is rather uncertain. Other authors have attributed oscillatory behaviour in the OCP with cycles of substrate oxide growth and etching.[75,76] However, oscillations were observed before salt addition. Even so, oxide growth and etching may still be responsible, since cleaned but otherwise unreacted substrates reveal an etched substrate texture similar to that observed for 10^{-5} and 10^{-4} mol/L $AgNO_3$, except without metal deposition. It may be helpful to see if these oscillations of period ~1 s continue at longer deposition times. Because oxide growth is related to metal coverage on the substrate and since the amount of background deposition may be periodic, OCP measurements at higher deposition times may also show if the average potential (the nodes of these waves) shows another larger period on the order of tens of minutes or even hours. Though the growth of the large structures may also be periodic, it is expected that the determination of this phenomenon would be more difficult, since the sizes of the structures vary considerably within a sample, besides sample-to-sample variation. The periodic nature of any

growth/dissolution process (for the oxide, background deposition, and stacked structures) may not be a perfect sinusoidal wave, but it may be damped and/or have a lengthened period as the reaction progresses. OCP measurements (plus SEM imaging) should also be performed on different types of GaAs wafers (e.g., level and type of doping, orientation), as it has been suggested that the semiconductor properties may play a role.[77]

3.3.5 Ag on Ge

3.3.5.1 Results

When silver was deposited on Ge(100) with BMT, the deposition consisted of nut-like particles (slightly facetted, dimpled, 200-400 nm in size) and large, complex structures, the latter of which became more dominant and larger towards the edges (Figure 3.31). Many of the particles coalesced and the large structures appear to be the result of a combination of coalescence and greater

Figure 3.31. Ag on Ge in the presence of BMT. (a) and (b) Small particles and large structures can be seen by the edge of the substrate. (c) Close-up of small structures (obtained from the centre of the substrate).

chemical activity due to the global cathodic nature of the edges. The particles and structures appear to have spiral-like features.

For silver deposited on Ge(100) with SDS, the product consisted of a tangled web of wires and plates, with the plates becoming more dominant at higher concentrations (Figure 3.32). The wires were about 50 nm in diameter and the plates about the same thickness and a few hundred nanometres in width. The wires and plates actually appear to be part of a continuum as they are highly networked along with ribbons. When the reaction time increased for 10^{-3} mol/L SDS, there was simply more of the same product as at lower reaction times (Figure 3.33). EDX confirms that the deposits consist of silver (Figure 3.32d).

3.3.5.2 Discussion

Since inukshuk-like and other related dendritic structures are formed when germanium is immersed in a solution of silver salt only, the effect of surfactants was investigated. BMT seemed to produce blocky structures in which there may be seen slight spirals or screws, which are also present in the inukshuks and their related structures,[78] as dendrites may grow via a screw dislocation mechanism, though this mechanism was unconfirmed for the inukshuks.[73] The synthesis with SDS produced tangled networks of plates, ribbons, and wires. Although it is unclear as to why these structures are formed, we see that bath additives certainly have an effect on the structure of the products. SDS appears to have a larger effect on the product morphology, as there is no obvious screw or spiral structure present. More work will be needed to properly examine the effects of these additives and other parameters which may be controlled to possibly give other (more ordered) structures.

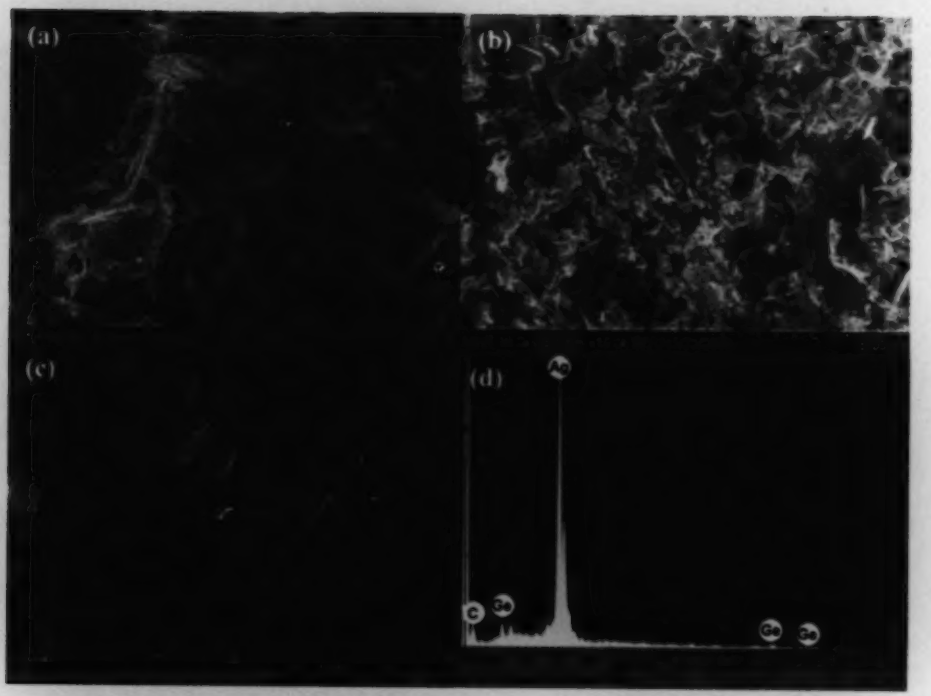

Figure 3.32. Ag on Ge with SDS for 3 h. (a) 10^{-3} mol/L SDS, centre of substrate. (b) 10^{-3} mol/L SDS, corner of substrate, showing more material. (c) 8.0×10^{-2} mol/L SDS, centre of substrate, showing a greater dominance of plates compared to at lower concentrations. (d) EDX spectrum of product. The C signal comes from surface contamination. This particular spectrum was taken from the sample synthesized with 2×10^{-3} mol/L SDS for 24 h.

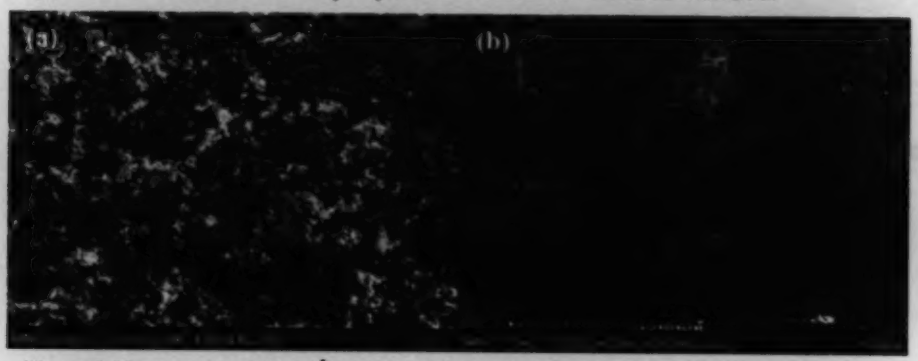

Figure 3.33. Ag on Ge with 10^{-3} mol/L SDS for 24 h. (a) and (b) show different magnifications.

3.3.6 Si nanowires and Ag dendrites (Ag on Si)

3.3.6.1 Results

A typical sample substrate of the silicon nanowire etching synthesis is shown in the optical photograph in Figure 3.34.

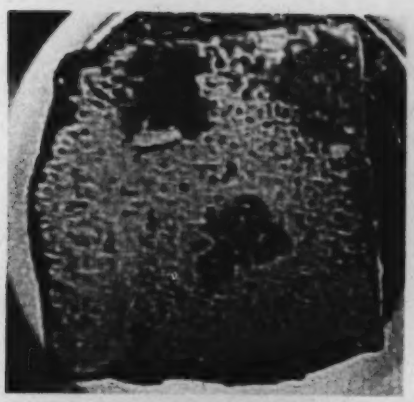

Figure 3.34. Optical photograph of Si substrate etched with $HF/AgNO_3$. The light area is the silver dendrite film. The dark area is the etched substrate where the film has delaminated.

While the products were still immersed in the bath, the dull, grey film of silver appeared spongy and came off very easily. Upon removal of the substrate from the solution, the film quickly lost volume and became thin. As the film dried after rinsing, it became white. If the concentration of silver nitrate used was high enough, small specks of shiny silver metal could be seen with the naked eye. The underlying etched substrate appeared dull and grey-brown.

SEM images giving an overview are shown in Figure 3.35, clearly showing the porous nature of the silver dendrite film. The tops of the silicon nanowires can be seen through the openings in the film. Figure 3.36 shows silicon nanowires and pillars of various sizes. Wires that are as thin as 20 nm or longer than 100 μm can be found. Figure 3.36b shows structures that are a few tens of nanometres thick but about 200 nm wide, indicating that there is potential to etch the width down further to produce thin wires. Figure 3.36e shows a curved nanowire, demonstrating the flexibility expected of nanomaterials since the strain is reduced. The EDX and XRD spectra (Figure 3.36g, h, respectively) corroborate that the material is crystalline silicon.

The silver film consisted of dendrites of various forms. Figure 3.37 shows inukshuk-like dendrites, dendrites with short arms spiralling out, fish-spine-like dendrites with round arms, filamentary dendrites that appear rather disordered, and fish-spine-like dendrites with flat arms. The structures closer to the substrate

Figure 3.35. Etching synthesis of Si nanowires: overview of products. The porous film consists of dendrites (left side of (c)). The silicon nanowires (right side of (c) and also (d)) can be seen through the holes in the film.

adopt features about 200-300 nm, such as the first three forms mentioned here. As the film grows farther away from the substrate, the structures become larger, with features on the order of 1 μm or more, like the fish-spine-like structures with flat arms. The disordered structure may be one of the smaller forms in a stage of coalescence, if at an intermediate distance from the substrate. This may be understood from looking at the outer surface of the film (Figure 3.38). There are chunky dendrites (feature size of several microns), coalescence, and even large particles (tens of microns). Although difficult to tell for certain, the particles are probably not strictly separate particles but a result of the chunky dendrites coarsening more and/or coalescence. EDX and XRD (Figure 3.37g, h, respectively) confirm these dendrites are made of crystalline silver.

A feature of note is that etching seems to occur in directions other than directly vertically into the substrate. Figure 3.39a shows a detached block with directions of etching perpendicular to each other. Figure 3.39b shows a similar but less pronounced effect on a block of substrate not detached. Though not clear

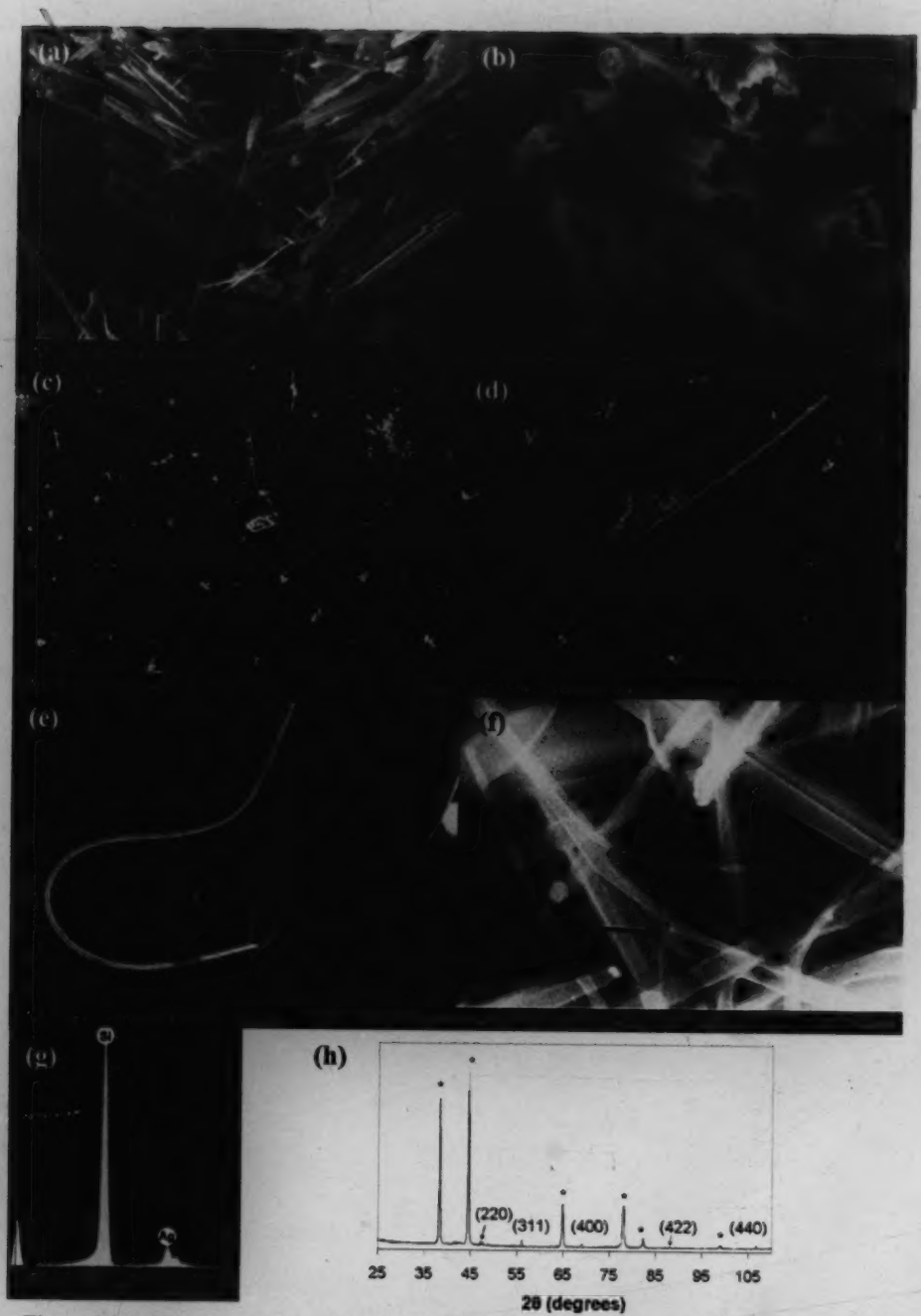

Figure 3.36. Silicon nanowires. (a) Different sizes of pillars and wires. (b) Small pillars showing some small possible nanowire diameters. (c) Several very long wires. (d) Close-up of long wire about 115 μm long. The diameter gradually varies from 500 nm to 1 μm, giving an aspect ratio of over 100. (e) Bent wire demonstrating flexibility. (f) Thin wires. The one indicated by the arrow is about 20 nm in diameter. (g) EDX spectrum. (h) XRD spectrum showing the Si reflections, with Ag peaks marked by asterisks. There is clearly much silver.

Figure 3.37. Silver dendrites. (a) Inukshuk-like dendrites. (b) Dendrites with spiralling arms. (c) Fish-spine-like dendrites with round arms. (d) Disordered, filamentary dendrites. (e) Fish-spine-like dendrites with flat arms. (f) Large fish-spine-like dendrite with flat arms and of a higher order. (g) EDX spectrum of dendrites mounted directly on carbon paste and aluminum stub. (h) XRD spectrum confirming the presence of silver.

Figure 3.38. Silver dendrites farther from substrate surface. (a) Chunky dendrites. (b) Chunky dendrites and coalescence of dendrites (bottom of image). (c) Coalescence of dendrites. (d) Dendrites with a particulate nature.

why different etching directions exist, it is possible that it is related to the dendritic formation between pillars and wires and coarsening of these dendrites. Corrugations on pillars and wires can be seen as well (Figure 3.39e) and this is probably a templating effect of dendrites within the substrate.

Not commonly seen is a more intermediate stage of etching. Figure 3.40 shows the substrate with holes rather than leftover pillars and wires.

Post-synthesis etching to refine the silicon nanostructures proved to be unsuccessful as the FTIR spectra obtained did not contain any SiH_x modes. However, some silicon nanostructures were still present as was seen in the SEM.

3.3.6.2 Discussion

Silicon nanowires were formed with the concomitant formation of silver dendrites. The silicon nanowires were similar to those described previously,[41-43] with both loose wires and undetached pillars that have not been etched down

Figure 3.39. Etching in different directions. (a) A loosened block of the substrate with etching directions that are perpendicular to each other. (b) An attached block of the substrate with slight etching in a direction parallel to the surface. (c) Dendrites among the nanowires and pillars. (d) Dendrites among the nanowires and pillars that show a degree of coalescence and coarsening. (e) Corrugations along the sides of pillars.

as much as the wires. Even though the latter appeared more dominant, the pillars often had a dimension that was similar to the diameter of the thinnest nanowires (tens of nanometres). These flatter pillars may be seen as nanobelts, a transition between the thin nanowires and large pillars. The nanostructures were easily freed from the substrate via scraping or sonication of the substrate, yielding free-standing nanowires and pillars of various dimensions.

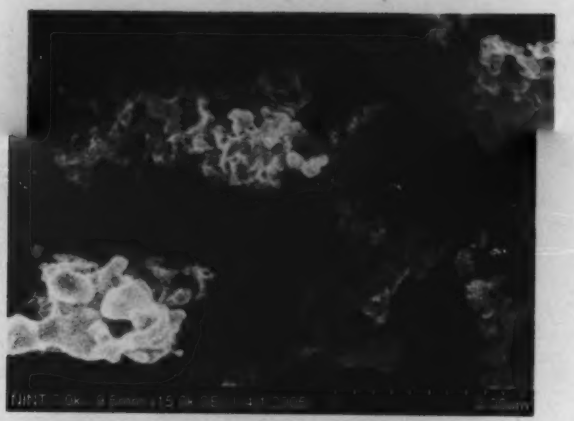

Figure 3.40. Less etched Si substrate. Holes can be seen rather than the leftover wires and pillars normally seen.

Besides silicon nanostructures of varying size and morphology, the silver nanostructures obtained displayed an array of sizes and shapes as well. These included inukshuk-like dendrites,[38] dendrites with spiralling arms, fish-spine-like dendrites with round arms, and filamentary dendrites close to the substrate surface; and fish-spine-like dendrites with flat arms, chunky dendrites, and dendrites with a particulate nature farther away from the surface. The latter structures, along with coalescence, probably do not affect the nanostructure of the silicon very much, as the silver appears to simply be coarsening. The structure of the silver close to the surface, however, is suspected to be related to that of the silicon.[43] It was found by others that, by changing the $AgNO_3$ concentration or the temperature of the synthesis, one can achieve a different type of silver dendrite and a corresponding silicon nanostructure.[42,43] The temperature change was not attempted in the current experiments. Rather, in some instances, the salt concentration was increased. This should lead to more extensive etching and, therefore, more free wires and dendrites. However, a greater amount of free wires could not be conclusively confirmed. The only noticeable difference is that more shiny silver metal can be seen with the naked eye. The reasons why the results at different concentrations do not appear to be much different may be that the experimental set-up was different from those used by other groups[41-43,79] (i.e., lack of sealed autoclave) and there are local variations within the samples obtained, besides some sample-to-sample variation.

In support of the newly proposed mechanism[44] for the nanowire formation is the curvature seen of the sides of the wires and pillars. The cross-section has curved sides of negative curvature (concave), because the etched areas have sides of positive curvature (convex). The etched areas consist of overlapping, (approximately) cylindrical pores, as seen in Figure 3.39 and illustrated schematically in Figure 3.41a. If the old mechanism were true, then the areas left standing should consist of overlapping, cylindrical columns (Figure 3.41b), which is clearly not the case. Further proof is in Figure 3.40, in which spatially separate, round pores are seen. SEM of as-grown products also reveals that there is much dendritic formation between the silicon nanostructures. Corrugations on the sides of pillars may be due to clusters that have sunk to the bottom of the wires/pillars and that have also formed dendrites that reach to the top of the substrate. Though unclear as to which would have a larger effect, it is possible that both the thickening and lengthening of the dendritic arms can cause the corrugations. In further support of the new mechanism, these corrugations also exhibit negative curvature.

Further etching of the silicon nanostructures was attempted in order to reduce and refine the thick pillars and to hydride-terminate them. Nitric acid is used to oxidize the surface of the silicon nanowires to SiO_2, while HF etches the SiO_2 formed. The pertinent equations are as follows.

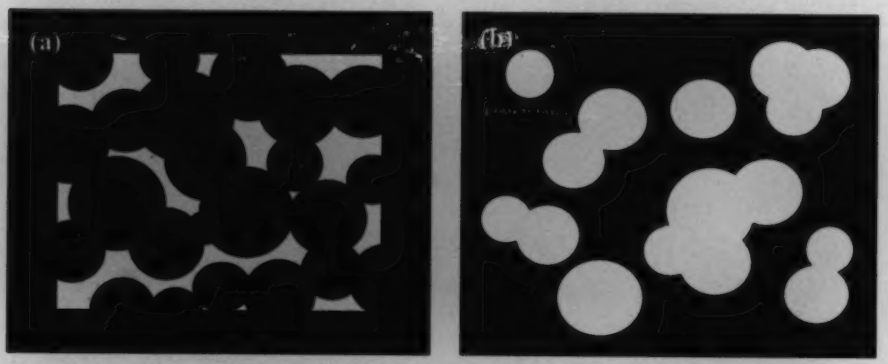

Figure 3.41. Cross-sections of silicon wires/pillars. The dark areas are where the substrate was etched away. The light areas are where the substrate remains. (a) Cross-section according to new mechanism. The etched areas are overlapping cylindrical pores, leaving the unetched areas to have surfaces of negative curvature. (b) Cross-section according to old mechanism. The unetched areas are overlapping cylindrical columns having positive curvature.

Oxidation $Si + HNO_3 + H_2O \rightarrow SiO_2 + HNO_2 + H_2$

Etching $SiO_2 + 6HF \rightarrow SiF_6^{2-} + 2H^+ + 2H_2O$

Overall $Si + HNO_3 + 6HF \rightarrow SiF_6^{2-} + HNO_2 + H_2O + 2H^+ + H_2$

After a rinsing procedure to eliminate HNO_3, the wires were then treated with HF alone to etch any remaining SiO_2 and to generate a hydride-terminated surface. As is the case with the silicon nanowires produced via the oxide-assisted growth method, it proved difficult to obtain SiH_x vibration modes in the FTIR spectrum, though there were still some nanowires left over after the etching treatment as seen with the SEM. The parameters will have to be optimized in order to successfully etch the nanowires and with as high a yield as possible. Other researchers working with silicon nanoparticles have also found that most of their product gets etched away when using HF/HNO_3.[80] The XRD pattern of an unetched dispersion (Figure 3.36h) shows that there is much silver, even though the first dispersion obtained was discarded and the substrate was sonicated again in fresh solvent. SEM of etched products reveals that there are products other than the silicon nanowires, which may be silver and/or an etching by-product due to reactions with the silver. Another factor to be considered is that the concentration of the silicon nanostructures may not be high enough to obtain an adequate signal in the FTIR spectrometer. It is possible that the wires did have a hydride-terminated surface, but it was simply not evident in the FTIR spectra. Thus, a better method will have to be developed to isolate the nanowires effectively in order to obtain a purer and more concentrated product and to avoid possible unwanted reactions with the silver.

3.4 Conclusion

Various morphologies of different metals (Au, Pt, and Ag) were shown to deposit on different semiconductors (InP, GaAs, Ge, and Si) via galvanic displacement. Of note, gold deposits as regular (or quasi-regular) geometric shapes on InP in the presence of an acid. These shapes include the icosahedron,

decahedron, decahedral prism, truncated tetrahedron, hexagonal plate, and triangular plate. These shapes can be explained through twinning.

The silver plates on GaAs were also very intriguing and require much further study. The plates are very thin and can grow very large, resulting in a high aspect ratio. They consist of close-packed planes and arrange themselves into complex stacks (with $AgNO_3$). They stabilize into a hexagonal shape and eventually coalesce. The plates nucleate on each other at probably 70.5° on close-packed lines of atoms. XRD indicates the presence of both phases of silver when $AgNO_3$ is used as the salt. Purging of the $AgNO_3$ solution before reaction causes the (large) plates to be decorated with smaller hexagonal plates that are discontinuous with the (large) plate. When Ag_2SO_4 is used, cubic phase silver results and the plates are very large and lie parallel to the substrate on a bed of small plates, suggesting that the sulphate ion adsorbs more strongly than the nitrate ion to silver. Twinning, in conjunction with dendritic formation, appears to be responsible for the growth of the plates. An Ostwald ripening process (along with twinning) may account for the growth of the plates into stacked structures. The OCP exhibits oscillatory behaviour. More SEM and OCP for different reaction times are required to determine if these oscillations are permanent and if there is another waveform to explain the growth and dissolution of the background plates. TEM may also be instrumental in obtaining more information on the phase and degree of crystallinity of the plates.

The silicon nanostructures synthesized with HF/HNO_3 had varying sizes and morphologies. Some were wires as thin as 20 nm. There were also nanobelts and large pillars. The silver dendrites formed also had various sizes and shapes. The morphologies included inukshuk, spiralling arms, fish-spine (some with round arms, others with flat arms), and filamentary. At the top of the silver film, there was much coarsening and coalescence of the dendrites. The newly proposed mechanism of the etching synthesis was supported by the negative curvature seen in the sides of the silicon nanostructures. Attempts to further etch to refine the wires were ineffectual. In order to accomplish this, a more effective method needs to be developed to isolate and concentrate the silicon nanostructures.

As this work has shown, there is much potential in developing nanostructures of a desired size and shape. However, much more work still needs to be done in order to fully realize this potential and to exploit the findings for real applications.

3.5 References

(1) El-Sayed, M. A. *Acc. Chem. Res.* **2001**, *34*, 257.

(2) El-Sayed, M. A. *Acc. Chem. Res.* **2004**, *37*, 326.

(3) Sun, X.-H.; Wong, N.-B.; Li, C.-P.; Lee, S.-T.; Kim, P.-S. G.; Sham, T.-K. *Chem. Mater.* **2004**, *16*, 1143.

(4) Yu, Y.-Y.; Chang, S.-S.; Lee, C.-L.; Wang, C. R. C. *J. Phys. Chem. B* **1997**, *101*, 6661.

(5) Charnay, C.; Lee, A.; Man, S.-Q.; Moran, C. E.; Radloff, C.; Bradley, R. K.; Halas, N. J. *J. Phys. Chem. B* **2003**, *107*, 7327.

(6) Kim, F.; Connor, S.; Song, H.; Kuykendall, T.; Yang, P. *Angew. Chem. Int. Ed.* **2004**, *43*, 3673.

(7) Chen, S.; Fan, Z.; Carroll, D. L. *J. Phys. Chem. B* **2002**, *106*, 10777.

(8) Maillard, M.; Giorgio, S.; Pileni, M. P. *J. Phys. Chem. B* **2003**, *107*, 2466.

(9) Chen, S.; Carroll, D. L. *J. Phys. Chem. B* **2004**, *108*, 5500.

(10) Jin, R.; Cao, Y.; Mirkin, C. A.; Kelly, K. L.; Schatz, G. C.; Zheng, J. G. *Science* **2001**, *294*, 1901.

(11) Semiconductor Industry Association. *2005 Annual Report: 2020 Is Closer Than You Think;* Paulus, J., Ed.; San Jose, CA, 2005.

(12) Sau, T. K.; Murphy, C. J. *J. Am. Chem. Soc.* **2004**, *126*, 8648.

(13) Sun, Y.; Xia, Y. *Science* **2002**, *298*, 2176.

(14) Chen, S.; Wang, Z. L.; Ballato, J.; Foulger, S. H.; Carroll, D. L. *J. Am. Chem. Soc.* **2003**, *125*, 16186.

(15) Germain, V.; Li, Jing.; Ingert, D.; Wang, Z. L.; Pileni, M. P. *J. Phys. Chem. B* **2003**, *107*, 8717.

(16) Puntes, V. F.; Zanchet, D.; Erdonmez, C. K.; Alivisatos, A. P. *J. Am. Chem. Soc.* **2002**, *124*, 12874.

(17) Chen, S.; Carroll, D. L. *Nano Lett.* **2002**, *2*, 1003.

(18) Puntes, V. F.; Krishnan, K.; Alivisatos, A. P. *Top. Catal.* **2002**, *19*, 145.

(19) Caswell, K. K.; Bender, C. M.; Murphy, C. J. *Nano Lett.* **2003**, *3*, 667.

(20) Gao, Y.; Song, L.; Jiang, P.; Liu, L. F.; Yan, X. Q.; Zhou, Z. P.; Liu, D. F.; Wang, J. X.; Yuan, H. J.; Zhang, Z. X.; Zhao, X. W.; Dou, X. Y.; Zhou, W. Y.; Wang, G.; Xie, S. S.; Chen, H. Y.; Li, J. Q. *J. Cryst. Growth* **2005**, *276*, 606.

(21) Gao, Y.; Jiang, P.; Song, L.; Liu, L. F.; Yan, X Q..; Zhou, Z. P.; Liu, D. F.; Wang, J. X.; Yuan, H. J.; Zhang, Z. X.; Zhao, X. W.; Dou, X. Y.; Zhou, W. Y.; Wang, G.; Xie, S. S. *J. Phys. D Appl. Phys.* **2005**, *38*, 1061.

(22) Yin, Y.; Rioux, R. M.; Erdonmez, C. K.; Hughes, S.; Somorjai, G. A.; Alivisatos, A. P. *Science* **2004**, *304*, 711.

(23) Magagnin, L.; Maboudian, R.; Carraro, C. *J. Phys. Chem. B* **2002**, *106*, 401.

(24) Vereecken, P. M.; Binstead, R. A.; Deligianni, H.; Andricacos, P. C. *IBM J. Res. Dev.* **2005**, *49*, 3.

(25) Porter, L. A.; Choi, H. C.; Ribbe, A. E.; Buriak, J. M. *Nano Lett.* **2002**, *2*, 1067.

(26) Carraro, C.; Magagnin, L.; Maboudian, R. *Electrochim. Acta* **2002**, *47*, 2583.

(27) Porter, L. A.; Choi, H. C.; Schmeltzer, J. M.; Ribbe, A. E.; Elliott, L. C. C.; Buriak, J. M. *Nano Lett.* **2002**, *2*, 1369.

(28) Porter, L. A.; Ribbe, A. E.; Buriak, J. M. *Nano Lett.* **2003**, *3*, 1043.

(29) Gorostiza, P.; Allongue, P.; Diaz, R.; Morante, J. R.; Sanz, F. *J. Phys. Chem. B* **2003**, *107*, 6454.

(30) Niwa, D.; Homma, T.; Osaka, T. *J. Phys. Chem. B* **2004**, *108*, 9900.

(31) Zambelli, T.; Munford, M. L.; Pillier, F.; Bernard, M.-C.; Allonge, P. *J. Electrochem. Soc.* **2001**, *148*, C614.

(32) Harraz, F. A.; Tsuboi, T.; Sasano, J.; Sakka, T.; Ogata, Y. H. *J. Electrochem. Soc.* **2002**, *149*, C456.

(33) Takano, N.; Niwa, D.; Yamada, T.; Osaka, T. *Electrochim. Acta* **2000**, *45*, 3263.

(34) Kim. C.; Oikawa, Y.; Shin, J.; Ozaki, H. *Microelectron. J.* **2003**, *34*, 607.

(35) Magagnin, L.; Bertani, V.; Cavallotti, P. L.; Maboudian, R.; Carraro, C.; *Microelectron. Eng.* **2002**, *64*, 479.

(36) D'Asaro, L. A.; Nakahara, S.; Okinaka, Y. *J. Electrochem. Soc.* **1980**, *127*, 1935.

(37) Lin, H.; Mock, J.; Smith, D.; Gao, T.; Sailor, M. J. *J. Phys. Chem. B* **2004**, *108*, 11654.

(38) Aizawa, M.; Cooper, A. M.; Malac, M.; Buriak, J. M. *Nano Lett.* **2005**, *5*, 815.

(39) Wang, Z. L.; Gao, R. P.; Nikoobakht, B.; El-Sayed, M. A. *J. Phys. Chem. B* **2000**, *104*, 5417.

(40) Gorostiza, P.; Kulandainathan, M. A.; Diaz, R.; Sanz, F.; Allongue, P.; Morante, J. R. *J. Electrochem. Soc.* **2000**, *147*, 1026.

(41) Peng, K. Q.; Yan, Y. J.; Gao, S. P.; Zhu, J. *Adv. Mater.* **2002**, *14*, 1164.

(42) Peng, K. Q.; Yan, Y. J.; Gao, S. P.; Zhu, J. *Adv. Funct. Mater.* **2003**, *13*, 127.

(43) Peng, K. Q.; Zhu, J. *Electrochim. Acta* **2004**, *49*, 2563.

(44) Peng, K. Q.; Wu, Y.; Fang, H.; Zhong, X. Y.; Xu, Y.; Zhu, J. *Angew. Chem. Int. Ed.* **2005**, *44*, 2737.

(45) Tsuboi, T.; Sakka, T.; Ogata, Y. H. *J. Appl. Phys.* **1998**, *83*, 4501.

(46) Hormozi Nezhad, M. R.; Aizawa, M.; Porter, L. A., Jr.; Ribbe, A. E. Buriak, J. M. *Small,* **2005,** in press.

(47) Lofton, C.; Sigmund, W. *Adv. Funct. Mater.* **2005,** *15,* 1197.

(48) Ascencio, J. A.; Perez, M.; Jose-Yacaman, M. *Surf. Sci.* **2000**, *447*, 73.

(49) Rupprechter, G.; Hayek, K.; Rendón, L.; José-Yacamán, M. *Thin Solid Films* **1995,** *260*, 148.

(50) Gillet, M.; Renou, A. *Surf. Sci.* **1979,** *90,* 91.

(51) Li, B. Q.; Zuo, J. M. *Phys. Rev. B* **2005,** *72,* 085434.

(52) Meerson, O.; Sitja, G.; Henry, C. R. *Eur. Phys. J. D* **2005,** *34,* 119.

(53) Gao, Y. Song. L. Jiang, P.; Liu, L. F.; Yan, X. Q.; Zhou, Z. P.; Liu, D. F.; Wang, J. X.; Yuan, H. J.; Zhang,, Z. X.; Zhao, X. W.; Dou, X. Y.; Zhou, W. Y.; Wang, G.; Xie, S. S..; Chen, H. Y.; Li, J. Q. *J. Cryst. Growth* **2005,** *276,* 606.

(54) Johnson, C. J.; Dujardin, E.; Davis, S. A.; Murphy, C. J.; Mann, S. *J. Mater. Chem.* **2002,** *12,* 1765.

(55) Kuo, C.; Chiang, T.; Chen, L.; Huang,, M. H. *Langmuir* **2004,** *20,* 7820.

(56) Salzemann, C.; Urban J.; Lisiecki, I.; Pileni, M. *Adv. Funct. Mater.* **2005,** *15,* 1277.

(57) Chen, Y.; Gu, X.; Nie, C.; Jiang, Z.; Xie, Z.; Lin, C. *Chem. Commun.* **2005,** *33,* 4181.

(58) Wiley, B.; Sun, Y.; Mayers B.; Xia, Y. *Chem. Eur. J.* **2005,** *11,* 454.

(59) Hofmeister, H.; Tan, G. L.; Dubiel, M. *J. Mater. Res.* **2005,** *20,* 1551.

(60) Bögels, G.; Meekes, H.; Bennema, P.; Bollen, D. *J. Phys. Chem. B* **1999,** *103,* 7577.

(61) Wiley, B.; Herricks, T.; Sun, Y.; Xia Y. *Nano Lett.* **2004,** *4,* 1733.

(62) Tadmor, E. B.; Bernstein, N. *J. Mech. Phys. Solids* **2004,** *52,* 2507.

(63) Wang, J.; Tian, M.; Mallouk, T. E.; Chan, M. H. W. *J. Phys. Chem. B* **2004,** *108,* 841.

(64) Gleiter, H.; Klein, H. P. *Philos. Mag.* **1973,** *27,* 1009.

(65) Bögels, G.; Meekes, H.; Bennema, P.; Bollen, D. *Philos. Mag. A* **1999,** *79,* 639.

(66) Goessens, C.; Schryvers, D.; Van Landuyt, J. *Microsc. Res. Techniq.* **1998,** *42,* 85.

(67) Hamilton, D. R.; Seidensticker, R. G. *J. Appl. Phys.* **1960,** *31,* 1165.

(68) Hamilton, J. F.; Brady, L. E. *J. Appl. Phys.* **1964,** *35,* 414.

(69) Berriman, R. W.; Herz, R. H. *Nature* **1957,** *180,* 293.

(70) Shirokoff, J.; Hui, K. C.; Erb, U. *J. Physique* **1988,** *49,* C5-165.

(71) Redmond, P. L.; Hallock, A. J.; Brus, L. E. *Nano Lett.* **2005,** *5,* 131.

(72) Lee. S. T.; Wang, N.; Lee, C. S. *Mater. Sci. Eng. A* **2000,** *286,* 16.

(73) Saratovkin, D. D.*Dendritic Crystallization*; Consultants Bureau, Inc.: New York, 1959.

(74) Wiley, B.; Sun, Y.; Xia, Y. *Langmuir* **2005,** *21,* 8077.

(75) Lehmann, V. *J. Electrochem. Soc.* **1996,** *143*, 1313.

(76) Parkhutik, V. P.; Matveeva, E. *Electrochem. Solid-State Lett.* **1999**, *2*, 371.

(77) Sasano, J. Understanding and Control of Metal Deposition Behavior onto Porous Silicon. Ph. D. Thesis, Kyoto University, Kyoto, Japan, March 2004.

(78) Cooper, A. M.; Aizawa, M.; Buriak, J. M. National Institute for Nanotechnology, National Research Council of Canada and Department of Chemistry, University of Alberta, Edmonton, Canada. Unpublished work, 2004.

(79) Qiu, T.; Wu, X. L.; Mei, Y. F.; Wan, G. J.; Chu, P. K.; Siu, G. G. *J. Cryst. Growth* **2005,** *277,* 143.

(80) Li, X.; He, Y.; Swihart, M. T. *Langmuir* **2004**, *20*, 4720.

4 Conclusion

4.1 Silicon nanowires

For the silicon nanowires, two methods of synthesis—oxide-assisted growth and electrochemical etching—were employed. The OAG method produced various other silicon nanostructures as well and their growth was dependent on substrate temperature. The electrochemical etching synthesis had concomitant formation of other products too, namely, silver dendrites of various morphologies. Though there was limited success in etching the wires (from both syntheses) to facilitate for further surface reaction, valuable insight into their preparation has been gained and some suggestions are offered concerning further experimentation. It was demonstrated that the OAG-synthesized wires could be dispersed in a solvent for TEM characterization and that they could be etched with HF vapour. It is therefore likely that dispersal followed by etching with HF vapour should work. Unfortunately, the yield of fine nanowires with the OAG method may be too low to be of practical value in real applications, unless synthesis parameters are optimized. A similar dispersal/etching method may prove useful in etching the electrochemically prepared wires. The etching procedure using HF/HNO_3 may also be effective with certain concentration combinations. After achieving satisfactory yield with the etching step, UV hydrosilylation may be utilized to functionalize the nanowires and attach them to a bulk silicon surface, either flat or porous.

4.2 Metal nanostructures on semiconductor substrates

Valuable, preliminary results have been obtained with regard to metal deposition on semiconductor substrates. Various morphologies of metal nanostructures were deposited onto various semiconductors, including regular and semi-regular polyhedral gold nanostructures on indium phosphide and stacked silver plates on gallium arsenide. Twinning was determined to be particularly important in the formation of these structures. Still, more work needs to be done

in order to fully exploit the findings. The parameters to be varied in synthesis include the metal salt, possible bath additives, their respective concentrations, semiconductor substrate (including orientation and dopant type and level), deposition time, and even cleaning procedure, reaction temperature, and exposure to light. More characterization techniques are required as well.

Specifically, for the case of silver on gallium arsenide, the variables that must be explored more fully include metal salt, concentration, and deposition time. It is very clear that the salt has a significant effect on the deposition morphology and probably overall growth rate. Since, for the same concentration but increasing reaction times, there appears to be a fluctuating amount of 'background' deposition on the substrate while the large structures grow, it is worthwhile to investigate the amount of both types of deposition (background, large structures) with respect to time. The other factor in the level of exposure to salt is the salt concentration. It may be instructive to map out the amount of deposition with respect to both concentration and time for each salt that is used. Varying these parameters would also allow study of the large structures; for example, how and why do the large, coalesced, leaf-like structures (seen after 21 h with 1 mmol/L $AgNO_3$) form?

Since there were a limited number of trials performed and some variation existed for those of similar deposition times, not only are more trials necessary, but different pre-synthesis cleaning and even post-synthesis rinsing procedures may be required to ensure reproducibility. For example, UV irradiation may be used as the last step in cleaning. Though fresh surface is generated during etching, this step may help in achieving more even deposition. Varying the pH of the bath or the post-reaction rinsing solution may also affect the products via Ostwald ripening. It may also be interesting to see if leaving the substrate in a bath (of varying pH and without the salt) for different periods of time after synthesis would have an effect on the Ostwald ripening process.

It is well known that defects corrode more easily than the rest of the crystal as they are thermodynamically less stable than the bulk crystal. Etching the products and examining them (for example, under the TEM) may allow one to

gain more insight into the twinning mechanism. Though unlikely that dislocations play a major role in the growth of the silver plates, this aspect may also be studied by immersing the deposition products in acid and analyzing them. This technique is particularly suggested for the silver structures on other substrates, especially germanium, with or without bath additives, as a screw dislocation mechanism is likely.

The effects of oxygen, chloride, Fe^{2+}, and Fe^{3+} should be investigated. It seems that a deoxygenated bath solution certainly has some effect on the final structures; therefore it would be worthwhile to fully explore the effects of these and other etchants/additives.

Another possible experiment would be to leave the substrate in water and add the salt (and any additives) at various rates. One possible effect is that formation of the stacked structures may be favoured or disfavoured with different rates of addition. Furthermore, if any additives are used, the order of addition of the bath components may be important.

Besides more wet chemistry (synthesis, etching), more characterization is necessary as well. On the basis of the current SEM observations, some plates within the large structures appear to have spaces between them, while other structures seem to have the plates very tightly packed. TEM may lend insight into this matter. Because the plates will have to be dispersed in a solvent, it should be possible to determine if they break apart leaving a smooth interface or not, or if they break apart at all, and therefore to see if there is any continuation of the crystal structure from one plate to the next and how often this occurs. TEM also has higher resolution than SEM. In addition, diffraction may be performed to provide more information on the crystal structure. Both imaging and diffraction may be done with different orientations (tilting of the sample). Furthermore, plates dispersed in epoxy may be aligned with a shear force such that the plates are parallel to the electron beam to view the probable re-entrant grooves and ridges on the edges. Diffraction would also be particularly useful for substrates prepared with purging of the bath beforehand, as there are small plates decorating the edges of the large plates.

More XRD characterization, particularly in the form of pole figures, would be necessary to determine any textural information regarding the plates formed with Ag_2SO_4.

If there is a certain nucleus size before a particle will start growing rapidly into a plate, atomic force microscopy (AFM) may be useful in determining this size. It is difficult to say what the nucleus size is under the SEM, since the SEM gives lateral and not depth information.

X-ray photoelectron spectroscopy (XPS) is needed to provide information on the nature of bonding at the interface of the metal and the semiconductor. It is important that the metal be adherent to the semiconductor substrate for applications in the microelectronics and microfabrication industry.

As these experiments are electrochemical in nature, more extensive OCP and other electrochemical experimentation is crucial to developing a more complete mechanistic picture.

Information on the amount of deposition may also be useful. To measure the film thickness and examine its uniformity, the substrate may be fractured (very carefully) and then examined under the SEM. The mass may be determined by performing inductively coupled plasma mass spectrometry (ICPMS) *in situ*.

Since metallic nanostructures exhibit unusual electrical and optical properties dependent on their size and shape, these properties may be investigated to explore the science and potential technological utility of these plates (and possibly stacked structures). Spectroscopies may include surface plasmon resonance and absorption in UV-visible light.

If the silver plates can be grown in a controllable fashion such that they lie flat against the substrate without a bed of small particles underneath, then further research may involve creating different metallization patterns to demonstrate utility in the microelectronics and microfabrication industry and for possible use as a resist.

The large surface area of the background deposition, stacked plate structures, and the dendrites (Ag on Si) may also be of potential use in catalysis and sensors.

Though most of this discussion is specific for silver on gallium arsenide, the synthetic procedures, characterization, and possible applications are also generally applicable to other metal-semiconductor systems. For the gold on indium phosphide system, it would be worthwhile to determine if there is any epitaxial relationship and to study these particles using TEM diffraction since they are twinned.

The platinum on indium phosphide system was not studied in detail, as there was little deposition remaining on the substrate. However, if the analysis on the formation of the coiled nanowire is accurate, then one possible avenue to be explored is making platinum nanowires of different sizes by scribing an indium phosphide substrate (for example, with an AFM tip) and immersing it into the platinum salt bath. Of course, an effective method would be needed to harvest the nanowires. Other than straight lines for nanowires, complex patterns may be scribed as well and therefore networked platinum structures may be formed. Thicknesses may even be varied within a structure.

The metal-semiconductor systems investigated in this work all involve a single metal on a semiconductor. However, co-deposition of different metals would possibly allow the formation of alloyed or heterogeneous nanostructures. A further extension is allowing nanostructures to grow in one bath (of single or multiple metal ions), then placing them into another bath (of single or multiple metal ions). All of these complex systems could be very interesting to study.

Since multiple metals may be used, one may also consider the use of more complex semiconductors, such as a quaternary compound like InGaAsP.